The Implications of Climate Change on Pavement Performance and Design

By Qiang Li, Leslie Mills and Sue McNeil

A report submitted to the University of Delaware University Transportation Center (UD-UTC)

September 25, 2011

DISCLAIMER*:*

The contents of this report reflect the views of the authors, who are responsible for the facts and the accuracy of the information presented herein. This document is disseminated under the sponsorship of the Department of Transportation University Transportation Centers Program, in the interest of information exchange. The U.S. Government assumes no liability for the contents or use thereof.

Table of Contents

Abstract

Pavements are designed based on historic climatic patterns, reflecting local climate and incorporating assumptions about a reasonable range of temperatures and precipitation levels. Given anticipated climate changes and the inherent uncertainty associated with such changes, a pavement could be subjected to very different climatic conditions over the design life and might be inadequate to withstand future climate forces that impose stresses beyond environmental factors currently considered in the design process.

This research explores the impacts of potential climate change and its uncertainty on pavement performance and therefore pavement design. Two tools are integrated to simulate pavement conditions over a variety of scenarios. The first tool, MAGICC/SCENGEN (Model for the Assessment of Greenhouse-gas Induced Climate Change: A regional Climate Scenario Generator), provides estimates of the magnitude of potential climate change and its uncertainty. The second tool, the Mechanistic-Empirical Pavement Design Guide (MEPDG) software analyzes the deterioration of pavement performance.

Three important questions are addressed: (1) How does pavement performance deteriorate differently with climate change and its uncertainty? (2) What is the risk if climate change and its uncertainty are not considered in pavement design? and (3) How do pavement designers respond and incorporate this change into pavement design process?

This research develops a framework to incorporate climate change effects into the mechanistic-empirical based pavement design. Three test sites in the North Eastern United States are studied and the framework is applied. It demonstrates that the framework is a robust and effective way to integrate climate change into pavement design as an adaptation strategy.

Acronyms

ΔT2x – Climate Sensitivity

A1 – family of emissions scenarios including A1F1 –fossil intensive, A1T - non-fossil energy sources, and A1B – balanced across all sources.

AADTT – Annual Average Daily Truck Traffic

AASHTO – American Association of State Highway and Transportation Officials

AC – Asphalt concrete

AMDTT – Average Monthly Daily Truck Traffic

AOGCM - atmosphere/ocean global climate mode

AVC – Automated vehicle counts

B1 and B2 – families of emission scenarios

CDF – Class Distribution Factor

CGCM3- Canadian Centre for Climate Modeling

CRCP – Continuously reinforced concrete pavement

ECHAM5/MPI-OM - Max Planck Institute for Meteorology (Germany)

EICM – Enhanced Integrated Climatic Model

GB – Granular base

GCM – General Circulation Model

GFDL CM2.0 and CM2.1- Geophysical Fluid Dynamics Laboratory Climate Models

GHG – Green house gas

GMT – Global Mean Temperature

GPS – Global Positioning System

GS- unbound granular subbase

HadCM3 and HadGEM1 - Hadley Centre for Climate Prediction and Research (United Kingdom)

HATT – Hourly Average truck traffic for one-hour time period

HCD – file extension for hourly climatic database files used by MEPDG

HMA – Hot mix asphalt

ICM – file extension for climate files generated by MEPDG

IPCC – Intergovernmental Panel on Climate Change

IPSL_CM4 - Institute Pierre Simon Laplace (France) Climate Model

IRI – International Roughness Index

JPCP – Jointed plain concrete pavement

LTPP – Long term pavement performance program

MAGICC/SCENGEN – Model for the Assessment of Greenhouse-gas Induced Climate Change: A regional Climate Scenario Generator

MEPDG – Mechanistic Empirical Pavement Design Guide

MIROC 3.2 - Center for Climate System Research (Japan) (medium resolution)

MRI-CGCM 2.3.2 - Meteorological Research Institute (Japan))

MSLP – Mean Sea Level Pressure

NCAR CCSM - National Center for Atmospheric Research CCSM

NCDC – National Climatic Data Center

NFS – Non-frost susceptible

PCC – Portland Cement Concrete

SRES – Special Report on Emissions Scenarios

SS – Sand soil

TB – Bound treated base

TMG – Traffic Monitoring Guide

TMI – Thornwaite Moisture Index

TRB – Transportation Research Board

UKCIP – United Kingdom Climate Impacts Programme

WIM – Weigh in motion

Symbols

a, b, c = calibration constants

a_i, b_j, c_j = regression coefficients

Age = Age after construction, years

Age= pavement age in years

$(\mathrm{BC})_{\mathrm{T}}$ = Total area of block cracking (low, medium, and high severity levels), percent of total lane area, %

C_1 through C_7 = calibration constants

$\mathrm{C}_1, \mathrm{C}_2$ = calibration constants

CDFj = Class distribution factor for vehicle class j

Ci – default value of Ci

$(\mathrm{COV}_{\mathrm{RD}})$ = Rut depth coefficient of variation, percent

$\mathrm{DE}_{\mathrm{i}} =$ Differential deformation energy accumulated during month$\mathrm{i}$.

D_{i} = accumulated fatigue damage at the end of i^{th} monthly increment

$\mathrm{distress}$ – estimated distress using default calibration factors

E = Stiffness of the material

EROD= Base/subbase erodibility factor

$\mathrm{E}_{\mathrm{distress}}^{\mathrm{Ci}}$ - Elasticity of factor Ci for the associated distress condition

$\mathrm{Fault}_{\mathrm{m}}$= Mean joint faulting at the end of month$\mathrm{m}$, in.

$\mathrm{FAULTMAX}_{\mathrm{i}} =$ Maximum mean transverse joint faulting for month$\mathrm{i}$, in

$(\mathrm{FC})_{\mathrm{T}}$ = Total area of fatigue cracking (low, medium, and high severity levels), percent of wheel path area, %

FD = total fatigue damage

Fenv =composite environmental effects adjustment factor,

FF = adjustment factor for frozen condition

FI = Average annual freezing index.

FR = adjustment factor for recovering conditions

FR = Base freezing index defined as percentage of time the top base temperature is below freezing $(32^{\circ}\mathrm{F})$ temperatures.

FU = unbound layer modulus adjustment factor for unfrozen conditions

h = Thickness of layer/sub-layer

h^i = Thickness of sub-layer i.

HDFi = Hourly distribution factor for ith one-hour time period

i = age (accounts for change in PCC modulus rapture, layer bond condition, deterioration of shoulder Load Transfer Efficiency)

IRI_0 = IRI measured within six months after construction, m/km

j = month (accounts for change in base and effective dynamic modulus of subgrade reaction)

k = axle type

k_1, k_2, k_3 = Laboratory regression coefficients

l = load level (incremental load for each axle type)

$(LC_{NWP})_{MH}$ = Medium and high severity sealed longitudinal cracks outside the wheel path, m/km.

$(LC_{SNWP})_{MH}$= Medium and high severity sealed longitudinal cracks outside the wheel path, m/km

m = temperature difference

MAFi = Monthly adjustment factor for month i

M_j = change in smoothness due to maintenance activities

MR = Unbound material adjustment factor

MR_i = PCC modulus of rapture at age i, psi

N = Number of load repetitions

N = Number of traffic repetitions

n = traffic path

N_f = Number of repetitions to fatigue cracking

$N_{i,j,k,...}$ = allowable number of load applications at condition i, j, k, l, m, n

$N_{i,j,k,...}$ = allowable number of load applications at conditioni, j, k, l, m, n.

$n_{i,j,k,...}$ = applied number of load applications at condition i, j, k, l, m, n

$nsublayers$ = number of sublayers

$(P)_H$= Area of high severity patches, percent of total lane area, %

$PATCH$ = pavement surface area with flexible and rigid patching (all severities), percent

$PATCH$ = percentage pavement surface with patching (M-H severity flexible and rigid)

$P_{0.02}$= Percent passing thee 0.02 mm sieve

$P_{0.075}$= Percent passing the 0.075 mm sieve

P_{200} = Percent subgrade passing #200 sieve

P_{200}= percent subgrade material passing the 0.075-mm sieve.

PD = pavement permanent deformation

PI = Plasticity index

PO_i = total predicted number of punchouts per mile at the end of i^{th} monthly increment

PUNCH = number of medium- and high-severity punchouts/km

P_s = Overburden on subgrade, lb

R_m= Average annual rainfall, mm

R_{SD}= Standard deviation in the monthly rainfall, mm

RF = Reduction factor due to thawing

RR=Recovery ratio

S = degree of saturation

S(*t*) = pavement smoothness at a specific time *t*

S_0 = initial smoothness immediately after construction

$S_{D(t)}$ = change of smoothness due to the *i*th distress at a given time *t* in the analysis period (*i*=1 to *n*)

(SD_{RD}) = Standard deviation of the rut depth, mm.

SDP (%) - Standard deviation of the percentage change in precipitation

SDT (%) - Standard deviation of temperature

Sequil = degree of saturation at equilibrium

SF = site factor

SF = site factor

S_j = change in smoothness due to site factors (subgrade and age)

SLR (cm) - sea level rise

Sopt = degree of saturation at optimum conditions

SPALL = percentage of joints with spalling (all severities)

T = Mix temperature (deg F)

TC = percentage of slabs with transverse cracking (all severities)

TC= number of medium- and high-transverse cracks/km

$(TC_S)_H$= Average spacing of high severity transverse cracks, m

$(TC_L)_T$ = Total length of transverse cracks (low, medium, and high severity levels), m/km

$TFAULT$ = total joint faulting cumulated per km, mm

V_a= air voids (%)

V_b = effective binder content (%)

$WetDays$ = Average annual number of wet days (greater than 0.1 in rainfall).

β_1 = Calibration factor for the unbound granular and subgrade materials

β_{f1}, β_{f2}, β_{f3} = Calibration parameters

β_{r1}, β_{r2}, β_{r3} = Calibration factors for the asphalt mixtures rut model

δ_a = Permanent deformation for the layer /sub-layer

$\delta_{curling}$ = Maximum mean monthly slab corner upward deflection PCC due to temperature curling and moisture warping

ε_0, β, ρ = Material properties

ε_0, β, ρ. ε_v= Average vertical resilient strain in the layer/sub-layer as obtained from the primary response model

ε_p = Accumulated permanent strain

ε_p^i = Total plastic strain in sub-layer i

ε_r = Resilient strain

ε_r= Resilient strain imposed in laboratory test to obtain material properties

ε_t = Tensile strain at the critical location

$\sigma_{i,j,k,...}$ = applied stress at condition i, j, k, l, m, n

$\partial(Ci)$ - change in the factor Ci

$\partial(distress)$ - change in the estimated distress associated with a change in the factor Ci

$\Delta Fault_i$= Incremental change (monthly) in mean transverse joint faulting during month i, in.

ΔP (%) - Percentage change in precipitation

ΔT (C) -Change in temperature

θsat = saturated volumetric water content

θ w = volumetric water content

1. Introduction

Problem Statement

Pavement structures represent a significant infrastructure investment that is critical to the well-being, growth and expansion of any geographic location. As such pavements are expected to be durable and resilient, and to perform satisfactorily throughout their service lives. In designing durable pavements, several factors are assessed and one such primary factor is the climate of the proposed highway location. Climate serves as an essential input in pavement design and depending on its variability can have significant impact on pavement performance. Climate data for a particular region in which a highway is located provides engineers with useful information when deciding on the combination of pavement layers and materials that can withstand the elements of the environment peculiar to that region and perform adequately in the face of adverse weather conditions. Climatic indicators also provide an expectation as to the type and extent of climate-induced deterioration that the highway is susceptible to. Pavements are designed based on typical historic climatic patterns, reflecting local climate and incorporating assumptions about a reasonable range of temperature and precipitation levels. As such changes in global and more specifically regional climate have the potential to affect pavement design and subsequent pavement performance once it is put in service.

According to the Intergovernmental Panel on Climate Change (IPCC), warming of the earth's climate system is unequivocal and most of the observed increase is due likely to an increase in anthropogenic greenhouse gas emissions (IPCC, 2007a). It is projected further that profound consequences will occur to human life as well as natural and built systems if this trend in anthropogenic climate change were to continue unabated. Such systems include civil infrastructure systems, meaning any significant future change in climate pertaining to temperature, precipitation or sea-level rise will only serve to create adverse effects for these systems. However, in all these systems there is uncertainty as studies of climate change do not know the exact amount or rate of change due to complexities in the climate system and in the modeling process (Foley, 2010). As a result, translating this uncertainty to the design and performance of civil infrastructure systems is challenging. There is a sharp divide in the way climate scientists and pavement designers analyze systems in their respective disciplines. Climate scientists describe the future in probabilistic terms with a portfolio of plausible scenarios and outcomes that are refined as new knowledge becomes available, where as pavement professionals tend to focus on "knowns" and work with the "best available" data (Transportation Research Board, 2008). Although current pavement design standards are robust and conservative in many occasions, they need to be evaluated in light of changing environmental factors recognizing uncertainty. In addition pavement engineers have to determine whether their systems are adequate to withstand climate forces that are beyond environmental factors currently considered in the design process.

This research explores how the uncertainty associated with climate change affects the design of pavements and influences their performance after construction. Presently, the majority of research conducted is based on an average change of environmental factors without

considering the uncertainty of the change. This research represents a disconnect between knowledge and actual conditions since the science of climate change is characterized by limitations as to the extent and magnitude of the change that will occur. The research therefore seeks to explore how uncertainty as applied to climate change could affect the design of pavements and influence their performance after construction. Questions like how pavement performance deteriorates differently with climate cha*n*ge and its uncertainty, what is the risk if climate change and its uncertainty are not considered in pavement design and how do pavement designers respond and incorporate this change into the pavement design process?

Background

Environmental Effects on Pavement Design

Environmental conditions have significant impact on pavement design and performance. These conditions are represented as the effects of weather and climate on the strength, durability and load bearing capacity of the pavement. In essence, they impact the structural and functional integrity of any highway. Pavements of all types are susceptible to conditions within the environment and each has its unique way of responding to a harsh environment or climate. Environmental conditions, in combination with factors such as traffic related loads, construction methods, constituent layer materials and maintenance and rehabilitation regimens are key variables in the assessment of pavement performance. The interaction between these variables and their effect on pavement performance is shown in Figure 1.1 (Haas et al, 2004).

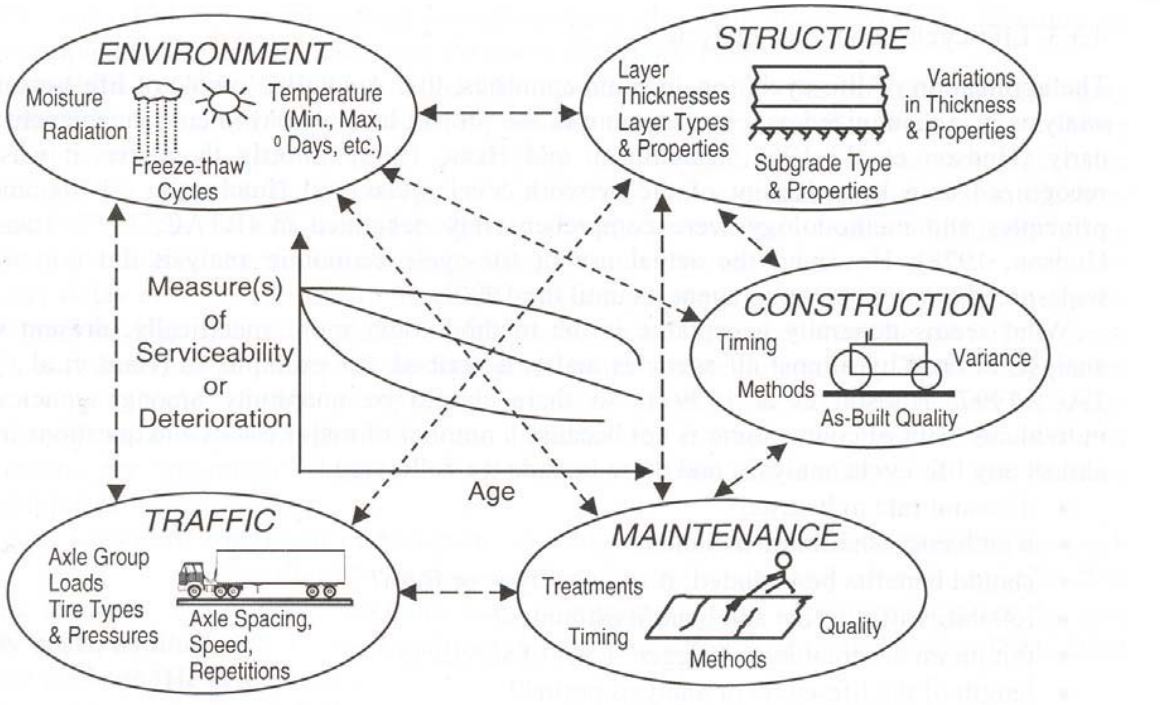

Figure 1.1 Factors affecting road performance (Haas et al, 2004)

Notable environmental factors discussed in the literature include temperature, precipitation, subsurface moisture and freeze-thaw cycles. Generally these factors lead to distress formation, which contributes to pavement deterioration and ultimate failure if left unchecked. The effect of temperature on pavements primarily results in thermal cracking and pavement distortion comprising rutting, shoving and corrugation (Baladi, 1990). Precipitation is characterized by its intensity and duration and affects the amount of water infiltrating the pavement surface and the amount of moisture within the pavement section. An example of a distress caused by sustained precipitation is pumping in rigid pavements (ERES Consultants Inc, 1987,Yoder and Witzcak, 1979). Subsurface moisture is a major contributor to the growth of ice lenses beneath pavements in wet freeze regions and directly influences the amount and rate of frost heave (Moulton, 1980). Moisture-related pavement distresses and/or failures are characterized by excessive deflection, cracking, reduced load-bearing capacity and concrete deterioration due to durability cracking (Carpenter et al, 1981). Freeze-thaw cycles are associated with accumulated ice underneath the pavement surface and lead to the formation of voids and tensile strain at the surface of the pavement (Haas et al, 2004).

To counter distress formation due to environmental factors, at the highway design stage engineers examine years of climate records for the geographic area where the highway is to be located and select pavement structures and materials that will perform well under the stated climatic conditions. Climate-induced deterioration patterns of existing highways are studied and used as input for new pavement designs. Laboratory tests are then run to determine how proposed structures will perform under worst-case environmental conditions. This level of detail is also adopted during the construction phase where contractors use methods that minimize the effect of the environment on constructed highways.

Climate Change and its Impact

Climate at the global, regional or local level is subject to change periodically due to natural and manmade factors. In all cases, changes in climate are generally unpredictable and climatologists take a period of time, on average 50 years, to establish trends for a particular jurisdiction. However, since the second half of last century climate science has observed significant extreme climatic events that tend to suggest departures from events usually observed in the past. Given that these departures are attributed to an increase in human activities that affect climate, even more profound climatic events are projected should these human activities continue unchecked (IPCC, 1990). If these projections prove to be right, both natural and built systems will be affected and this makes potential climate change a phenomenon worth investigating.

Overview of Global Climate Change

A primary ingredient that serves as a trigger for climate change is the green house gas effect. Greenhouse gases accumulate in the atmosphere from natural or manmade sources and comprise gases such as water vapor, carbon dioxide, methane, nitrous oxides and ozone. Once they accumulate in the atmosphere, these gases trap long-wave terrestrial radiation and affect its balance with short-wave solar radiation. Studies have shown that over the past century, anthropogenic sources of greenhouse gas emissions have increased substantially since pre-industrial times, which has made the impact of the greenhouse effect greater than it should be

and has led to additional warming of the Earth's surface (IPCC, 1990). Further investigation into anthropogenic induced climate change revealed that human activities such as fossil fuel use, land use change and agriculture are likely to have produced a positive radiative forcing of climate, tending to warm the earth's surface and triggering other changes in climate (IPCC, 1995). Some of these changes have presently been observed where as others have been projected to occur in future. Among those observed presently are rise in global average sea level, a decrease in the extent of ice and snow cover and for the past four decades, a temperature rise in the lowest eight kilometers of the atmosphere. For future changes, global model simulations and a variety of scenarios predict an increase in mean precipitation with more intense precipitation events, higher maximum temperatures and more hot days over nearly all land areas, higher minimum temperatures and fewer cold and frost days over nearly all land areas, increased tropical cyclone intensities and increased summer continental drying with associated risk of drought (IPCC, 2001, IPCC, 2007). In all these reports, the authors cite limitations with regards to model uncertainty, future emissions and uncertainties in climate variability. These are intended to be reduced as more data and scientific understanding of yet to be explained climate phenomena become available.

Impacts of Climate Change on Transportation

The Transportation Research Board's (TRB) Special Report 290 (Transportation Research Board, 2008) catalogs the potential impacts of climate change on transportation in the United States. From the report, climate change will have significant impacts on the way transportation professionals plan, design, construct, operate and maintain infrastructure. It further states that impacts from increases in several types of weather and climate extremes will vary by mode of transportation, geographical location and condition of the infrastructure. The report then lists five climate changes of particular importance to transportation as increases in very hot days and heat waves, increases in Arctic temperatures, rising sea levels, increases in intense precipitation events and increases in hurricane intensity. Based on these, the potentially greatest impact of climate change on North America's transportation system is identified as flooding of coastal roads, railways, transit systems and runways as a result of global sea level rise, coupled with storm surges and exacerbated in some locations by land subsidence. Table 1.1, exerted from the TRB Special Report 290 shows potential impacts to US transportation due to the five projected changes in climate listed above.

An example of a detailed study on the impact of climate change on transportation at the regional level is the United States' Gulf Coast (U.S. Climate Change Science Program, 2008). The study identified four key "climate drivers" in the Gulf region as rising temperatures, changing precipitation patterns, rising sea levels and increasing storm intensity. Findings from the study showed that the region's highways, pipelines, ports, rail lines and airports would suffer severe damage should extreme changes in regional climate occur. These would cause major and minor disruptions to the provision of transportation services within the Gulf and adversely affect the quality of life in the region.

Table 1.1: Potential Climate Changes and Illustrative Impacts on Transportation (Transportation Research Board, 2008)

Potential Climate Change	Examples of Impacts on Operations	Examples of Impacts on Infrastructure
Increases in very hot days and heat waves	Impact on lift-off load limits at high-altitude or hot-weather airports with insufficient runway lengths; limits on construction activity due to health and safety concerns	Thermal expansion of bridge expansion joints; rail-track deformities
Increases in Arctic temperatures	Longer ocean transport season and more ice-free ports in northern regions; possible availability of a northern sea route or a northwest passage	Thawing of permafrost, causing subsidence of rail beds, bridge supports, pipelines and runway foundations
Rising sea levels, combined with storm surges	More frequent interruptions to coastal and low-lying roadway travel and rail service due to storm surges; more severe storm surges requiring evacuation or changes in development plans; potential for closure of airports in coastal zones	Inundation of rail lines and airport runways in coastal areas, more frequent or severe flooding of underground tunnels and low-lying infrastructure; erosion of bridge supports; reduced clearance under bridges; changes in harbor and port facilities to cope with tides
Increases in intense precipitation events	Increases in weather-related delays and traffic disruptions; increased flooding of evacuation routes; increases in airline delays	Increases in flooding of rail lines, subterranean tunnels and runways; damages to rail bed support structures; damages to pipes
More frequent strong hurricanes (Category 4-5)	More frequent interruptions to air service; more frequent and potentially more extensive emergency evacuations; more debris on roads and rail lines, interrupting travel	Greater probability of infrastructure failures; increased threat to stability of bridge decks; adverse impacts on harbor infrastructure from waves and storm surges.

In related studies, researchers have expanded the impact of climate change on transportation beyond infrastructure and operations to include its influence on decision-making processes and consequently, policy formulation (Transportation Research Board, 2008, U.S. Climate Change

Science Program, 2008, Transportation Research Board, 2009). For example, TRB Special Report 299 *(*Transportation Research Board, 2009*)* lays out a decision framework for transportation professionals to use in addressing impacts of climate change on U.S. transportation infrastructure and involves the following steps:

1. Assess how climate changes are likely to affect various regions of the country and modes of transportation.
2. Make an inventory of transportation infrastructure essential for maintaining network performance in light of climate change projections to determine whether, when, and where the impacts could be consequential.
3. Analyze adaptation options to assess the trade-offs between making the infrastructure more robust and the costs involved. Consider monitoring as an option.
4. Determine investment priorities, taking into consideration the criticality of infrastructure components as well as opportunities for multiple benefits (e.g., congestion relief, removal of evacuation route bottlenecks).
5. Develop and implement a program of adaptation strategies for near and long term scenarios. Periodically assess the effectiveness of adaptation strategies and repeat Steps 1 through 5.

Other studies have looked into how transportation planning vis-à-vis land use planning could minimize the effect of climate change and how improvements in the US fuel economy and introduction of alternative fuels could affect total transportation greenhouse gas emissions. What serves as a recurrent theme in a majority of these studies is the vulnerability of the nation's transportation sector with increasing risk of climate change.

Impacts of Climate Change on Pavements

All pavement types are susceptible to deterioration given a potential change in climate occurs (Meyer et al, 2010, Meyer and Wiegel, 2011). From distresses at the surface to collapse of constituent layers, pavements are likely to undergo drastic deformation should they experience extremes in weather or climate. Under normal climate change conditions, rigid pavements suffer from distresses like scaling, D-cracking, pumping, faulting, curling, corner cracking and punch outs. Flexible pavements under the same conditions are affected by bleeding, weathering, bumps, rutting, depressions, potholes, longitudinal and transverse cracking (Baladi, 1990). Some of these distresses are formed in combination with traffic loads and or material defects. If extreme climate changes were to occur, these distresses will clearly be exacerbated and new distresses may be formed. Listed are some of the potential problems pavements will face under extreme climate scenarios (Transportation Research Board, 2008).

- Long periods of extreme heat may lead to thermal expansion of paved surfaces and may compromise flexible pavement integrity e.g. soften asphalt, increase rutting from traffic and cause migration of liquid asphalt.
- Increases in Arctic temperatures could cause permafrost to thaw and lead to

subsidence of roads and shorter seasons for ice roads, whose frozen beds trucks take advantage of to carry heavier loads during winter.

- Rising sea levels combined with storm surges could inundate roads or erode road bases where as increases in intense precipitation events would cause roadways to flood and lead to increases in road washouts.

Specific studies undertaken for pavements in Southern Canada (Mills et al, 2007) analyzed the effects of potential climate change on pavement infrastructure. Two case studies were analyzed based on midcentury climate predicted by selected global climate models. The first study examined deterioration-relevant climate indicators and showed that low temperature cracking would be less problematic, pavement structures would freeze later and thaw earlier with shorter freeze season lengths and potential rutting could occur for in-service pavements experiencing high temperatures. The second study used the Mechanical Empirical Pavement Design Guide (Applied Research Associates Inc, 2004a) to assess the impact of climate change, traffic loads and the structural and material properties of the pavement on incremental and terminal pavement deterioration and performance. Results showed rutting and longitudinal and alligator cracking would be exacerbated by climate change.

In studies undertaken for the Gulf Coast of the United States (U.S. Climate Change Science Program, 2008), researchers observed that key potential impacts on the highway network would be largely due to sea level rise and storm surge. Temperature and intense precipitation would also have some impacts but would be lower compared to those resulting from sea level rise. Extreme heat is expected to increase highway maintenance and construction costs as some pavement materials will degrade faster due to higher temperatures. Intense precipitation events will lead to increase in accidents, washouts, flooding, landslides, and cause undue stress for stormwater management infrastructure. Sea level rise and storm surge would affect highways in low-lying areas of the region and would cause inundation. Prolonged inundation can lead to long-term weakening of pavements.

As stated above, both general and specific studies describing the impacts of climate change indicate that pavements will be adversely affected by this phenomenon. It is imperative therefore for all stakeholders to research ways to preserve pavements and minimize these impacts so as to reduce losses that would be incurred in the event of unexpected changes in climate.

Project Objectives

Given anticipated climate changes and the inherent uncertainty associated with such changes, a pavement could be subjected to very different climatic conditions over its design life. The objective of this research is to explore the impacts of potential climate change and its uncertainty on pavement performance deterioration and therefore pavement design. There are three fundamental sources of uncertainty to be addressed:

- Greenhouse and other gas emissions: The IPCC Special Report Emission Scenarios (SRES) project (IPCC, 2011) a very wide range of emissions of key greenhouse gases (GHG);

- Climate sensitivity: How much global mean temperature (GMT) will warm for a CO_2 doubling has traditionally been thought to be between 1.5 to 4.5^0C;
- Patterns of regional change: This third source of uncertainty concerns relative regional changes in temperature and precipitation. Both global temperatures and precipitation will rise, but some areas will warm more than others and some areas receive increased precipitation while others face decreases.

To accomplish this main objective, the following sub-objectives are explored:

- Review of the potential impact of climate change on pavement performance
- Exploration of climate change scenarios and uncertainties using the MAGICC/SCENGEN tool (Wigley, 2008)
- Simulation of pavement performance deterioration over time for a selection of sites with various climate change levels and pavement structures
- Analysis to assess the significance of climate change pavement performance
- Development of guidance on when and how to integrate climate change into pavement design as an adaption strategy.

Overview of the Methodology

The research focuses on how potential climate change in the North Eastern part of the United States could affect road pavements at different locations within the region. Three locations were chosen, one in each of the following states: Delaware, New Jersey and Connecticut. The pavement types selected were jointed plain concrete pavement (JPCP), continuously reinforced concrete pavement (CRCP), a composite pavement and an asphalt concrete pavement.

Using data from the Long-Term Pavement Performance (LTPP) database (FHWA, 2010) and the Mechanistic-Empirical Pavement Design Guide (MEPDG) (TRB, 2010) as a design tool, pavements were designed with similar in-situ structures to simulate how they would perform overtime should changes in climate occur. In determining climatic factors to be considered in the research, a review of past research on climatic impacts on pavement performance was done and narrowed down to climatic factors of relevance to pavements within each of the selected locations. Of key interest is how uncertainty in projecting future changes in these factors can be characterized.

To explore uncertainty, climate models and climate change scenarios developed based on research by the Intergovernmental Panel and United Kingdom Climate Impacts Programme (UKCIP) (Department for Environment, Food and Rural Affairs, 2010) are primarily used. Data on climatic factors were obtained from the National Climatic Data Center (NCDC) (National Oceanographic and Atmospheric Administration, 2010) and served as input for different climate change scenarios. Thus climate models were developed and projections of future climate were done along the guidelines and within the framework set by the IPCC and UKCIP. A tool, “Model for the Assessment of Greenhouse-gas Induced Climate Change: A regional Climate Scenario Generator” (MAGICC/SCENGEN), was used in effecting climate change scenarios (Wigley, 2008).

By combining pavement structures, current and projected climatic agents and different traffic levels in experimental designs, the performance of pavements over their design lives were analyzed using MEPDG. This involved comparing the performance deteriorations of two parallel designs, one which considers the impacts of climate change with its different scenarios and one which does not consider climate change. This is achieved by using a set of performance indicators for each pavement type.

Of particular interest is how pavement distresses evolve under uncertainty in the different emission and climate change models. To tailor distresses to meet local pavement conditions, sensitivity analysis is conducted to locally calibrate distresses. Subsequent analysis in the research is based on results obtained from the parallel comparisons between potential climate change and no changes to climate. The methodology is illustrated in the flowchart in Figure 1.2.

Report Outline

To support the overarching goal of investigating the potential impacts of climate change on road pavements and its underlying uncertainty, chapters within the report are arranged so readers can appreciate the extent to which this phenomenon can affect pavement design and ultimately performance. This chapter provides an overview of the problem, including a review of past studies, study objectives and an overview of the methodology.

Chapter 2 investigates how environmental effects pertaining to climate are captured in MEPDG. It specifically looks at how the various climatic factors are incorporated in the design process and how these affect the overall performance of each pavement type. The science of climate change is presented in Chapter 3 and the knowledge established so far by leading research institutions is tabulated. MAGICC/SCENGEN is also introduced in this chapter. Additionally, the process by which it can be used to explore uncertainties related to potential climate change is demonstrated. Chapter 4 looks at how climatic factors and their related uncertainty, as discussed in Chapter 3, are employed in the MEPDG software. The chapter also shows how pavement performance is achieved in MEPDG using distress prediction models and how these can be calibrated to suit local conditions in which the different pavement types can be found. A case study is used in Chapter 5 to illustrate the process by which the various stages of the research are put together to determine in depth the implications of climate change on pavement design. Conclusions and recommendations are presented in Chapter 6.

Appendices document model inputs and comprehensive results.

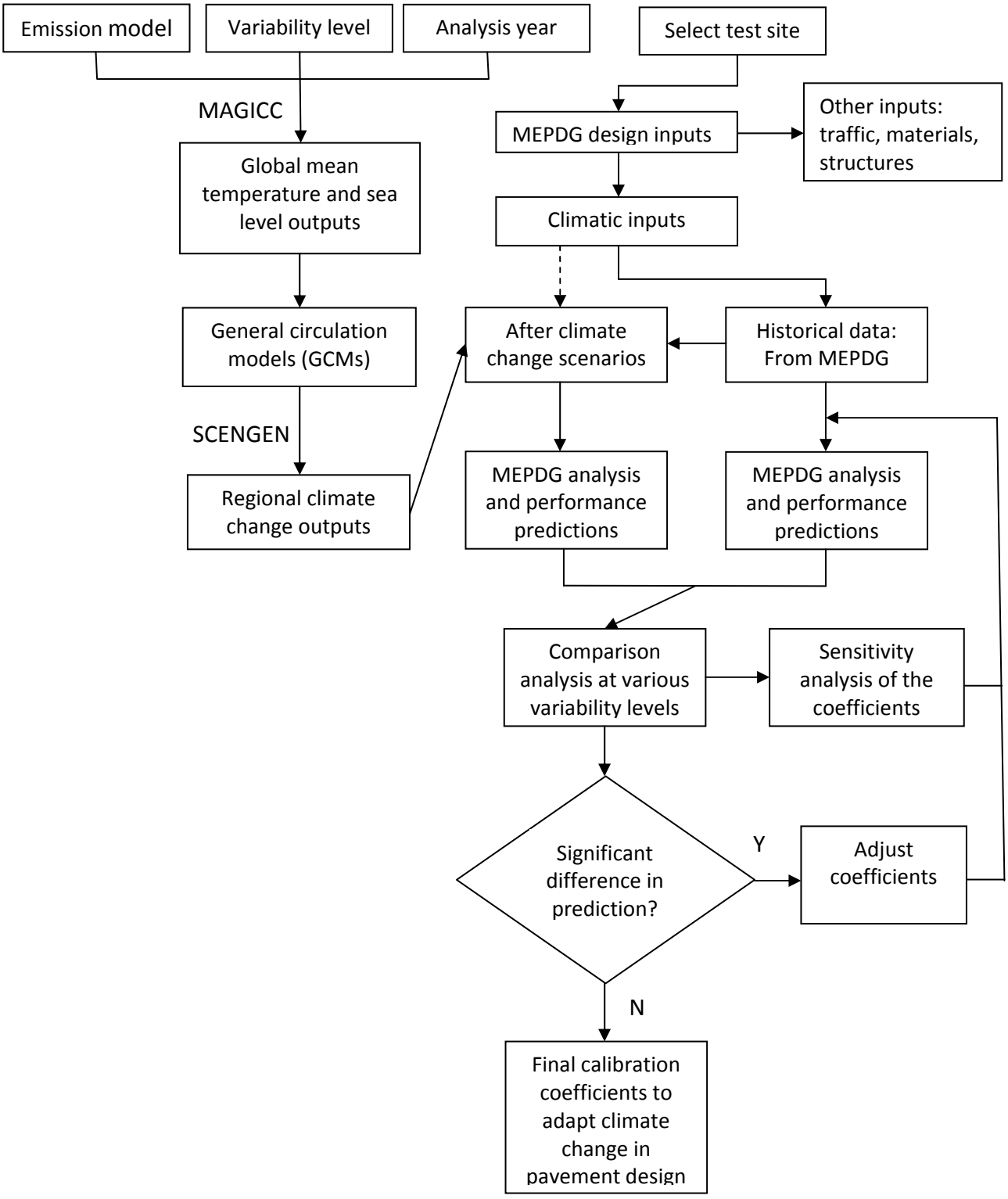

Figure 1.2 Flowchart representing the methodology

2. Environmental Effects in the Mechanistic Empirical Pavement Design Guide (MEPDG)

Introduction

A pavement must be able to function and perform effectively within the environment in which it is built. The environment varies across the globe at any one time and it can also vary greatly across time at any one place. Environmental variations can have a significant impact on pavement materials and the underlying subgrade, which in turn can drastically affect pavement performance. Certainly every environmental constituent (e.g., solar flux, heat, wind, humidity, etc.) can have an incremental effect on pavement. However, there are several constituents that exert an overriding influence. These variables are temperature, precipitation, and freeze/thaw cycles. Each variable is briefly described in terms of the damage caused.

Temperature

Temperature variations can cause severe pavement damage due to expansion, contraction and (in the case of rigid pavements) slab curling. Small amounts of expansion and contraction are typically accommodated without excessive damage, however extreme temperature variations can lead to catastrophic failures. Flexible and rigid pavements can suffer large transverse cracks as a result of excessive contraction in cold weather.

The effect of temperature on asphalt pavements is different from that of concrete pavements. Temperature affects the resilient modulus of asphalt layers, while it induces curling of concrete slab. In rigid pavements, due to differences in temperature between the top and bottom of slab, temperature stresses or frictional stresses are developed. While in flexible pavement, dynamic modulus of asphaltic concrete varies with temperature. Rigid pavements are also prone to slab buckling as a result of excessive expansion in hot weather and flexible pavement prone to rutting due to channelized traffic and high temperature.

Precipitation

The quantity and intensity of precipitation, in the form of rain and snow, affects the quantity of surface water infiltrating into the subgrade and the depth of ground water table. Poor drainage may reduce shear strength, or cause pumping or loss of support. Moisture (in the form of accumulated water or rainfall) affects pavements in several phases of the pavement life cycle:

- *Design*. Certain types of soils can be highly expansive when wet. Structural design must account for this expansiveness.
- *Construction*.
    - Subgrade should be compacted at optimal moisture content. Excessive rainfall can raise subgrade moisture content well beyond this value and make it virtually impossible to compact.
    - Hot mix asphalt (HMA) and Portland cement concrete (PCC) should not

be placed in wet conditions.

- *Driving Conditions*. Rainfall reduces skid resistance and can cause hydroplaning in severely rutted areas or other areas where water ponds on the road surface.

Freeze/Thaw

Frost action is a critical pavement structural design concern in parts of the country that regularly experience ground freezing. There are two basic types of frost action with which to contend:

- **Frost heave**: An upward movement of the subgrade resulting from the expansion of accumulated soil moisture as it freezes. Frost heaving of soil is caused by crystallization of ice within the larger soil voids and usually a subsequent extension to form continuous ice lenses, layers, veins, or other ice masses. An ice lens grows through capillary rise and thickens in the direction of heat transfer until the water supply is depleted or until freezing conditions at the interface no longer support further crystallization. As the ice lens grows, the overlying soil and pavement will "heave" up, potentially resulting in a cracked, rough pavement. This problem occurs primarily in soils containing fine particles (often termed "frost susceptible" soils), while clean sands and gravels (small amounts of fine particles) are non-frost susceptible (NFS). The three elements necessary for ice lenses and thus frost heave are:
  - Frost susceptible soil (significant amount of fines).
  - Subfreezing temperatures (freezing temperatures must penetrate the soil and, in general, the thickness of an ice lens will be thicker with slower rates of freezing).
  - Water (must be present, either from the groundwater table, infiltration, an aquifer, or held within the voids of fine-grained soil).
  - Frost heave causes differential settlements and pavement roughness.
- **Thaw weakening**: A weakened subgrade condition resulting from soil saturation as ice within the soil melts. Thawing is essentially the melting of ice contained within the subgrade. As the ice melts and turns to liquid it cannot drain out of the soil fast enough and thus the subgrade becomes substantially weaker (less stiff) and tends to lose bearing capacity. Therefore, loading that would not normally damage a given pavement may be quite detrimental during thaw periods (e.g., spring thaw).

Climatic Inputs in MEPDG

Changing temperature and moisture profiles in the pavement structure and subgrade over the design life of a pavement are considered in MEPDG through the Enhanced Integrated Climatic Model (EICM). The EICM is a one-dimensional coupled heat and moisture flow program that

simulates changes in the behavior and characteristics of pavement and subgrade materials in conjunction with climatic conditions over several years of operation. It is fully linked to the MEPDG software and internally performs all the necessary computations. The user inputs to the EICM are entered through interfaces provided as part of the MEPDG software. The EICM processes these inputs and feeds its outputs to the three major components of the MEPDG framework — materials, structural responses, and performance prediction. The following information throughout the entire pavement/subgrade profile are predicted: temperature, resilient modulus adjustment factors, pore water pressure, water content, frost and thaw depths, frost heave, and drainage performance (Applied Research Associates Inc, 2004a).

The inputs required by the climatic model fall under the following broad categories:

- General information
- Weather-related information
- Ground water related information
- Drainage and surface properties
- Pavement structure and materials

The use of the new Thornthwaite Moisture Index (TMI) model in the MEPDG software makes the entry of drainage path and infiltration unnecessary. The pavement structure and materials related data are out of the scope and excluded from this study.

General Information

The general information, such as pavement structure, construction dates, traffic opening time, is required to initialize the moisture model in the EICM. Under this category, the following inputs specifically relate to the climatic model:

- Base/Subgrade Construction Completion Month and Year.
- Existing Pavement Construction Month and Year.
- Pavement Construction Month and Year
- Traffic Opening Month and Year

Weather-Related Data Input

To accomplish the climatic analysis required for incremental damage accumulation, MEPDG requires five weather-related parameters on an hourly basis over the entire design life for the design project (*21*):

- Hourly air temperature
- Hourly precipitation
- Hourly wind speed
- Hourly percentage sunshine (used to define cloud cover)

- Hourly relative humidity

In MEPDG, the weather-related information is primarily obtained from weather stations located near the project site. The MEPDG software provides over 800 weather stations containing hourly data across the United States from the National Climatic Data Center (NCDC) database. All the data sets for each station are saved in a file with HCD extension and can be downloaded from the website for NCHRP 1-37A project (http://www.trb.org/mepdg) (TRB, 2011). In the MEPDG report, it states that "several of the major weather stations have approximately 60 to 66 months of climatic data at each time step (1 hour) needed by the EICM. Other weather stations could have less than this amount of data, however, the Design Guide software requires at least 24 months of actual weather station data for computational purposes" (Applied Research Associates Inc, 2004a). The climatic database can be tapped into by simply specifying the latitude, longitude, and elevation of the project site in MEPDG software. Once the global positioning system (GPS) coordinates and elevation are specified for the design project site, the MEPDG software highlights the six closest weather stations to the site from which the user may select any number of stations to generate a virtual project weather station. After selecting the climate stations and inputting the water table depth for the design, click "generate" button and all the climatic data sets required are saved in a file with an "icm" extension through the EICM numerical engine. The climate generating screen window is shown in Figure 2.1.

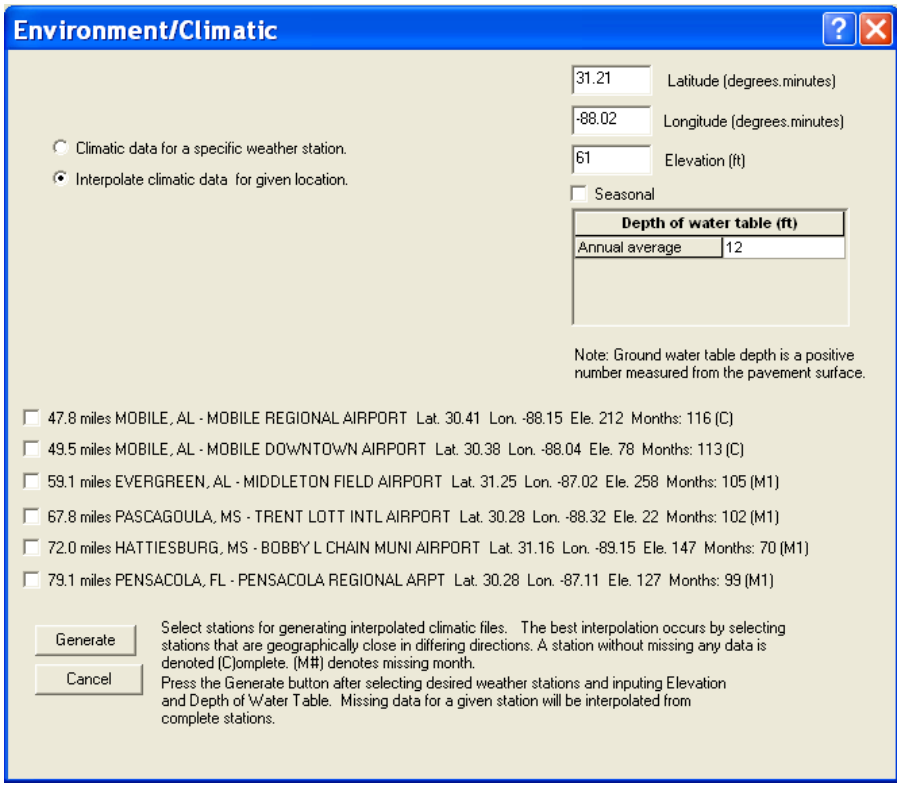

Figure 2.1 Climatic Generating Window in MEPDG

In the climate data generation process, there are three types of files that are used by the EICM numerical engine in the MEPDG software: “icm” file, “hcd” file, and “station.dat” file As shown above, “icm” files are generated from “hcd” files and “station.dat” file. Each file has its unique file format, which is documented in Appendix A.

Groundwater Table Depth Input

The groundwater table depth, intended to be either the best estimate of the annual average depth or the seasonal average depth, is another important parameter needed to be input to the MEPDG software. At input Level 1, it could be determined from profile characterization borings prior to design. At input Level 3, an estimate of the annual average value or the seasonal averages can be provided, such as using the data produced by the United States Geological Survey (USGS).

Major Outputs of the EICM

The output of the EICM can be described on two fronts—internal and external. Both forms of outputs of the EICM are transparent to the user with the difference being that the internal outputs are not passed on to other components of the Design Guide software (e.g., structural response calculation module or the performance prediction module), while the external outputs are. However, the user has full control over the inputs that drive both these outputs (e.g., water table depths, climatic information for the project site).

Regarding the internal output of the EICM, the computational engine of the EICM determines values of volumetric water content, θ_w, and temperature at each node over time based on above mentioned climatic input. The values of θ_w are divided by the saturated volumetric water contents, θ_{sat}, to get values of degree of saturation, S. With no oscillations in the input groundwater table and no cracks in the AC layer, values of S are essentially values at a state of equilibrium, S_{equil}, unless freezing or thaw recovery is in progress. Values of S_{equil}, together with values of degree of saturation at optimum conditions, S_{opt}, are then used to compute the unbound layer modulus adjustment factor for unfrozen conditions, F_U, at each node. The output temperatures are used to signal freezing at a node and an adjustment factor for frozen condition, F_F, is computed at each freezing node. Thawing normally follows freezing, as signaled by the rise in temperature above the freezing point. During the recovery period, material type/properties are used to compute the recovery ratio, RR, at recovering nodes. These RR values, together with reduction factors due to thawing, RF, are used to compute and adjustment factor for recovering conditions, F_R, at each recovering node.

The external EICM outputs feed directly into the materials characterization, structural response computation, and performance prediction modules of the MEPDG software, including the following:

- Unbound material M_R adjustment factor as function of position and time—values of composite environmental effects adjustment factor, F_{env}, are computed for every sublayer from the values of F_F, F_R, or F_U at each node. The sublayering is internally defined by the EICM and is a function of the frost penetration depth,

among other factors. These F_{env} factors are sent forward to structural analysis modules of the MEPDG software.

- Temperatures at the surface and at the midpoint of each asphalt bound sublayer—these values are subjected to statistical characterization for every analysis period. The mean, standard deviation, and quintile points are sent forward for use in the fatigue and permanent deformation prediction models.
- Values of hourly temperature at the surface and at a set depth increment (every inch) within the bound layers for use in the thermal cracking model.
- Volumetric moisture content—an average value for each sublayer is reported for use in the permanent deformation model for the unbound materials.
- Temperature profile in the PCC—hourly values are generated for use in the cracking and faulting models for JPCP and CRCP pavements.
- Number of freeze thaw cycles and freezing index are computed for use in JPCP performance prediction.
- Relative humidity values for each month are generated for use in the JPCP and CRCP modeling of moisture gradients through the slab.

3. Climate Change and Variability

Introduction

The world's leading climate scientists have reached consensus that human activity in the form of greenhouse gas (GHG) emissions is warming the planet in ways that will have profound and unsettling impacts on natural resources, energy use, ecosystems, economic activity, and potentially quality of life. Many studies have already examined the potential impacts of climate change on broad sectors of the economy, such as agriculture and forestry, but few have studied the impacts on transportation (Transportation Research Board, 2008, Walther, 2002, Kheshgil et al, 2000).

Transportation infrastructure systems are designed for typical weather patterns, taking into consideration local climate and making projections based on its history within the locality. Should any profound future climate change occur, transportation will be primarily affected through increases in several types of weather and climate extremes, such as very hot days; intense precipitation events; intense hurricanes; drought; and rising sea levels, coupled with storm surges and land subsidence (Transportation Research Board, 2008). The impacts will vary by transportation mode and region of the country, but they will be widespread and costly in both human and economic terms and will require significant changes in every facet of the provision of transportation infrastructure.

IPCC Special Report Emissions Scenarios

Green house gas emissions from anthropogenic sources have been associated with changing global climatic trends and have been increasing steadily over the past few decades (*10*). Estimates of future GHG emission levels begin with identifying a range of possible future scenarios that relate to such features as population and economic growth, and type of power generation. The scenarios used in this research were adopted from the IPCC Special Report on Emissions Scenarios (SRES) (IPCC, 2011). There are six SRES scenarios being widely used based on four families:

- The A1 scenario family describes a future world of very rapid economic growth, global population that peaks in mid-century and declines thereafter, and the rapid introduction of new and more efficient technologies. The A1 scenario family develops into three groups that describe alternative directions of technological change in the energy system: fossil intensive (A1FI), non-fossil energy sources (A1T), or a balance across all sources (A1B).
- The A2 scenario family describes a very heterogeneous world. The underlying theme is self-reliance and preservation of local identities. Economic development is primarily regionally oriented and per capita economic growth and technological change are more fragmented and slower than in other scenarios.
- The B1 scenario family describes a convergent world with the same global population that peaks in midcentury and declines thereafter, as in the A1 storyline,

but with rapid changes in economic structures toward a service and information economy, with reductions in material intensity, and the introduction of clean and resource-efficient technologies. The emphasis is on global solutions to economic, social, and environmental sustainability.

- The B2 scenario family describes a world in which the emphasis is on local solutions to economic, social, and environmental sustainability. It is a world with continuously increasing global population at a rate lower than A2, intermediate levels of economic development, and less rapid and more diverse technological change than in the B1 and A1 scenarios.

Climate Change Variability

There is broad consensus that anthropogenic warming is occurring. However, the obvious limitations to performing scientific experiments on the global climate system and its extremely complicated nature render our understanding incomplete. The 2007 IPCC report on the physical science basis of climate change includes many models which show the wide range of temperature increase predictions (IPCC, 2007b). Figure 3.1 gives a sense of the uncertainties involved in climate change modeling for the 10 models (Andronova, 2001; Annan, 2005; Forest, 2002; Forest, 2006; Forster, 2006; Frame, 2005; Gregory, 2002; Hegerl, 2006; Knutti, 2002;Schneider, 2006 as cited in IPCC, 2007b). Each model attempts to take what we know about the climate system and determine the probability that the climate will stabilize with a global mean temperature increase from 0-10°C. While there is broad agreement across the models that temperature increases will occur, the distributions vary considerably.

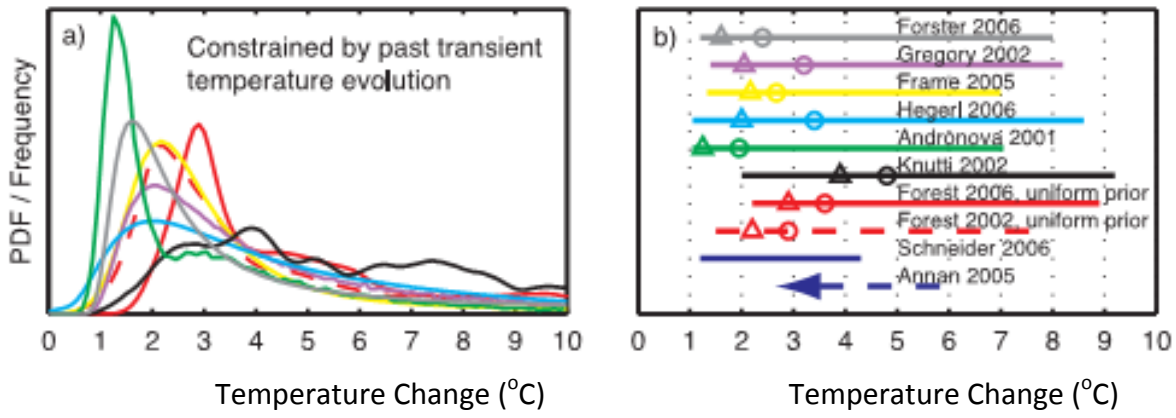

a) Probability of equilibrium temperature change (climate sensitivity) in different climate models.

b) Confidence interval (5%-95%) for temperature change Circles represent the median temperature and triangles the maximum probability.

Figure 3.1 Probabilities of Equilibrium Temperature Increases in Sample of Different Climate Models (as cited in IPCC, 2007b)

As a result, there are a myriad of uncertainties individuals confront when making decisions that affect, or are affected by climate change. In general, there are three fundamental sources of uncertainty to be addressed:

1. Greenhouse and other gas emissions: Various emission models have been developed worldwide but predictions vary significantly. For example, the IPCC SRES models project a very wide range of emissions of key greenhouse gases (GHG);
2. Climate sensitivity: Climate sensitivity is a measure of how responsive the temperature of the climate system is to change in the radiative forcing. It is usually expressed as the temperature change associated with a doubling of the concentration of CO^2 in the earth's atmosphere. How much global mean temperature (GMT) will warm for a CO^2 doubling has not been fully understood;
3. Pattern of regional change: This third source of uncertainty concerns relative regional changes. Some areas will warm more than others and some areas will receive increased precipitation while others face decreases in precipitation.

Quantifying uncertainty is challenging. There are aspects of climate change about which we are almost certain (the physical chemistry), and areas in which uncertainty is significant (e.g. the effect of clouds, the ocean, the response of biological processes, climate change mitigation). As a result, various approaches may be adopted to characterize the uncertainty. The simplest but widely used approach is to assume the climatic parameters are subject to normal distributions. For example, for a temperature record that is stationary, the distribution is assumed to be normal (the "bell curve") and characterized by two statistical parameters, the mean and variance. If the climate change undergoes a warming without any change in the variance then the whole bell curve moves sideways. The consequence of a shift to a higher mean is that there are fewer cold days and more hot days, and a higher probability that previous record high temperatures will be exceeded. If however, there is an increase in variance but no change in the mean the bell curve becomes fatter and lower. The consequence is that there are cooler and hotter days and a high probability that previous records for both the coldest and hottest days will be broken. If both the mean and the variance increase then the bell curve shifts sideways and becomes lower and fatter. The effect is for relatively little change in the frequency of cold weather or the occurrence of extreme low temperatures, but a big increase in hot weather and previous record high temperatures being exceeded far more often. The three combinations of the mean changing over time and the variance around the mean are shown in Figure 3.2.

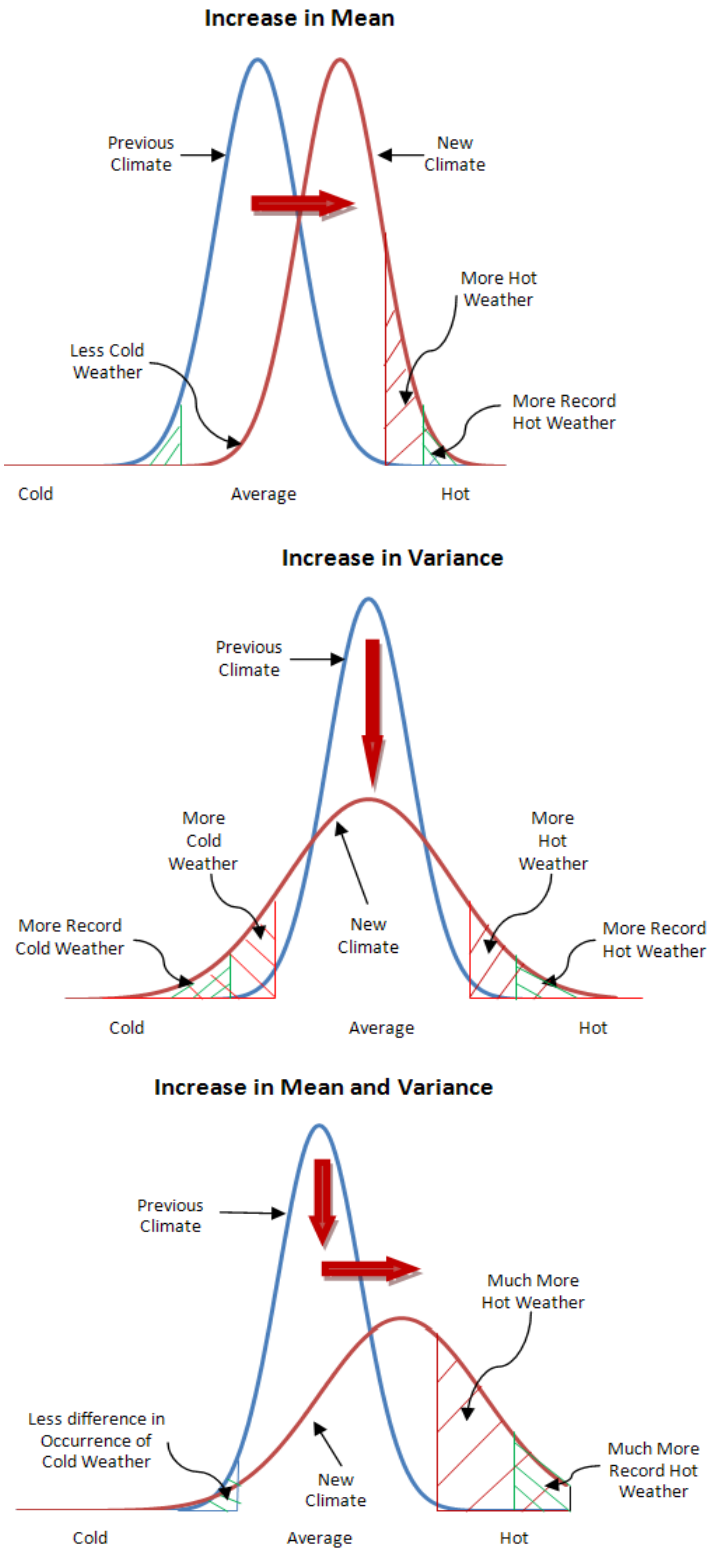

Figure 3.2 Climate Change Uncertainties

MAGICC/SCENGEN Software

MAGICC and SCENGEN are a suite of models that determine the regional details of future climatic change for specified emissions scenarios, together with estimates of their uncertainties (Wigley, 2008). It is a coupled gas-cycle/climate model (MAGICC; **M**odel for the **A**ssessment of **G**reenhouse-gas **I**nduced **C**limate **C**hange) that drives a spatial climate-change **SCEN**ario **GEN**erator (SCENGEN). A flow chart describing how MAGICC/SCENGEN is configured as shown in Figure 3.3.

MAGICC has been one of the primary models used by IPCC since 1990 to produce projections of future global-mean temperature and sea level rise. The climate model in MAGICC is an upwelling-diffusion, energy-balance model that produces global and hemispheric-mean temperature output together with results for oceanic thermal expansion. The MAGICC climate model is coupled interactively with a range of gas-cycle models that give projections for the concentrations of the key greenhouse gases. Climate feedbacks on the carbon cycle are therefore accounted for. The years 1990 and 2100 are the default start and end output years used by the software, but they can be changed by the user. The main aims of MAGICC are:

- To compare the global-mean temperature and sea level implications of two different emissions scenarios. For convenience, MAGICC refers to these as a "Reference" scenario and a "Policy" scenario. However, any two scenarios may be compared.
- To determine the sensitivity of the temperature and sea level results for any chosen emissions scenario to changes in and uncertainties in model parameters, such as the climate sensitivity. Basic uncertainty ranges and a "best-estimate" result are calculated by default. In addition, the user may select a set of model parameters that differs from the best-estimate set to examine uncertainties associated with model parameter uncertainties in more detail.

Global-mean temperatures from MAGICC are used to drive SCENGEN. SCENGEN uses a version of the pattern scaling method described in Santer et al. (1990) to produce spatial patterns of change from a database of atmosphere/ocean global climate model (AOGCM). The pattern scaling method is based on the separation of the global-mean and spatial-pattern components of future climate change, and the further separation of the latter into greenhouse-gas and aerosol components. Spatial patterns in the database are —normalized and expressed as changes per 1^0C change in global-mean temperature. These normalized greenhouse-gas and aerosol components are appropriately weighted, added, and scaled up to the global-mean temperature defined by MAGICC for a given year, emissions scenario and set of climate model parameters. For the SCENGEN scaling component, the user can select from a number of different AOGCMs for the patterns of greenhouse-gas-induced climate.

Projections of absolute (rather than relative) future climate conditions for any future date covered by the input emissions data can be obtained as well. To produce these projections, SCENGEN adds the climate change information to observed baseline climate data (1980-99 means). These results are given as array files on a standard 2.5x2.5 degree latitude/longitude grid and displayed as maps.

User-choices in the production of such future climate or climate change scenarios are: a future date; a climate variable (temperature, precipitation or Mean Sea Level Pressure (MSLP)); either a specific month or season or the annual mean; and one or more of the AOGCMs in SCENGEN's library of model results. Climate change fields are constructed using a pattern scaling method. Beyond simple climate change scenario construction (i.e., changes in the mean climate state), SCENGEN produces spatial pattern results for: changes in inter-annual variability; two different forms of signal-to-noise ratio (to assess the significance of changes); probabilistic output (the default being the probability of an increase in the chosen climate variable); and a wide range of model validation statistics for individual models or combinations of models to assist in the selection of models for scenario development.

As can be seen, the tool MAGICC/SCENGEN can be used to address the three uncertainties and allows users to explore:

- GHG emission scenarios, thus addressing uncertainty #1;
- Climate model uncertainties, including climate sensitivity, aerosol feedbacks, carbon cycle, thermohaline circulation, and ice melt, thus addressing uncertainty #2;
- SCENGEN uses the regional pattern of relative changes across 20 General Circulation Models (GCMs) to average regional GCMs outputs because it controls for differences in climate sensitivity across models. As a result, the third variability is addressed.

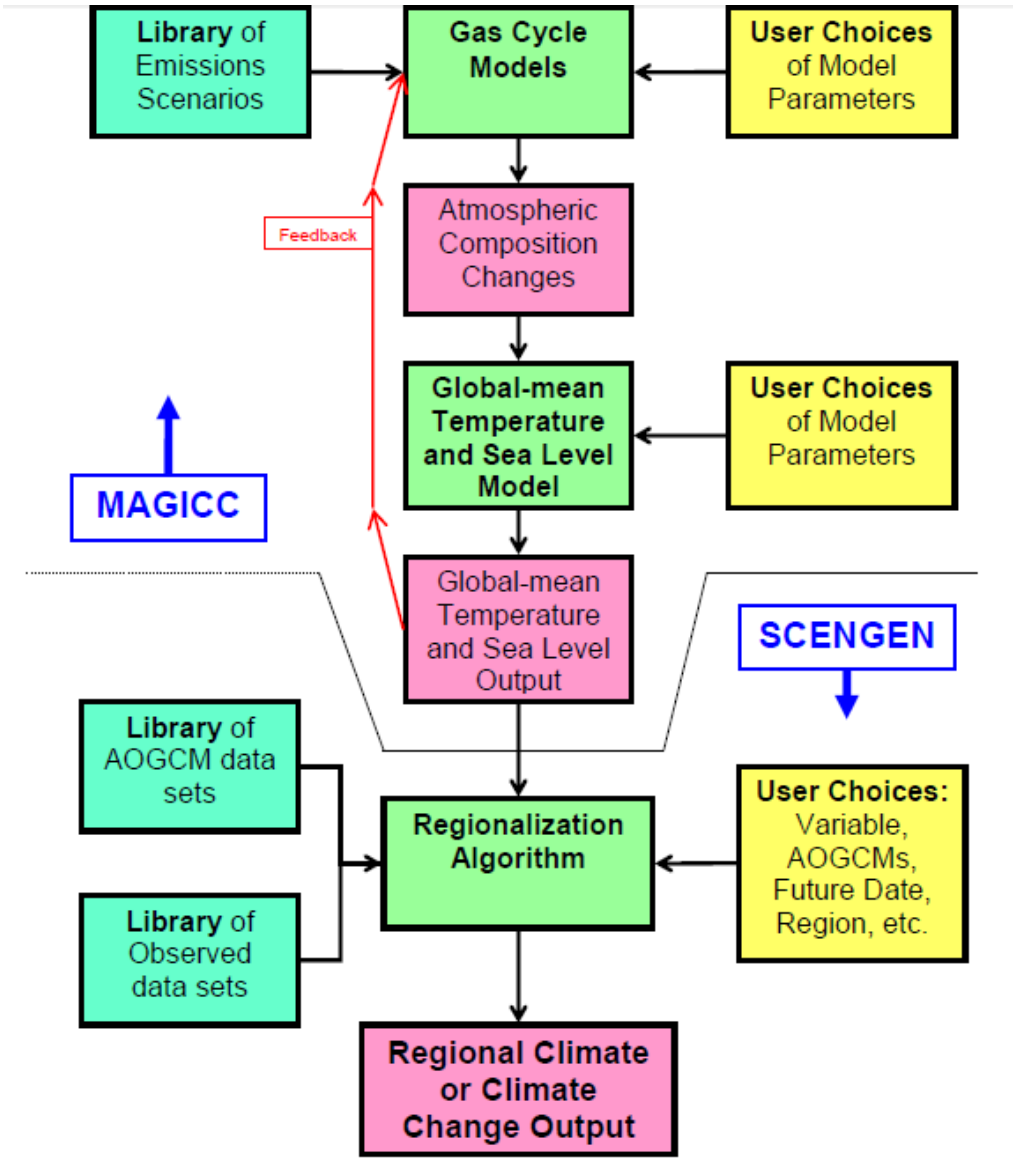

Figure 3.3 Structure of the MAGICC/SCENGEN Software (Wigley, 2008)

4. Incorporating Climate Change into the M-E Pavement Design

Introduction

MEPDG is largely based on mechanistic engineering principles that provide a fundamental basis for the structural design of pavement structures. The design procedures were calibrated using historical climate data (without considering the potential of climate change), design inputs and performance data largely from the national LTPP database. Whatever bias included in this calibration data is naturally incorporated into the distress prediction models. Because of the differences between national conditions and local conditions such as climate, material properties, traffic patterns, construction and management techniques, the national calibration may not be entirely adequate for specific regions of the country thus a more local or regional calibration and validation are needed for local conditions. In addition, the distress mechanisms are far more complex than can be practically modeled; therefore, the use of empirical factors and calibration is necessary to obtain realistic performance predictions.

Pavement Performance Prediction in MEPDG

Pavement performance is primarily concerned with functional and structural performance. The structural performance of a pavement relates to its physical condition (such as fatigue cracking and rutting for flexible pavements, and joint faulting and slab cracking for rigid jointed pavements). Several of these key distress types can be predicted directly using mechanistic concepts and are considered in the design process.

Ride quality is the dominant characteristic of functional performance, as measured by the International Roughness Index (IRI). In MEPDG, IRI is estimated incrementally over the entire design period by incorporating distresses such as cracking, rutting, faulting, and punchouts as major factors influencing the loss of smoothness of a pavement. The general hypothesis of smoothness models is that the various distresses resulting in significant changes in smoothness are represented by separate components within the MEPDG models, as shown in Equation 4.1 (Applied Research Associates Inc, 2004b).

$$S(t)=S_0+(a_1S_{D(t)1}+\cdots+a_nS_{D(t)n})+b_jS_j+c_jM_j \qquad \text{(Eqn.4.1)}$$

Where $S(t)$ denotes pavement smoothness at a specific time t; S_0 initial smoothness immediately after construction; $S_{D(t)}$ (i=1 to n) change of smoothness due to the ith distress at a given time t in the analysis period; $a(i=1, \ldots, n)$, b_j, c_j are regression coefficients; S_j change in smoothness due to site factors (subgrade and age); M_j change in smoothness due to maintenance activities.

The following section examines the different performance models as used in this research in detail.

Flexible Pavement Performance Models

Performance models for flexible pavements were used in analyzing the following distresses: rutting, bottom-up cracking and roughness. In MEPDG, rutting is defined as a load-associated distress in flexible pavement systems normally appearing as longitudinal depressions in wheel paths accompanied by small upheavals to the sides (Applied Research Associates Inc, 2004c). The width and depth of a rutting profile is highly dependent on the pavement structure (layer thickness and quality), traffic matrix and quantity and the environmental conditions at the design site. Rutting results from densification and permanent deformation under loads combined with displacement of pavement materials (Mills et al, 2007). Pavements afflicted by rutting pose as safety concerns by modifying drainage characteristics of the roadway, thereby contributing to vehicle aquaplaning and reducing skid resistance. Rutting also reduces riding quality of the roadway.

Rutting can occur in all layers of a pavement system and designers model total permanent deformation as a product of cumulative ruts in all layers. For MEPDG, a predictive rutting system was developed to evaluate permanent deformation in all rut susceptible layers within the pavement structure. Layers generally analyzed for rutting are the asphaltic layer and all unbound material layers. Considering the different layers, the field-calibrated rutting model used in the Design Guide for asphaltic mixtures is given as:

$$\frac{\varepsilon_p}{\varepsilon_r} = \beta_{r1} 10^{-3.15552} T^{1.734 \times \beta_{r2}} N^{0.39937 \times \beta_{r3}} \quad \text{(Eqn. 4.2)}$$

Where β_{r1}, β_{r2}, β_{r3} = Calibration factors for the asphalt mixtures rut model. ε_p = Accumulated permanent strain. ε_r = Resilient strain. T = Mix temperature (deg F). N = Number of load repetitions.

The basic relationship used for characterizing permanent deformation in unbound layers as stated in the Design Guide is given as:

$$\delta_a(N) = \beta_1 \left(\frac{\varepsilon_0}{\varepsilon_r}\right) e^{-\left[\frac{\rho}{N}\right]^{\beta}} \varepsilon_v h \quad \text{(Eqn. 4.3)}$$

Where δ_a = Permanent deformation for the layer /sub-layer. N = Number of traffic repetitions. ε_0, β, ρ = Material properties. ε_r= Resilient strain imposed in laboratory test to obtain material properties, ε_0, β, ρ. ε_v= Average vertical resilient strain in the layer/sub-layer as obtained from the primary response model. h = Thickness of layer/sub-layer. β_1 = Calibration factor for the unbound granular and subgrade materials.

Individual and cumulative rut depths are found as a function of time and traffic repetitions. Damage induced by rutting is estimated for each sub-season at the mid-depth of each sub-layer within the pavement and the plastic strain accumulated is computed at the end of each sub-season. The overall permanent deformation at the end of the season is given by

$$PD = \sum_{i=1}^{nsublayers} \varepsilon_p^i h^i \quad \text{(Eqn. 4.4)}$$

Where PD = pavement permanent deformation. $nsublayers$ = number of sublayers. ε_p^i = Total plastic strain in sub-layer i. h^i = Thickness of sub-layer i. The process is repeated for each load-level, month and sub-season of the analysis period.

Fatigue cracks are a series of interconnected cracks caused by fatigue failure of the asphaltic surface (or stabilized base) by repeated loading (*32*). The action of repeated or traffic loads induces tensile and shear stresses in layers and cause fatigue cracks to initiate at points where these critical strains and stresses occur. The most important factors in the location of critical strains or stresses are the layer stiffness and the load configuration (Applied Research Associates Inc., 2004d). The more common form of fatigue cracking initiates at the bottom of the asphaltic layer and propagates up to the surface. This phenomenon is known as bottom-up cracking. A more recent form of fatigue cracking, top-down cracking, which starts from the surface and propagates downwards, has also been observed and is undergoing further research. As such, only bottom-up cracking is analyzed in this study. Fatigue cracking leads to a loss in the structural integrity of the flexible pavement and reduces it overall serviceability. Cracks allow water, typically run-off, to seep into the pavement structure and weaken underlying layers. Fatigue cracks can also contribute to the formation of other distresses such as roughness. The most commonly used fatigue models are those developed by Shell Oil (Bonnaure et al, 1980) and the Asphalt Institute (Asphalt Institute, 1982). The overall general form of these two models is governed by a mathematical relationship given as:

$$N_f = Ck_1 \left(\frac{1}{\varepsilon_t}\right)^{k_2} \left(\frac{1}{E}\right)^{k_3} \qquad \text{(Eqn. 4.5)}$$

Where N_f = Number of repetitions to fatigue cracking. ε_t = Tensile strain at the critical location. E = Stiffness of the material. k_1, k_2, k_3 = Laboratory regression coefficients. C = Laboratory to field adjustment factor

The differences between the two models lie in the laboratory regression coefficients and the laboratory to field adjustment factor. In MEPDG, fatigue cracking prediction was achieved by focusing on these two models. The modified model used in the Design Guide to calibrate fatigue cracking to actual field performance is represented by the relationship:

$$N_f = 0.00432 \times C \times \beta_{f1} k_1 \left(\frac{1}{\varepsilon_t}\right)^{k_2 \beta_{f2}} \left(\frac{1}{E}\right)^{k_3 \beta_{f3}} \qquad \text{(Eqn. 4.6)}$$

$$C = 10^M \qquad \text{(Eqn. 4.7)}$$

$$M = 4.84\left[\frac{V_b}{V_a + V_b} - 0.69\right] \qquad \text{(Eqn. 4.8)}$$

Where V_b = effective binder content (%). V_a= air voids (%). β_{f1}, β_{f2}, β_{f3} = Calibration parameters.

In MEPDG, the chosen functional performance indicator is pavement smoothness as indicated by the International Roughness Index (IRI) (Applied Research Associates Inc., 2004). The American Society of Testing and Materials defines roughness as the deviation from a true planar surface with characteristic dimensions that affects vehicle dynamics, ride quality,

dynamic loads, and drainage (American Society of Testing Materials, 2006). Road roughness has an appreciable impact on vehicle operating costs and on the safety, comfort, and speed of travel. It also increases the dynamic loading imposed by vehicles on the surface, accelerating the deterioration of the pavement structure. Roughness can also have adverse effects on drainage, causing water to pond on the surface, with subsequent impacts on both the performance of the pavement and vehicle safety (Saleh et al, 2000). International Roughness Index (IRI) is the widely accepted standard for measuring road roughness. Research has shown IRI is significantly affected by distresses such as rutting, fatigue cracking, potholes, depressions and swellings caused by soil movements. Other factors that affect IRI are design, site and climatic parameters as well as the initial as constructed IRI of the pavement (Applied Research Associates Inc, 2004b). The approach utilized in the Design Guide for predicting roughness was to predict it over time as a function of the initial IRI and key distress types. The basic design premise for the Design Guide was that incremental increases in surface distress cause incremental increases in surface roughness. Using base type, three equations were developed for new flexible pavements and these are shown below:

For Conventional Flexible Pavement with Thick Granular Base:

$$IRI = IRI_0 + 0.0463\left(SF\left[e^{\frac{Age}{20}} - 1\right]\right) + 0.00119(TC_L)_T + 0.1834(COV_{RD}) + 0.00384(FC)_T + 0.00736(BC)_T + 0.00155(LC_{SNWP})_{MH} \quad \text{(Eqn. 4.9)}$$

Where IRI_0 = IRI measured within six months after construction, m/km. $(TC_L)_T$ = Total length of transverse cracks (low, medium, and high severity levels), m/km. (COV_{RD})= Rut depth coefficient of variation, percent. $(FC)_T$ = Total area of fatigue cracking (low, medium, and high severity levels), percent of wheel path area, %. $(BC)_T$ = Total area of block cracking (low, medium, and high severity levels), percent of total lane area, %. $(LC_{SNWP})_{MH}$= Medium and high severity sealed longitudinal cracks outside the wheel path, m/km. Age = Age after construction, years.

$$SF = \left[\frac{(R_{SD})(P_{0.075}+1)(PI)}{2\times10^4}\right] + \left[\frac{\ln(FI+1)(P_{0.02}+1)(\ln(R_m+1))}{10}\right] \quad \text{(Eqn. 4.10)}$$

Where R_{SD}= Standard deviation in the monthly rainfall, mm. R_m= Average annual rainfall, mm. $P_{0.075}$= Percent passing the 0.075 mm sieve. $P_{0.02}$= Percent passing thee 0.02 mm sieve. PI= Plasticity index. FI = Average annual freezing index.

For Flexible Pavement with Asphalt Treated Base:

$$IRI = IRI_0 + 0.0099947(Age) + 0.0005183(FI) + 0.00235(FC)_T + 18.36\left(\frac{1}{(TC_S)_H}\right) + 0.9694(P)_H \quad \text{(Eqn. 4.11)}$$

Where $(TC_S)_H$= Average spacing of high severity transverse cracks, m. $(P)_H$= Area of high severity patches, percent of total lane area, %. FI = Average annual freezing index. Age = Age after construction, years.

For Flexible Pavement with Cement Treated Base:

$$IRI = IRI_0 + 0.00732(FC)_T + 0.07647(SD_{RD}) + 0.0001449(TC_L)_T + 0.00842(BC)_T + 0.0002115(LC_{NWP})_{MH} \quad \text{(Eqn. 4.12)}$$

Where $(LC_{NWP})_{MH}$ = Medium and high severity sealed longitudinal cracks outside the wheel path, m/km. (SD_{RD}) = Standard deviation of the rut depth, mm.

Pavement Performance Models for JPCP

Performance of jointed plain concrete pavements (JPCP) under different climate change scenarios was analyzed using the following distresses as benchmarks: faulting, and transverse cracking. Joint faulting is the difference in elevation between adjacent joints at a transverse joint (Applied Research Associates Inc, 2004e). Faulting is usually caused by pumping, which is simply the movement of erodible material by water pressure within the pavement structure under the action of heavy axle loads or inadequate load transfer at the joints. This forms a buildup of material beneath the approach corner of a slab, whilst forming a void under the lead corner of the adjacent slab, thereby creating differential elevation between the two slabs. Faulting can also be caused by slab settlement, curling and warping; and is a contributing factor of roughness in rigid pavements (WSDOT, 2011). In formulating a mechanistic-empirical model for faulting, the Design Guide examined four main components: damage due to axle load applications, inadequate load transfer, erodibility of underlying materials and the presence of free water. The Guide then used incremental damage accumulation as its approach in developing the faulting model, where increments are observed monthly. The faulting at each month is determined as a sum of faulting increments from all previous months in the pavement life since traffic opening using this model:

$$Fault_m = \sum_{i=1}^{m} \Delta Fault_i \quad \text{(Eqn. 4.13)}$$

$$\Delta Fault_i = C_{34} \times (FAULTMAX_{i-1} - Fault_{i-1})^2 \times DE_i \quad \text{(Eqn. 4.14)}$$

$$FAULTMAX_i = FAULTMAX_0 + C_7 \times \sum_{j=1}^{m} DE_j \times Log(1 + C_5 \times 5^{EROD})^{C_6} \quad \text{(Eqn. 4.15)}$$

$$FAULTMAX_0 = C_{12} \times \delta_{curling} \times \left[Log(1 + C_5 \times 5^{EROD}) \times Log\left(\frac{P_{200} \times WetDays}{P_S}\right)\right]^{C_6} \quad \text{(Eqn. 4.16)}$$

Where $Fault_m$= Mean joint faulting at the end of month m, in. $\Delta Fault_i$= Incremental change (monthly) in mean transverse joint faulting during month i, in. $FAULTMAX_i$ = Maximum mean transverse joint faulting for month i, in. $FAULTMAX_0$ = Initial maximum mean transverse joint faulting, in. $EROD$= Base/subbase erodibility factor. DE_i = Differential deformation energy accumulated during month i. $\delta_{curling}$ = Maximum mean monthly slab corner upward

deflection PCC due to temperature curling and moisture warping. P_s = Overburden on subgrade, lb. P_{200} = Percent subgrade passing #200 sieve. WetDays = Average annual number of wet days (greater than 0.1 in rainfall).

$$C_{12} = C_1 + C_2 \times FR^{0.25} \qquad \text{(Eqn. 4.17)}$$

$$C_{34} = C_3 + C_4 \times FR^{0.25} \qquad \text{(Eqn. 4.18)}$$

Where FR = Base freezing index defined as percentage of time the top base temperature is below freezing ($32^{\circ}F$) temp. C_1 through C_7 are calibration constants

Transverse cracking, a primary structural fatigue distress type of JPCP, is characterized by its initiation from one longitudinal edge of a concrete slab followed by a diagonal progression across the slab to the other longitudinal joint or a transverse joint (*39*). They are usually caused by a combination of heavy load repetitions and stresses due to temperature gradient, moisture gradient and drying shrinkage (Huang, 2004). Another cause could be as a result of poor construction (Papagiannakis and Masad, 2008). For the Design Guide, the mechanistic-empirical prediction for transverse cracking includes an iterative damage accumulation algorithm where damage is accumulated on a monthly basis over the analysis period. The algorithm considered truck axle loadings, thermal gradients and moisture gradients in the development of the prediction model. As such traffic information, climatic factors, design features and information on materials used in different layers within the JPCP structure serve as useful sources of information for transverse crack prediction. The incremental damage algorithm used in the Design Guide is presented as follows:

$$FD = \sum \frac{n_{i,j,k,l,m,n}}{N_{i,j,k,l,m,n}} \qquad \text{(Eqn. 4.19)}$$

Where FD = total fatigue damage. $n_{i,j,k,\ldots}$ = applied number of load applications at condition i, j, k, l, m, n. $N_{i,j,k,\ldots}$ = allowable number of load applications at condition i, j, k, l, m, n. i = age (accounts for change in PCC modulus rapture, layer bond condition, deterioration of shoulder Load Transfer Efficiency). j = month (accounts for change in base and effective dynamic modulus of subgrade reaction). k = axle type. l = load level (incremental load for each axle type). m = temperature difference. n = traffic path.

The applied number of load applications ($n_{i,j,k,l,m,n}$) is the actual number of axle type k of load level l that passed through traffic path n under each condition (age, season and temperature difference). The allowable number of load applications is determined using the following field calibrated fatigue model:

$$\log\left(N_{i,j,k,l,m,n}\right) = C_1 \left[\frac{MR_i}{\sigma_{i,j,k,l,m,n}}\right]^{C_2} + 0.4371 \quad \text{(Eqn. 4.20)}$$

Where $N_{i,j,k,\ldots}$ = allowable number of load applications at conditioni, j, k, l, m, n. MR_i = PCC modulus of rapture at age i, psi. $\sigma_{i,j,k,\ldots}$ = applied stress at conditioni, j, k, l, m, n. C_1, C_2 = calibration constants.

Analysis of roughness for JPCP followed that for flexible pavements. No one fundamental mechanism could be identified as the cause, but several factors came to play when considering roughness as a distress. These factors include other structural and non-structural distresses such as faulting, corner breaks, longitudinal and transverse cracking; surface defects such as initial smoothness; maintenance regimens; and other variables like age. Combining all these factors and variables, the equation for predicting JPCP roughness in the Design Guide is given as:

$$\mathrm{IRI} = \mathrm{IRI}_0 + 0.013 \times (\mathrm{TC}) + 0.007 \times (\mathrm{SPALL}) + 0.005 \times (\mathrm{PATCH}) + 0.0015 \times (\mathrm{TFAUL}) + 0.45 \times (\mathrm{SF}) \quad \text{(Eqn. 4.21)}$$

Where TC = percentage of slabs with transverse cracking (all severities). SPALL = percentage of joints with spalling (all severities). PATCH = pavement surface area with flexible and rigid patching (all severities), percent. TFAULT = total joint faulting cumulated per km, mm. SF = site factor = $\mathrm{Age} \times (1 + \mathrm{FI}) \times (1 + \mathrm{P}_{200})/1000000$, , in which Age= pavement age in years, FI = freezing index, 0C days, P_{200}= percent subgrade material passing the 0.075-mm sieve.

Pavement Performance Models for CRCP

Two distresses: roughness and punch outs were used as indicators to monitor the effect of potential climate change on continuously reinforced concrete pavements (CRCP). Roughness for CRCP followed the same description given in the sections for flexible and JPCP. As was the case for the afore mentioned pavement types, roughness in CRCP is also triggered by a number of factors such as age, initial roughness after construction and distresses formed as a result of interactions between traffic, site and environmental factors. Following JPCP, factors that influence roughness can be classified as structural, surface defects and maintenance-related. Examples of structural factors are punch outs, transverse cracks and pumping. Surface defects include initial IRI, scaling and map cracking. A maintenance related factor is patching. The model for predicting roughness for CRCP as used in the Design Guide is given as:

$$\mathrm{IRI} = \mathrm{IRI}_0 + 0.003 \times (\mathrm{TC}) + 0.008 \times (\mathrm{PUNCH}) + 0.45 \times (\mathrm{SF}) + 0.2 \times (\mathrm{PATCH}) \quad \text{(Eqn. 4.22)}$$

Where TC= number of medium- and high-transverse cracks/km. PUNCH = number of medium- and high-severity punchouts/km. PATCH = percentage pavement surface with patching (M-H severity flexible and rigid). SF = site factor = $\mathrm{Age} \times (1 + \mathrm{FI}) \times (1 + \mathrm{P}_{200})/1000000$, in which Age= pavement age in years, FI = freezing index, 0C days, P_{200}= percent subgrade material passing the 0.075-mm sieve.

Edge or structural punchout is a major structural distress of CRCP characterized first by a loss of aggregate interlock at one or two closely spaced transverse cracks at the edge of the pavement. The crack or cracks begin to fault and spall slightly, and with the application of heavy axle loads across this cracked section, a longitudinal crack is formed between the transverse cracks. As the cracks deteriorate with time, the steel within the concrete raptures and pieces of concrete punch down under load into the subbase and subgrade. The distressed area expands in size to

adjoining cracks and develops into a large area if left unchecked (Huang, 2004). CRCP punchouts are a combination of repeated heavy axle loads, loss of LTE across two closely spaced transfer cracks of which crack width is a primary factor, inadequate PCC slab thickness, free moisture beneath the CRCP, erosion of supporting subbase or subgrade material along edge of CRCP and negative slab curling and moisture warping. Punchouts reduce the ride quality of the roadway and influence the formation of other CRCP distresses (Applied Research Associates Inc, 2004g). In the Design Guide, one method for predicting CRCP performance is based on the incremental development of punchout distress. The prediction of punchout distress is achieved in terms of the accumulated fatigue damage associated with the formation of specific longitudinal cracks between two closely spaced transverse cracks (LaCourseiere et al, 1978, Selezneva et al, 2001, Selezneva, 2002, Zollinger et al, 1990, Darter, 1988). The calibrated model for punchout prediction as a function of accumulated fatigue damage due to slab bending in the transverse direction is given as

$$PO_i = \sum_{i=1}^{Life} \frac{a}{1+bD_i^c} \qquad \text{(Eqn. 4.23)}$$

Where PO_i = total predicted number of punchouts per mile at the end of i^{th} monthly increment. D_i = accumulated fatigue damage at the end of i^{th} monthly increment. a, b, c = calibration constants

Local Calibration Approach

Current highways are designed based on typical historic climatic patterns, reflecting local climate and incorporating assumptions about a reasonable range of temperatures and precipitation levels. Given anticipated climate changes and the inherent uncertainty associated with such changes, a pavement could be subjected to very different climatic conditions over the design life and might be inadequate to withstand future climate forces that impose stresses beyond environmental factors currently considered in the design process.

The MEPDG performance models were developed using historical data and didn't take climate change into consideration. In addition, the coefficients in the performance were based on national climate data sets. These national calibration factors may not be appropriate for specific regions of the country that have their own climate patterns. In order to generate more accurate performance predictions for a more robust pavement design in the light of potential climate change, the performance models need to be "locally" calibrated to consider the impact of the change.

The concept of "local calibration" in MEPDG is to eliminate bias between national models and local conditions, to reduce the standard error associated with the prediction equations and to consider the differences in materials, construction specifications, policies on pavement preservation and maintenance across the nation. The MEPDG software incorporates the local calibration coefficients for the performance models that can be changed by the users to make adjustments to the predicted performance values. Figure 4.1 shows a screen shot of the tools section where these values can be entered into the software for each performance indicator on a project basis. In this study, we expand this concept to local climate change conditions and

apply it to adapt to the change by calibrating the coefficients of the performance prediction models.

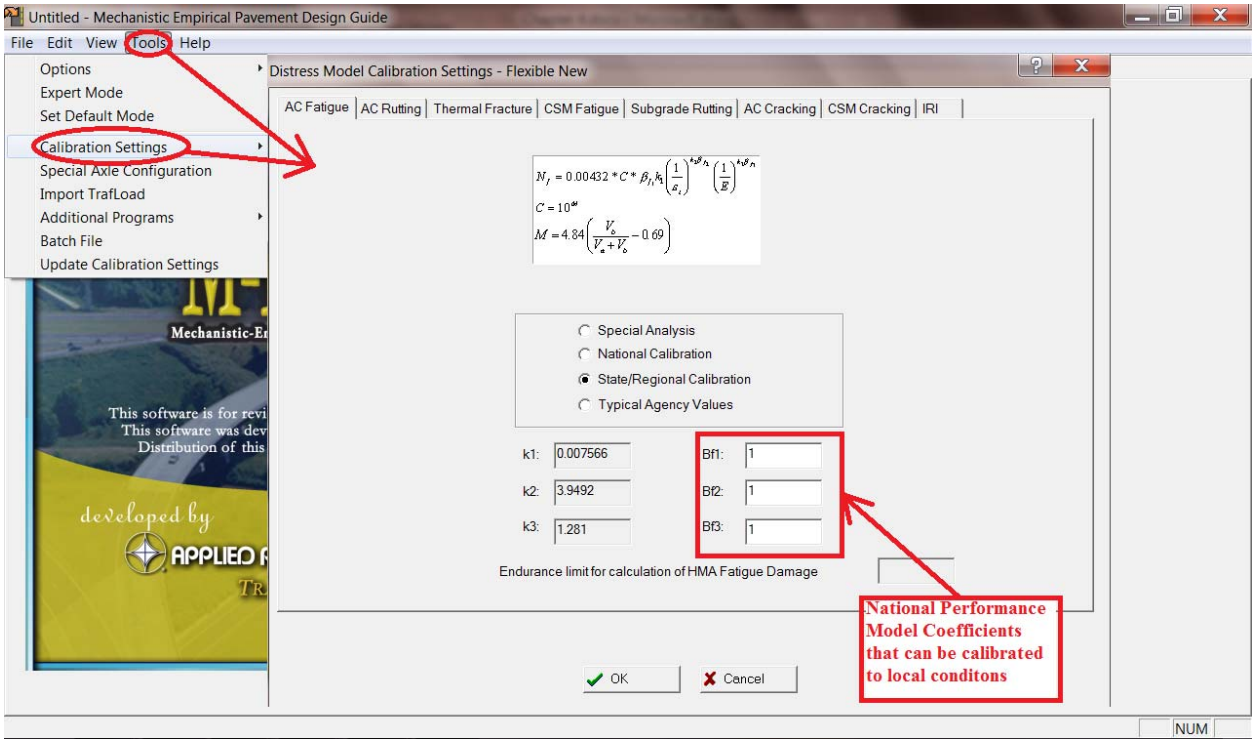

Figure 4.1 MEPDG Local Calibration Screen Shot

Overview of the Methodology

To tailor distresses to meet local pavement conditions, sensitivity analysis was conducted to locally calibrate distresses. Subsequent local calibration analysis in the research proceeded based on results obtained from the parallel comparisons between potential climate change and no changes to climate. The procedure of local calibration is a major iterative work effort. The calibration process, as developed, involves five basic steps as follows:

- Review all input data.
- Conduct sensitivity analysis.
- Conduct comparative studies.
- Conduct validation/calibration studies.
- Modify input defaults and calibration coefficients as needed.

Step 1: Review All Input Data

All inputs to the MEPDG software should be reviewed and the desired level and procedures for obtaining each input on various types of design projects be determined. Several inputs are very

critical but are not well defined in the MEPDG software and these are the ones the design entity should conduct sensitivity analysis on. The process is as follows:

- Determine if defaults provided with the MEPDG software are appropriate for the design entity and if not, modify as needed.
- Select allowable ranges for inputs for various types of projects within the geographical area of the designer (low volume, high volume, different geographic areas within the state).
- Select procedures to obtain these inputs for regular design projects (e.g., traffic volume and weight inputs). Determine the effects of the accuracy of input values on the resulting design.
- Conduct necessary testing to establish specific inputs (e.g., material characterization, axle load distributions) and acquire needed equipment for any testing required.
- Conduct analyses to establish the desired level of design reliability for various types of highways (e.g., Interstate, primary, secondary) or levels of traffic.

Step 2: Sensitivity Analysis

This is accomplished by selecting a typical design situation with all design inputs. The software is run and the mean distresses and IRI predicted over the design period. Then individual inputs are varied and the change in all outputs observed. Appropriate tables and plots are prepared, the results evaluated, and inputs divided into groups based on their sensitivity to outputs, such as those that have very significant effect, a moderate effect, and only minor effect. Those inputs that have significant impacts must be selected more carefully than those with minor effects. The above sensitivity may be repeated for low, medium and high traffic project designs to see if that has an effect on inputs.

Step 3: Comparative Studies

Conducting comparative studies using the MEPDG software can provide observations of various design inputs on pavement performance. In this study, the comparison analyses are conducted to examine how the climate change variability might affect the performance of pavement sections over time. This involved comparing the performance deteriorations of two parallel designs, one which considered the impacts of climate change with its different scenarios and one which did not consider climate change.

Step 4: Calibration to Local Conditions

A validation process should be developed to confirm that the national calibration factors or functions are adequate and appropriate for the construction, materials, climate, traffic, and other conditions that are encountered within the designer's highway system. Prepare a database of agency performance data and compare the design results with the performance of these "local" sections. This will require comprehensive experimental design and the selection of a statistically sufficient number of pavement sections for analysis. The goal of the calibration-

validation process is to confirm that the performance models accurately predict pavement distress and ride quality on a national basis. For any specific geographic area, adjustments to the national models may be needed to obtain reliable pavement designs.

Step 5: Modify the Calibrations/Inputs

If significant differences are found between the predicted and measured distresses and IRI for the agencies highways, appropriate adjustments must be made to the calibration coefficients. Make modifications to the default national coefficients in the performance models as needed based on all of the above results and findings. These results could then be used to establish a new standard deviation model for use in reliability design to provide a more cost effective design.

5. Case Study and Implementation

Study Sites and Pavement Structures

The potential impacts of climate change and its uncertainty on pavement performance and design were explored using sites in the North-Eastern region of the United States as the reference area of study. Three states, namely Delaware, New Jersey and Connecticut, were selected within the study region and flexible and rigid pavement types were chosen for experimental designs. Each of the pavement locations had climate conditions peculiar to the location and these conditions formed the platform from which expectations with respect to future climate changes were made. Pavement types analyzed were asphaltic concrete pavement, continuously reinforced concrete pavement (CRCP) and jointed plain concrete pavement (JPCP).

For each pavement type and a specific location, an existing Long Term Pavement Performance (LTPP) pavement section was identified and its characteristics such as pavement structure, traffic information and layer material properties were used as input in developing experimental units for the study. As such, the asphalt concrete pavement used in this research was a replica of Interstate 95 in New Jersey, the experimental design for CRCP was based on Interstate 495 in Delaware and that for JPCP followed the rigid section of Interstate 84 W in Connecticut. Pavement structures for all these highways were designed using information from the Long-Term Pavement Performance (LTPP) database. This section describes the development of pavement structures for the study.

The structure of the asphalt concrete pavement consisted of two layers: an asphalt layer and an unbound granular base, placed on top of an existing subgrade. The JPCP was made up of a Portland concrete layer and a granular base layer on top of its subgrade. The structure for CRCP consisted three constructed layers in addition to the subgrade. The additional layers were an unbound subbase, a treated base and a Portland concrete layer in ascending order. Thicknesses for each layer with the exception of the subgrade were provided in the LTPP database and were used for initial performance runs in MEPDG. Also contained in the LTPP database were the constituent materials of the layers and their respective properties and characteristics. The locations, pavement types, LTPP structures, and adjusted MEPDG designs for the three test sites are included in Table 5.1.

Given LTPP sections were designed using the AASHTO Guide for Design of Pavement Structure and recognizing that these structures are more conservative than those designed using the MEPDG software, the structural designs for the study were adjusted where necessary. This was done as follows: if the AASHTO design passed all the MEPDG performance criteria requirements, the surface layer thickness was reduced in increments of half an inch and MEPDG analysis was performed. This process was repeated until one of the performance criteria failed, then the MEPDG design thickness was that thickness plus 0.5 inches. On the other hand if the AASHTO design failed, analysis started with an increase of the thickness by half an inch and followed the same philosophy described above to achieve an acceptable MEPDG design.

Table 5.1 Test Sites of the Case Study

State ID	SHRP ID	Route	Type	LTPP Structure	Lat	Long	Elevation (ft)	MEPDG Adjusted Structure
NJ-34	6057	I-95	AC	1.8" AC 6.1" AC 7.5" GB 74.4" SS	40.27	74.83	222	1.8" AC 4.5" AC 7.5" GB 74.4" SS
CT-09	4008	I-84W	JPCP	10.4" PC 9.5" GB SS	41.80	72.56	155	8" PC 9.5" GB SS
DE-10	5004	I-495	CRCP	9" PC 4" TB 4" GS SS	39.74	75.51	14	9" PC 4" TB 4" GS SS

Note: AC – Asphalt Concrete; PC – Portland Concrete; GB – granular base; SS – sand soil; TB – bound treated base; GS – unbound granular subbase.

Historical Climatic Data

For any projected changes in climate to be made, a history of climatic data was first examined for the three test sites. The climatic data used in MEPDG was obtained from a database managed by the National Climatic Data Center which contains records for locations all over the country. For the three test sites, the most appropriate weather stations were the following stations: Bradley International Airport in Connecticut (station ID 14740) for the JPCP section, New Castle County Airport in Delaware (station ID 13781) for the CRCP and Trenton Mercer Airport in New Jersey for the asphalt section. The locations of these 3 weather stations are in Table 5.2.

In the MEPDG software, the historical climate data for each station are recorded hourly and saved in a file with an "HCD" extension using a predefined format. These HCD files, which store the historical data, represent the historical climatic patterns without considering climate change impacts. The five climate variables for each station are air temperature, precipitation, wind speed, percentage sunshine, and relative humidity. For pavements, the most significant climate variables were temperature and precipitation, whose values can be projected for various climate change scenarios using the MAGICC/SCENGEN software. The statistical summary of the historical temperature data is provided in Table 5.3.

Table 5.2 MEPDG Weather Stations for the three pavement sections

Weather Station	City/State	Location	Lat	Long	Elevat-ion (ft)	First data date	Used for Pavement section [1]	Distan ce
14740	Windsor Locks, CT	Bradley International Airport	41.56	-72.41	165	960701	09-4008	13.6
13781	Wilmington, DE	New Castle County Airport	39.4	-75.36	95	960701	10-5004	26.6
14792	Trenton, NJ	Trenton Mercer Airport	40.17	-74.49	197	980301	34-6057	15

[1] the pavement section is labeled as "State ID – SHRP ID". For example, 09-4008 indicates the pavement section in State 09 (NJ) with the SHRP ID of 4008. See Table 5.1.

Table 5.3 Statistical Summary of Historical Hourly Temperature Data

Location	Season	min	1st Quartile	Median	Mean	3rd Quartile	Max	SD	# Record
14740	Spring	-1	39	48	48.63	57.9	94	13.73	19872
	Summer	35	64.9	71	71.22	78	102	9.31	21360
	Fall	12	43	53	52.9	63	90	13.43	21840
	Winter	-7	24	31	30.2	37	74	10.70	21648
13781	Spring	17	44	53	52.74	61	91	12.82	19872
	Summer	46	69	74	74.1	80	98.1	8.14	21360
	Fall	18	48	57	57.01	66.9	91	12.81	21840
	Winter	2	29	35.1	35.67	42	73	10.23	21648
14792	Spring	12	42	51.1	51.7	60.1	93	13.22	17664
	Summer	44	67	73	73.42	80	100	8.83	17664
	Fall	21	47	56	55.93	65	90	12.39	17472
	Winter	2	27	34	33.9	40	75	10.75	17328

Traffic Inputs Required in MEPDG

The MEPDG requires four basic categories of traffic inputs as follows (Federal Highway Administration 2001):

- The base year traffic volume. One important input in this category is Annual Average Daily Truck Traffic (AADTT) of vehicle Classes 4 through 13. This information can be derived from weigh-in-motion (WIM), automated vehicle counts (AVC), or vehicle count data and is available within a state highway agency.
- The base year AADTT must be adjusted by using traffic volume adjustment factors, including monthly distribution, hourly distribution, class distribution, and traffic growth factors. These factors can be determined on the basis of classification counts obtained from WIM, AVC, or vehicle count data.
- Axle load distribution factors (axle load spectra). The axle load distribution factors represent the percentage of the total axle applications within each load interval for a specific axle type (single, tandem, tridem, and quad) and truck class (class 4 to class 13). The axle load distributions or spectra can be determined only from WIM data.
- General traffic inputs, such as number of axles per truck, axle configuration, and wheel base. These data are used in the calculation of traffic loading for determining pavement responses (Applied Research Association Inc., 2004i). The default values provided for the general traffic inputs are recommended if more accurate data are not available.

WIM data collected in accordance with the Traffic Monitoring Guide (TMG) (Federal Highway Administration, 2001) would meet the traffic characterization requirements for MEPDG to develop all the traffic input parameters.

Development of MEPDG Traffic Inputs

Analyses of WIM data based on the LTPP database showed that the differences between year-to-year and month-to-month load spectra were not significant (Tran and Hall, 2007). Therefore, the traffic data can be normalized on an annual basis for the development of traffic inputs for the MEPDG software.

Monthly Adjustment Factors

Based on the traffic counts by class obtained from WIM data, the monthly adjustment factors were calculated as follows:

- Determine the total number of trucks (in a given class) for each 24-hour period.
- Determine the Average Monthly Daily Truck Traffic for each month (AMDTT) in the year.
- Sum up the average daily truck traffic for each month for the entire year.

- Calculate the monthly adjustment factors by dividing the average daily truck traffic for each month by summing the average daily truck traffic for each month for the entire year and multiplying it by 12 as given below (NCHRP 1-37A, 2004):

$$MAF_i = 12 \times \frac{AMDTT_i}{\sum_{i=1}^{12} AMDTT_i} \quad \text{(Eqn. 5.1)}$$

Where MAF_i = Monthly Adjustment Factor for month i; $AMDTT_i$ = Average Monthly Daily Truck Traffic for month i.

Vehicle Class Distribution

The vehicle class distribution factors can be determined as a given formula (Applied Research Association Inc., 2004i). The sum of Class Distribution Factors (CDF) for all classes should equal 100%.

$$CDF_j = \frac{AADTT_j}{AADTT} \quad \text{..... (Eqn. 5.2)}$$

Where: CDF_j = Class Distribution Factor for vehicle class j; $AADTT_j$ = Annual Average Daily Truck Traffic for class j; AADTT = Annual Average Daily Truck Traffic for all classes

Hourly Truck Distribution

The hourly data are used to determine the percentage of total trucks within each hour as follows (*24*):

- Determine the total number of trucks counted within each hour of traffic data in the sample.
- Average the number of trucks for each of the 24 hours of the day in the sample.
- Total the 24 hourly averages from step 3.
- Divide each of the 24 hourly averages from step 2 by the total from step 3 and multiply by 100 and get the Hourly Distribution Factors (HDF), which is shown in Equation 3 (Applied Research Association Inc., 2004i). The sum of the percent of daily truck traffic per time increment must add up to 100%.

$$HDF_i = \frac{HATT_i}{\sum_{j=1}^{24} HATT_j} \quad \text{..... (Eqn. 5.3)}$$

Where: HDF_i = Hourly Distribution Factor for i^{th} one-hour time period; $HATT_i$ = Hourly Average Truck Traffic for i^{th} one-hour time period

Axle Load Distribution Factors

Axle load distribution factors can be calculated using WIM data to average the daily number of axles measured within each load interval of an axle type for a truck class divided by the total number of axles for all load intervals (Wang and Li, 2008). The procedure is given as:

- Find the range containing all weight data from a specific WIM station.
- Count the number of axles in each weight bin for different vehicle classes using the following load intervals:
  - Single axles: 3,000 lb to 40,000 lb at 1,000-lb intervals;
  - Tandem axles: 6,000 lb to 80,000 lb at 2,000-lb intervals;
  - Tridem and quad axles: 12,000 lb to 102,000 lb at 3000-lb intervals.
- Summarize the monthly axle load distribution in the previous step and determine the axle load spectra for the site.

WIM Data Sources and Results

At most LTPP sites, Weigh-In-Motion (WIM) equipment was installed to collect traffic data. It is widely recognized that WIM data are often erroneous due to uncalibrated sensors, pavement conditions and environmental issues. In order to obtain high quality data, the data obtained immediately after a system calibration are used to generate the traffic load spectra for the pavement section. The calibration details and the data availability are summarized in Table 5.4.

Table 5.4 WIM Calibration and Data Availability

Pavement Section	Calib Date	Equip Calib	Reason Calib	Quartz Piezo	Induct. Loops	Manufacturer	Availability
09-4008	27-04-00	3	2	N	Y	IRD	93 (1-9), 94, 95, 98 (1-11), 99, 06, 07 (no 9)
09-4008	09-06-05	3	2	Y	N	IRD	
10-5004							2008
34-6057	22-04-00	1	1	N	Y	DYNAX	2000, 2008 (5-12)
34-6057	12-05-01	1	1	N	Y	DYNAX	

Note: EQUIP_CALIB: 1 - WIM; 3 - Both WIM and AVC.
REASON_CALIB: 1 - Regularly scheduled visit; 2 – Research.

Based on the data available immediately after equipment calibration, 2006 data was used for 09-4008 JPCP pavement section, 2008 for 10-5004 Delaware CRCP section, and 2000 data for 34-6057 New Jersey flexible pavement section. For each WIM station, the load spectra for vehicle class 5 and 9 single axles, vehicle Class 9 tandem axles, and Vehicle class 7 and 10 Tridem axles, the monthly adjustment factors, and vehicle class distribution factors are presented as Figures in Appendix B.

The traffic module in the MEPDG software is shown in Figure 5.1, which allows designers to import all the traffic parameters required. All the importable inputs are saved in 11 files. These files, as summarized in Appendix C, require a specific format. The traffic data from these three WIM locations are prepared according to the file format so that the MEPDG software can directly import them for pavement analysis.

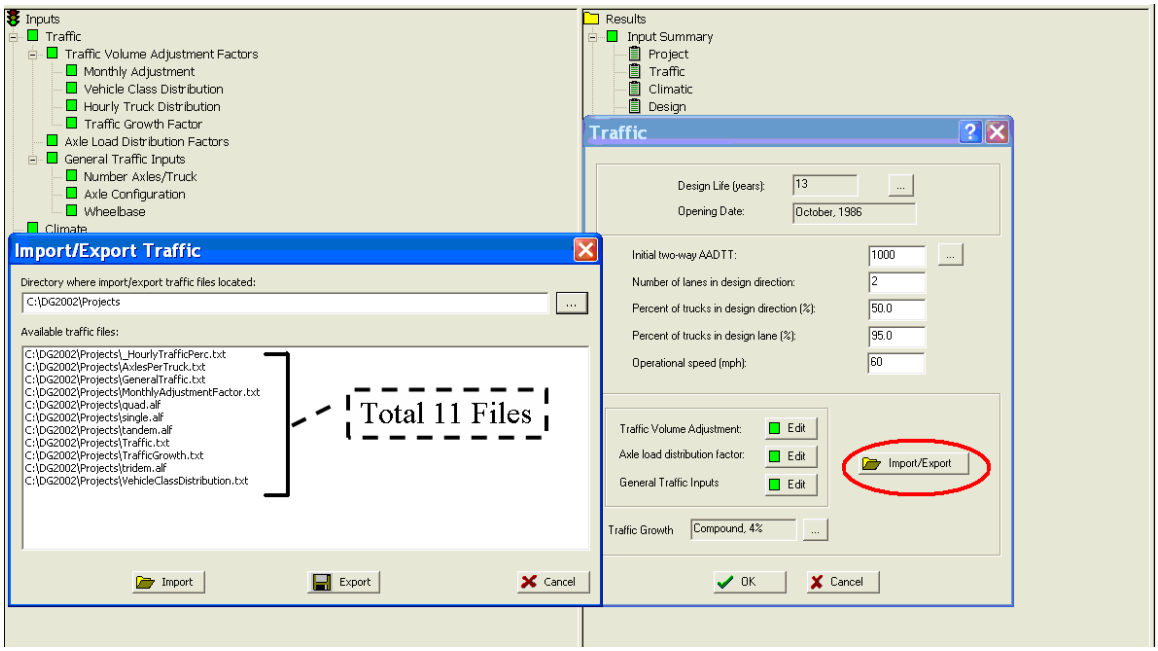

Figure 5.1 Traffic Input in the MEPDG Software

Material Input

Materials used in the constituent layers of the different pavement structures play a pivotal role in the overall performance of the pavement. Material inputs are required for pavement response models, distress models and climate models (Applied Research Associates Inc, 2004h). The MEPDG Design Guide catalogues some of the material properties that are required for the models. To predict the states of stress, strain and displacement within the pavement structure for the response model, MEPDG uses elastic modulus and Poisson ratio of the material in each of the pavement layers. Distress models use material parameters such as strength, expansion-contraction characteristics, friction between slab and base, modulus, Poisson ratio, erodibility of underlying layers, layer drainage characteristics, plasticity and gradation. Material-related inputs that affect climate models include engineering index properties, gradation parameters and thermal properties. The correct specification of material inputs in MEPDG is thus a significant ingredient in determining pavement performance overtime. Examples of material inputs for different material groups as required by MEPDG and as displayed in the Design Guide are shown in Table 5.5.

Table 5.5 Major material input considerations by material group

Materials Category	Materials inputs required
Hot-Mix Asphalt materials (covers surface, binder, base and subbase courses)	Time-temperature dependent dynamic modulus, Poisson's ratio, tensile strength, creep compliance, coefficient of thermal expansion, surface shortwave absorptivity
PCC materials (surface layer only)	Static modulus of elasticity adjusted with time, Poisson's ratio, unit weight, coefficient of thermal expansion, modulus of rapture, compressive strength, water-to-cement ratio
Chemically Stabilized materials (covers lean concrete, cement treated, soil cement, lime-cement-flyash, lime-flyash and lime stabilized layers)	Elastic modulus, resilient modulus, Poisson's ratio, unit weight, modulus of rapture, base erodibility, thermal conductivity and heat capacity of PCC.
Unbound Base/Subbase and subgrade materials	Seasonally adjusted resilient modulus, Poisson's ratio, unit weight, coefficient of lateral pressure, gradation parameters and base erodibility, plasticity index, specific gravity

As a start, information on pavement materials and their properties for each pavement design template was obtained from their respective in-service pavements as documented in the LTPP database. Information gathered included pavement layer configuration, layer composition, gradation of asphalt concrete, gradation of unbound layers, subgrade condition, results of strength tests and steel reinforcement characteristics amongst many others. Not all the information required by MEPDG was found in the LTPP database. Other pieces of information were inconsistent across the database and could not be used. When such cases arose, the authors used other pavement engineering resources and their own experience in designing pavements to formulate solutions. Using a combination of data inventory from LTPP, pavement design manuals and experience, Table 5.6 shows the different constituent layers for each of the pavement design types employed in the research.

The general approach used in selecting design inputs for materials in the Design Guide is the hierarchical system (Applied Research Associates Inc, 2004h). The hierarchical system is developed based on the philosophy that the level of engineering effort exerted in the pavement design process should be consistent with the relative importance, size and cost of the design process. There are three levels involved with the hierarchical system. Level 1 requires the use of comprehensive laboratory or field tests; Level 2 uses inputs that are estimated through correlations with other material properties that are measured in the laboratory or field; and Level 3 requires an estimation of the most appropriate design input value of the material property based on experience with little or no testing. This study used Level 3 inputs based on the sources from which information was obtained to design the pavement structures.

Table 5.6 Layer and material composition for pavement types

Pavement Type	Layer Configuration
Asphalt Concrete	AC Laver A-1-a A-1-b Poorly graded gravels
CRCP	CRCP Soil Cement A-3 Poorly graded sand
JPCP	JPCP A-1-a A-6

Climate Change Projections and MEPDG Climate Data Generation

The greenhouse gas emission scenarios used in this research were adopted from the IPCC Special Report on Emissions Scenarios (SRES) (*26*). The four scenarios used are described below:

- The A1B scenario describes a future world of very rapid economic growth, global population balanced across all sources.
- The A2 scenario describes a very heterogeneous world. The underlying theme is self-reliance and preservation of local identities.
- The B1 scenario describes a convergent world with the same global population that peaks in midcentury and declines thereafter.
- The B2 scenario describes a world in which the emphasis is on local solutions to economic, social, and environmental sustainability.

Only four out of six SRES scenarios are used. In the short term, the A1FI and A1T scenarios may not be practical, thus only A1B scenario was selected to represent the A1 family. Among these four scenarios, A2 generates the most GHG emissions followed by A1B, B2, and B1.

Climate Sensitivity

Climate sensitivity (ΔT2x) is a key variable in estimating future climate change. According to IPCC (2001), the best-estimate climate sensitivity is 3°C (5.4°F), which is used in this research for central estimates. To explore the impact of climatic sensitivity, the low variability is set to half the most likely value (which is 1.5°C) and the high end is doubled to 6°C. These ranges are consistent with those adopted in MAGICC/SCENGEN by Wigley (2008). The rates of melting of ice from glaciers and major ice sheets are assumed to be low, medium and high leveled for these three variability levels.

General Circulation Models (GCMs)

SCENGEN can be used to examine the extent to which the GCMs agree or disagree about regional projections of temperature and precipitation by calculating a signal-to-noise ratio for the models used. Studies suggest that 10 of the 20 climate AOGCM models best simulate the current US climate (Meyer et al, 2010, Meyer and Wiegel, 2011 and Wigley, 2008). The 10 models selected and used in this paper are:

- Canadian Centre for Climate Modeling (CGCM3)
- National Center for Atmospheric Research (NCAR CCSM)
- Geophysical Fluid Dynamics Laboratory (GFDL CM2.0 and CM2.1)
- Institute Pierre Simon Laplace (France) (IPSL_CM4)
- Center for Climate System Research (Japan) (MIROC 3.2, medium resolution)
- Max Planck Institute for Meteorology (Germany) (ECHAM5/MPI-OM)
- Meteorological Research Institute (Japan) (MRI-CGCM 2.3.2)
- Hadley Centre for Climate Prediction and Research (United Kingdom) (HadCM3 and HadGEM1)

Climate Change Projection Results

MAGICC gives projections of global-mean temperature and sea level change which are used by SCENGEN. SCENGEN gives the changes in absolute values of temperature and precipitation, changes in absolute values of temperature and precipitation variability, signal-to-noise ratios for temporal variability, and probabilities of temperature and precipitation change above a specified threshold on a 2.5 latitude by 2.5 longitude grid.

For the three test sites, the flexible pavement section on Interstate 95 in New Jersey and the JPCP section on Interstate 84W in Connecticut fell in the same GPS grid while the Delaware CRCP site belonged to another grid. Three scenario years: 2030, 2050, and 2100 were examined in the analysis. The MAGICC/SCENGEN climate change projection results for temperature and precipitation are summarized in Appendix D. As an example, the climate change projections for temperature and precipitation are summarized in Table 5.7 for the JPCP pavement section.

It should be noted that the change of absolute values and standard deviations are compared to those for the base year in 2010, which are obtained from the historical data at MEPDG provided weather stations as shown in Table 5.3.

Table 5.7 SCENGEN Projected temperature and precipitation change for the JPCP site

Year	Climate Indicator	Criteria	Spring	Summer	Fall	Winter
2030	Temperature	Mean change (C)	0.72	0.74	0.75	0.66
		Standard deviation (%)	2.1	14.21	2.31	-7.94
	Precipitation	Mean change (%)	3.54	-0.19	-0.09	2.05
		Standard deviation (%)	4.11	-0.36	2.58	-0.76
2050	Temperature	Mean change (C)	0.3	1.31	1.34	1.18
		Standard deviation (%)	3.73	25.26	4.11	-14.11
	Precipitation	Mean change (%)	6.3	-0.34	-0.16	3.65
		Standard deviation (%)	4.11	-0.65	4.59	-1.36
2100	Temperature	Mean change (C)	2.25	2.29	2.34	2.06
		Standard deviation (%)	6.53	44.17	7.19	-24.67
	Precipitation	Mean change (%)	11.01	-0.59	-0.28	6.38
		Standard deviation (%)	12.77	-1.13	8.03	-2.37

The projected sea level rise, which can be obtained from MAGICC, may have an impact on pavement performance as well. Among these three locations, only CRCP in Delaware was structured to include the impact of a rise in sea level. Sea level rise had no effect on the JPCP and asphalt concrete pavement because they were located more inland. The magnitude of the rise range from 9.54 ft to 9.88 ft in 2030 for the four emission models, from 9.11 to 9.81 ft in 2050, and from 7.37 to 9.66 ft in 2100. When considering climate effects on pavement performance, the sea level rise should be included.

Climate change is defined not simply as average temperature and precipitation change but also by the frequency and intensity of extreme weather events. For pavement design, the extreme temperature is a critical climatic input. As a result, the potential extreme temperature change should be considered. However, MAGICC/SCENGEN does not provide the capability to project this change. In this study, the results from the "Global climate change impacts in the United States" Report (U.S. Global Change Research Program, 2009) for the Northeast portion of the country are used and are summarized in Table 5.8.

Table 5.8 Projected Extreme Temperature Change (in ^{o}F) (U.S. Global Change Research Program, 2009)

Parameter	2030			2050			2100		
	Low	Med	High	Low	Med	High	Low	Med	High
Winter Min	1.45	2.55	4.36	2.18	3.82	6.55	4	7	12
Winter Max	1.09	2.55	4.36	1.64	3.82	6.55	3	7	12
Summer Min	1.82	1.82	1.82	2.73	2.73	2.73	5	5	5
Summer Max	1.09	2.55	4	1.64	3.82	6	3	7	11

Generation of HCD Data Files Considering Climate Change

Changing temperature and moisture profiles in the pavement structure and subgrade over the design life of a pavement are considered in MEPDG through the EICM engine. The EICM requires the following climatic data for MEPDG analysis:

- Hourly weather-related parameters: air temperature, precipitation, wind speed, percentage sunshine, and relative humidity;
- Others: elevation and water table depth.

For the weather-related information, the MEPDG software provides weather stations across the United States, which contain historical hourly data representing the base year climatic patterns without considering climate change impacts. These base year climatic data are saved in their respective HCD files. MAGICC/SCENGEN is capable of projecting the change of temperature and precipitation. By combining the base year HCD data and MAGICC/SCENGEN projected changes, a new HCD file considering climate change can be generated for MEPDG by following the steps:

- **Obtain historical data without climate change**. Based on the GPS coordinates and the surrounding geography of the test sites, select the most appropriate weather stations from the MEPDG climate database and obtain the HCD file from the MEPDG software website. The data in the HCD file represent the historical data without climate change. Statistical parameters are generated for these stations, as shown in Table 5.3.
- **Generate climate change statistics**. Identify the GPS gird box in the MAGICC/SCENGEN software for the test sites and generate the statistical parameters of the change (such as mean change and standard deviation) for each location. Example of results by season is illustrated in Table 5.7. The step-by-step guideline on how to generate climate change parameters can be referenced in the MAGICC/SCENGEN User's Manual (Wigley, 2008).
- **Generate after climate change HCD file**. With the base year statistics and the potential change in mean, standard deviation and possible extremes, the statistics of after climate change data can be determined. Historical data on hourly temperature was assumed to be normally distributed and this served as a platform to generate values that reflect changes should potential climate change occur. For precipitation, its percentage change under individual climate change scenarios was calculated and applied to the historic data. It is assumed that there will be no significant changes in wind speed, percentage sunshine or relative humidity should climate change occur at these locations and hence their original datasets were used throughout the study. This assumption is made because presently there is no software/tool which has the capability to project these changes under climate change. The newly generated data are then updated in the climatic files following the HCD file format requirements, and a new HCD file is created for that climate change scenario. Since multiple emission models, variability levels and analysis years exist, multiple new HCD files are

created for each location.

The newly generated HCD files represent climatic conditions after climate change and were imported into the MEPDG software to generate performance predictions for the after climate change scenarios.

Pavement Performance Comparisons and Analysis

The performance indicators used for flexible pavements in this study were alligator (bottom-up) cracking and rutting. For rigid pavement structures, the performance indicators were mean joint faulting and load related transverse slab cracking for JPCP and punchouts for CRCP. Functional performance for all pavement types was defined by time (pavement age) dependent pavement roughness quantified as a predicted International Roughness Index (IRI). As described in Chapter 4, IRI is predicted using a regression equation with computed pavement distresses, initial (as constructed) IRI, and "site/climate" factors as the primary independent variables. Different empirical functions are used for flexible pavement structures, JPCP and CRCP.

Comparing Performance Results

MEPDG allows the user to test various assumptions or scenarios using pavement performance variables. In doing so, it provides output concerning the progression of pavement deterioration and performance and the adequacy of various pavement designs. To examine how climate change and its variability might affect the performance of pavement sections over time, comparisons and analyses were performed by assessing the following:

- Three analysis years (2030, 2050, and 2100) to identify a range of changes in temperature and precipitation;
- Three levels of climate change variability (low, medium, and high) to represent the sensitivity of climate change to CO_2 emissions;
- Four emission models (A1B, A2, B1, and B2) to represent different future policy scenarios.

As noted earlier, the primary objective of the MEPDG analysis is to evaluate relative, not absolute, changes in pavement performance between baseline and future climate change scenarios. As a result, all the following results are presented in the format of relative performance change in percentage compared to the base year scenario in 2010. The performance comparisons for the three pavement sections are given in Appendix E.

For the purpose of illustration, only the results of the JPCP section are analyzed here. Figures 5.2, 5.3 and 5.4 show the relative change in IRI, faulting and transverse cracking for three scenarios considered for JPCP. The three scenarios are based on analysis year, climate change variability and emission models.

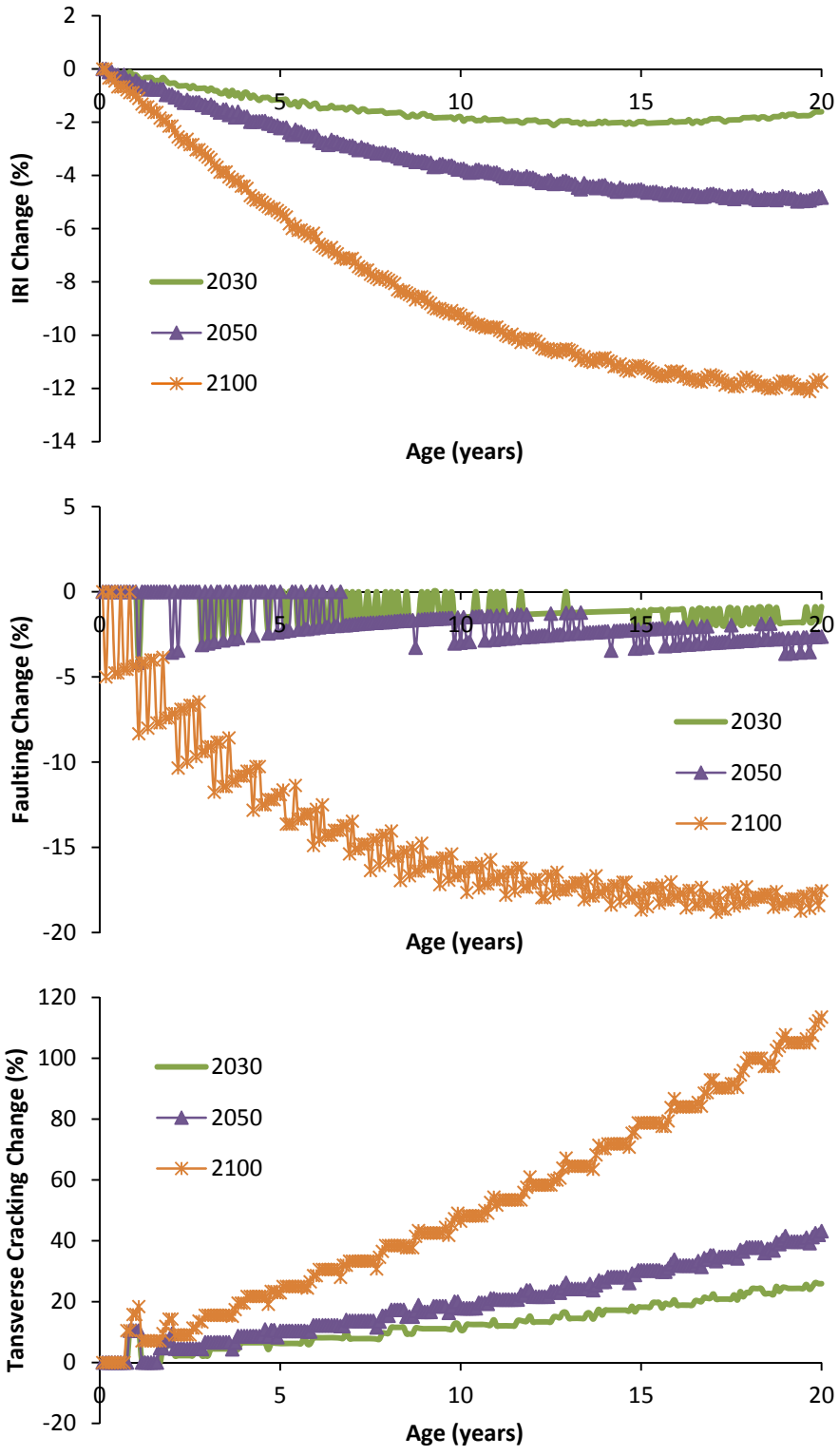

Figure 5.2 Analysis year comparisons (to the 2010 baseline design)

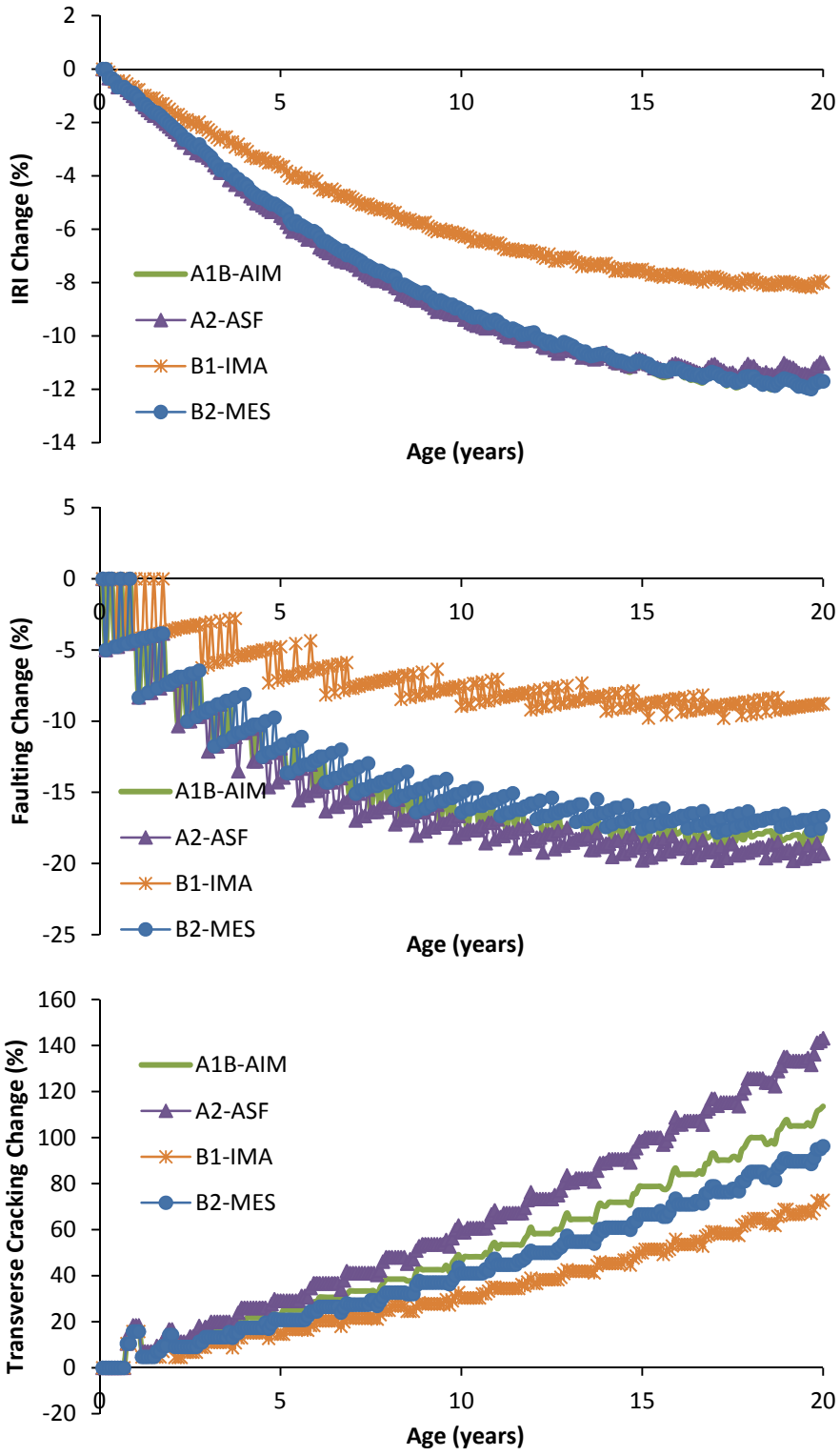

Figure 5.3 Emission model comparisons (to the 2010 baseline design)

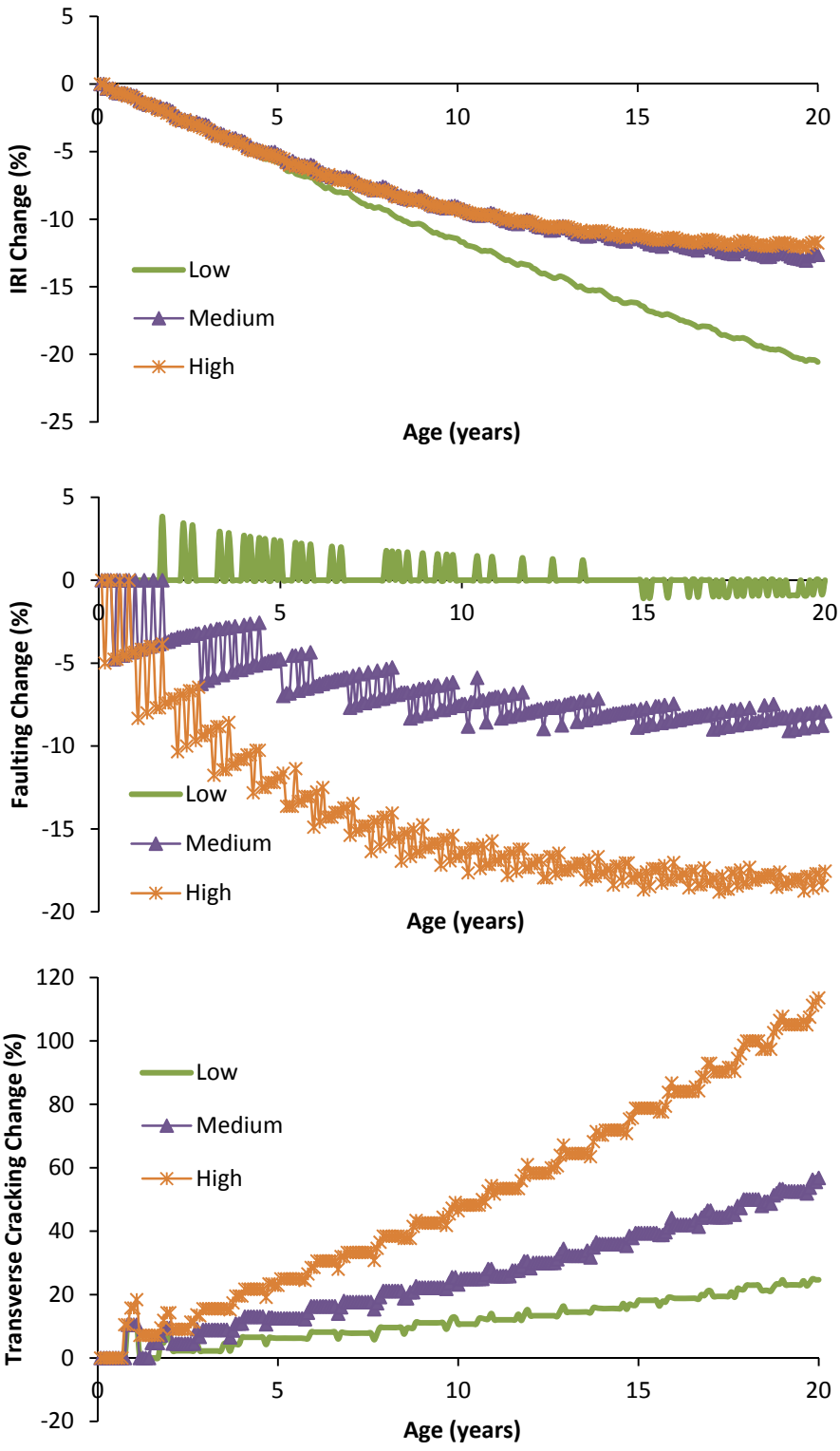

Figure 5.4 Climate change variability level comparisons (to the 2010 baseline design)

Influence of Analysis Year

For all three distresses, the most significant impact of climate change on pavement performance was observed in year 2100 as shown in Figure 5.2. This was due to a projected increase in extreme climate change events with time. Deterioration trends for roughness and faulting are identical and support the knowledge that faulting is a major contributing factor in the formation of roughness in rigid pavements (WSDOT, 2011). As respective relative percentages of roughness and faulting in 2010, the plot shows reduction in the two distresses with increasing years. The damage observed for both is however minimal and is less than 20%. A more profound impact of climate change is observed with transverse cracking. Transverse cracks are usually caused by a combination of heavy load repetitions and stresses due to temperature gradient, moisture gradient and drying shrinkage (Huang, 2004). The high relative percentages seen in Figure 5.2 for transverse could primarily be a result of extremes in temperature gradient, moisture gradient or drying shrinkage from 2030 to 2100. Such an increase in rate of transverse cracking could lead to the formation of other distresses and reduce pavement serviceability should climate change occur.

Influence of Variability level

Figure 5.3 shows the effect of different variability levels of carbon dioxide in the atmosphere on pavement performance. High levels of carbon dioxide represent the greatest propensity to climate change and produced the most pronounced deterioration for all three distresses. Following the plot in Figure 5.2, deterioration trends for roughness and faulting show reverse progression relative to 2010 distresses. These are minimal compared to the formation of transverse cracks. Generally, as observed in all three distresses, the plot supports the notion that activity in pavement distress formation has an increasing effect as carbon dioxide variability levels move from low to high.

Influence of emission models

The plot in Figure 5.4 illustrates how four climate change emission scenario families: A1, A2, B1 and B2 affect deterioration patterns for the three identified JPCP distresses used in the research. Observed trends for roughness and faulting show that maximum impact on pavement performance occur under the A1, A2 and B2 family scenarios where as B1 had a lower impact. This supports the scientific premise that of the four listed scenario families, climate change is significantly enhanced under A1, A2 and B2 families due to high emission levels of carbon dioxide for A1 and A2, and medium levels of emission for the B2 family (IPCC, 2011). B1 is characterized by low emission levels of carbon dioxide. The four emission scenarios are clearly distinguished in transverse cracking where A2 shows the most active deterioration pattern followed by A1, B2 and B1 in decreasing effect. This also supports the premise that A2 is associated with high emission levels, A1 with medium high emission levels, B2 with medium low emission levels and B1 with low emission levels.

Model Calibration to Local Climate Change Conditions

To evaluate the relative impact of each calibration coefficient to the model estimation, the concept of "elasticity" proposed at Washington Department of Transportation (Li et al, 2006, Li et al 2009) was adopted and defined as:

$$\mathrm{E}_{\mathrm{distress}}^{\mathrm{Ci}} = \frac{\partial(\mathrm{distress})/\mathrm{distress}}{\partial(\mathrm{Ci})/\mathrm{Ci}} \quad \text{(Eqn. 5.4)}$$

Where $\mathrm{E}_{\mathrm{distress}}^{\mathrm{Ci}}$ - Elasticity of factor Ci for the associated distress condition; $\partial(\mathrm{distress})$ - change in the estimated distress associated with a change in the factor Ci; $\partial(\mathrm{Ci})$ - change in the factor Ci; $\mathrm{distress}$ – estimated distress using default calibration factors; Ci – default value of Ci.

Elasticity can be zero, positive, or negative. Zero means the factor has no impact on the model; positive means the estimation increases as the factor increases; negative means the estimation decreases as the factor increases. The bigger the absolute value of elasticity, the greater impact the factor has on the model. The elasticity values may vary with the selected design parameters and related inputs. However, it is the order from high to low, not the values to rank the calibration factors, that is adjusted during the calibration process. Numerous MEPDG runs indicate that the order remained about the same (Li et al, 2006, Li et al 2009). Through this process, the numbers of MEPDG runs are significantly reduced, and the calibration process will begin with those factors ranking high based on the elasticity value.

Based on the best available information for the test sites, the elasticity results shown in Tables 5.9, 5.10, and 5.11 demonstrate that some coefficients are much more sensitive than others, which provides an order of the coefficients to be calibrated. In addition, due to the mathematical formation of the prediction models: (a) the asphalt concrete fatigue models should be calibrated before the longitudinal and alligator cracking models, (b) for the rutting model, calibration factors Br2 and Br3 should be adjusted before Br1, (c) the CRCP fatigue models should be calibrated before the punchout models.

Default values of the calibration coefficients are provided in the MEPDG software for each prediction model, as shown in Tables 5.9, 5.10, and 5.11. Based on sensitivity analysis results, the coefficients are calibrated in the order of high to low elasticity. First, a baseline MEPDG run without considering climate change is performed. By comparing the performance of baseline design and after climate change scenario, the direction of the coefficient change can be determined. For example, in Figure 5.3, the 2100 climate change scenario produces more transverse cracking than the baseline scenario. The sensitivity results show that the most sensitive coefficient is C1 with an elasticity of -7.579, which indicates that the predictions decrease as the coefficients increase. Thus for that case, the calibrated coefficients should be smaller than the default value in MEPDG, which is 2.0. The trial analyses can be developed with a decrement of 0.01 starting from the default value until the performance predictions are lower than those for the baseline. With two confidence lines: one generating higher predictions and the other lower, the calibrated coefficient can be linearly interpolated. This process is then repeated with the second ranked coefficient. The process will stop when the differences of the

performance predictions between those from the baseline and after climate change scenario converge to an acceptable level. The performance models were combined with the adjusted calibration coefficients and selected as the final calibration results.

The calibration results are shown in Tables 5.9, 5.10, and 5.11 for JPCP, CRCP, and flexible pavement sections respectively. The results are developed based on the A1B model using a high variability level in scenario year 2100. The same procedure can be applied to calibrate the coefficients for other scenarios. It was noted that most of the models converged after the second order coefficients were calibrated. Due to the fact that some elasticity values were relatively large, the calibrated coefficients did not demonstrate any significant difference to the default values. In other words, even though the changes of these model coefficients were minor, the impacts to performance prediction were substantial.

TABLE 5.9 Local Calibration Results for JPCP (A1B model, 3% traffic growth)

Calibration Factor		Elasticity Factor	National Default	Calibrated Coefficient		
				2030	2050	2100
Cracking	C1	-7.579	2	**1.971**	**1.961**	**1.894**
	C2	-7.079	1.22	**1.216**	**1.214**	**1.224**
	C4	0.658	1	1	1	1
	C5	-0.579	-1.98	-1.98	-1.98	-1.98
Faulting	C1	0.42	1.0184	1.0184	1.0184	1.0184
	C2	0.08	0.91656	0.91656	0.91656	0.91656
	C3	0.07	0.0021848	0.0021848	0.0021848	0.0021848
	C4	0.01	0.000883739	0.000883739	0.000883739	0.000883739
	C5	0.07	250	250	250	250
	C6	0.57	0.4	**0.396**	**0.391**	**0.313**
	C7	0.55	1.8332	1.8332	1.8332	1.8332
	C8	0.00	400	400	400	400
Smoothness	C1	0.011	0.8203	0.8203	0.8203	0.8203
	C2	0.003	0.4417	0.4417	0.4417	0.4417
	C3	0.077	1.4929	1.4929	1.4929	1.4929
	C4	0.003	25.24	25.24	25.24	25.24

Validation

The calibrated coefficients were used as input into the MEPDG software and runs were conducted. Figure 5.5 provides comparisons of the performance predictions for JPCP section before and after calibration assuming climate change occurred. It demonstrates that the local calibration approach is effective and that climate change effects can be fully incorporated into any pavement design process.

TABLE 5.10 Local Calibration Results for CRCP (A1B model, 3% traffic growth)

Calibration Factor		Elasticity Factor	National Default	Calibrated Coefficient		
				2030	2050	2100
Fatigue	C1	-0.5	2	**2.004**	**2.004**	**2.025**
	C2	-0.5	1.22	**1.224**	**1.224**	**1.224**
Punchout	C3	0.5	216.842	**227.841**	**226.579**	**225.402**
	C4	-0.25	33.1579	33.1579	33.1579	33.1579
	C5	-0.33	-0.58947	-0.58947	-0.58947	-0.58947
Smoothness	C1	-0.01	3.15	3.15	3.15	3.15
	C2	-0.02	28.35	28.35	28.35	28.35

TABLE 5.11 Local Calibration Results for Flexible Pavement (A1B model, 3% traffic growth)

Calibration Factor		Elasticity Factor	National Default	Calibrated Coefficient		
				2030	2050	2100
AC Fatigue Damage	Bf1	-3.3	1	1	1	1
	Bf2	-40	1	**0.999**	**0.999**	**0.998**
	Bf3	20	1	**1.002**	**1.003**	**1.004**
Longitudinal Cracking	C1	-0.2	7	**7.010**	**6.985**	**6.931**
	C2	1	3.5	**3.392**	**3.211**	**3.093**
	C3	0	0	0	0	0
	C4	0	1000	1000	1000	1000
Alligator Cracking	C1	1	1	**0.996**	**0.996**	**0.993**
	C2	0	1	1	1	1
	C3	0	6000	6000	6000	6000
Rutting	Br1	0.6	1	1	1	1
	Br2	20.6	1	**1.022**	**1.039**	**1.070**
	Br3	8.9	1	**1.001**	**1.001**	**1.001**
Smoothness	C1	NA	40	40	40	40
	C2	NA	0.4	0.4	0.4	0.4
	C3	NA	0.008	0.008	0.008	0.008
	C4	NA	0.015	0.015	0.015	0.015

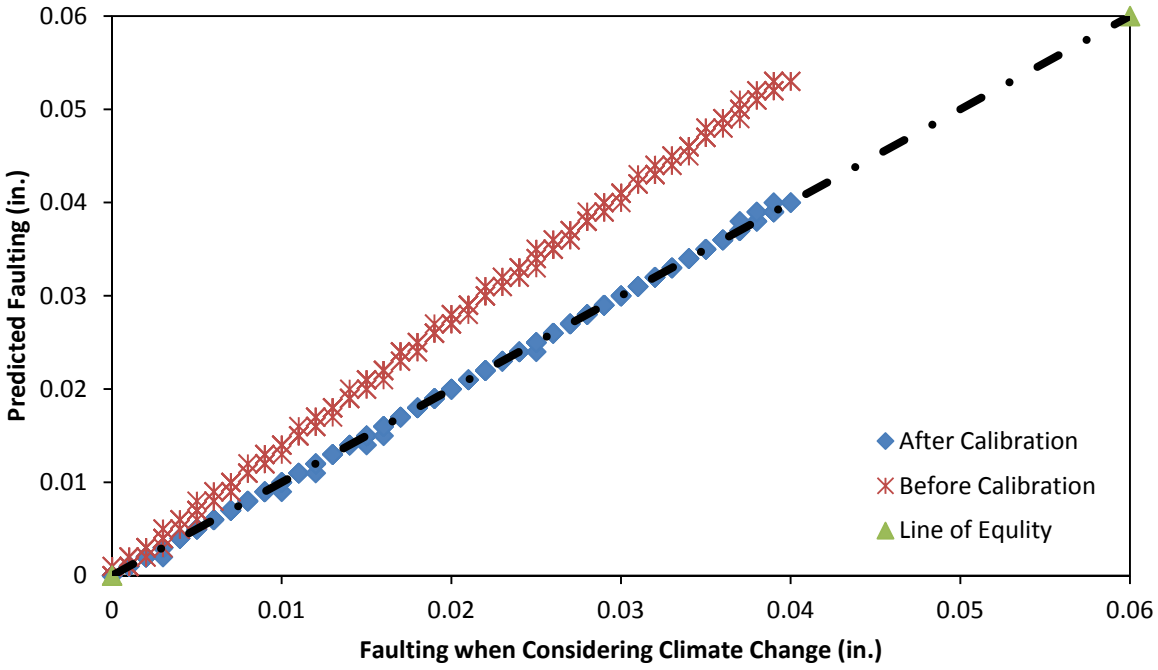

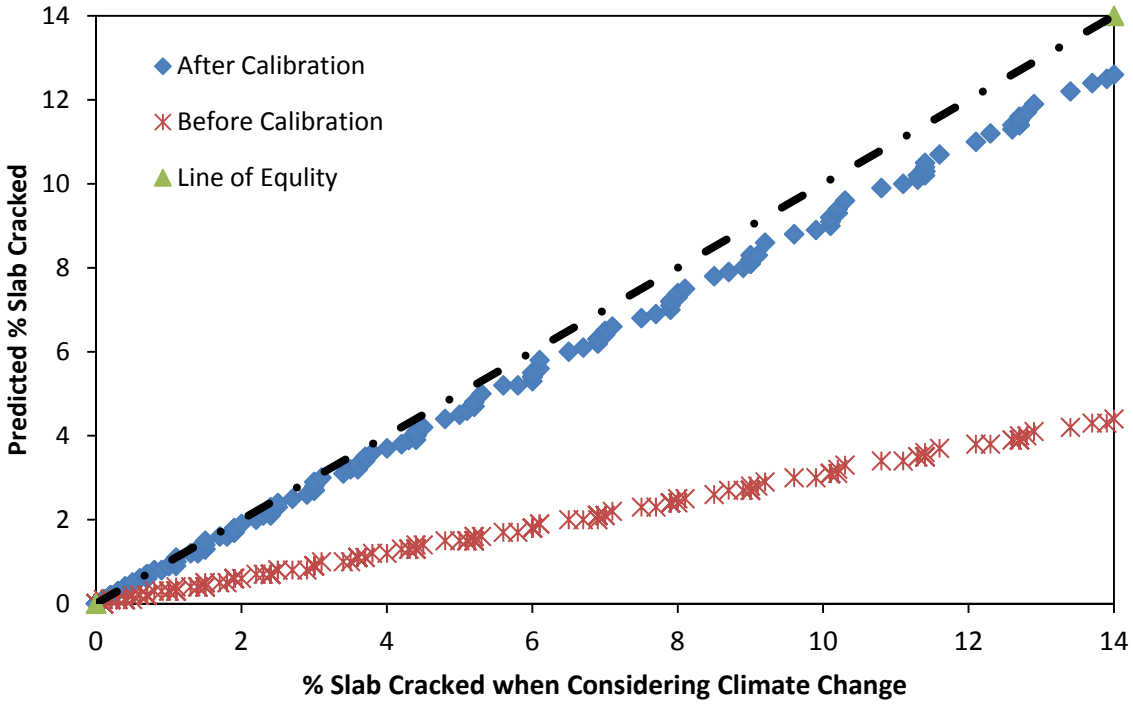

Figure 5.5 Validation of the calibration coefficients

6. Conclusions and Recommendations

Conclusions

Current and past pavement designs generally assume a static climate whose variability has not been considered. The notion of anthropogenic climate change challenges this assumption and raises the possibility that pavement performance may be altered leading to premature deterioration. Given anticipated climate changes and the inherent uncertainty associated with such changes, a pavement could be subjected to very different climatic conditions over the design life and might be inadequate to withstand future climate forces that impose stresses beyond environmental factors currently considered in the design process. To explore the impacts of potential climate change and its uncertainty on pavement performance and therefore pavement design, this study integrates two tools: MAGICC/SCENGEN to address the potential climate change and its uncertainty and the MEPDG software to analyze the deterioration of pavement performance. In the process, three important questions were addressed: (1) How does pavement performance deteriorate differently with climate change and its uncertainty? (2) What is the risk if climate change and its uncertainty are not considered in pavement design? and (3) How do pavement designers respond and incorporate this change into the pavement design process?

Based on the concept of local calibration for MEPDG prediction models, a framework to incorporate the climate change effects into the mechanistic-empirical based pavement design was developed by calibrating the coefficients performance models. Three test sites located in the northeast United States were identified to illustrate the application of the framework. This study has established a procedure for highway agencies to follow which shows how climate change can be integrated into pavement design as an adaptation strategy.

Limitations

Limitations encountered in developing the framework to model climate change uncertainty are listed below:

- The Transportation Research Board's Special Report 290 (*13*) noted the five climate changes of particular importance to transportation as increases in very hot days and heat waves, increases in Arctic temperatures, rising sea levels, increases in intense precipitation events and increases in hurricane intensity. In this study, the extremes of these changes could not easily be modeled.
- Secondly, MEPDG requires five climatic data inputs: temperature, precipitation, wind speed, cloud cover and humidity. Since MAGICC/SCENGEN only produces temperature and precipitation projections, the other three parameters are not included and their impacts not quantified.
- The three test sites used in the paper were based on available data in the LTPP database on pavements along the East Coast corridor. In actual design, calibration uses data from accessible databases as well as experimentation on

representative pavement sections. Conducting experiments on representative sections could be tenuous and was not undertaken in this research.

Recommendations

To overcome some of the limitations mentioned above, the following solutions are proposed:

- Where resources are available, experiments on representative pavement sections are needed, using subgroups amongst the selected sections. Subgroups need to be formed based on the most critical input factors such as traffic level, pavement types, and climatic regions and the calibration process should be conducted for these subgroups.
- The effort involved in exploring scenarios and variability should not diminish or be underestimated. As climate change researchers come to a better understanding of climate change sensitivity and focus on areas of its uncertainty, highway designers should streamline methods by which climate is incorporated into the design process.
- Finally, it should be realized that various inputs other than regional climate data and potential climate change impact are critical in designing pavements. Such inputs include local material characterization, construction specifications and pavement preservation and maintenance practices. In this study, only climatic inputs were considered in the local calibration process. Future research is required to include all these inputs such as those listed above in combination with climate change parameters into MEPDG and subsequently into the local calibration procedure.

The application of the framework to three pavement sections demonstrated significant impacts due to climate change. Incorporating future scenarios into pavement design is important.

7. References

American Society of Testing and Materials. E867. (2006). Standard Terminology Relating to Vehicle-Pavement System, www.astm.org.

Andronova, N.G., and M.E. Schlesinger, (2001). Objective estimation of the probability density function for climate sensitivity. *J. Geophys. Res.*, 106, 22605–22612.

Annan, J.D., et al., (2005). Efficiently constraining climate sensitivity with ensembles of paleoclimate simulations. *Scientific Online Letters on the Atmosphere*, 1, 181–184.

Applied Research Associates Inc. (2004a). *Guide for Mechanistic-Empirical Design of New and Rehabilitated Pavement Structures: Part 2 Chapter 3 Design Input - Climatic Effects*. ERES Consultants Division, Urbana Champion, IL.

Applied Research Associates Inc. (2004b). Guide for Mechanistic-Empirical Design of New and Rehabilitated Pavement Structures. *Smoothness Prediction Models for Flexible Pavements*. Appendix OO.

Applied Research Associates Inc. (2004c). Guide for Mechanistic-Empirical Design of New and Rehabilitated Pavement Structures. *Calibration of Permanent Deformation Models for Flexible Pavements*. Appendix GG.

Applied Research Associates Inc. (2004d). Guide for Mechanistic-Empirical Design of New and Rehabilitated Pavement Structures. *Calibration of Fatigue Cracking Models for Flexible Pavements*. Appendix II, 2004.

Applied Research Associates Inc. (2004e). Guide for Mechanistic-Empirical Design of New and Rehabilitated Pavement Structures. Transverse Joint Faulting Model. Appendix JJ.

Applied Research Associates Inc. (2004f). Guide for Mechanistic-Empirical Design of New and Rehabilitated Pavement Structures. Transverse Cracking for JPCP. Appendix KK.

Applied Research Associates Inc. (2004g). Guide for Mechanistic-Empirical Design of New and Rehabilitated Pavement Structures. Punchouts in CRCP. Appendix LL.

Applied Research Associates Inc. (2004h). Guide for Mechanistic-Empirical Design of New and Rehabilitated Pavement Structures. Part 2: Design Inputs; Chapter 2: Material Characterization.

Applied Research Associates Inc. (2004i). Guide for Mechanistic-Empirical Design of New and Rehabilitated Pavement Structures. Part 2: Design Inputs; Chapter 4: Traffic.

Asphalt Institute. (1982). *Research and Development of the Asphalt Institute's Thickness Design Manual (MS-1)*. 9th edition. Research Report 82-2, 1982.

Baladi, Gilbert Y. (1990) *Highway Pavement* (NHI Course No. 13114). FHWA, McLean VA, May.

Bonnaure, F., A. Gravois, and J. Udron. (1980). *A New Method of Predicting the Fatigue Life of Bituminous Mixes*. Journal of the Association of Asphalt Paving Technologist, Vol. 49, 1980.

Carpenter S.H., M. I. Darter and B.J. Dempsey. (1981) *A Pavement Moisture Accelerated Distress Identification System: Users Manual*, Volume 2.

Darter, M. I. (1988). CRCP Distress Study on I-77 Fairfield and Chester Counties, South Carolina. ERES Consultants, Inc.

Department for Environment, Food and Rural Affairs (Defra). (2010). UK Climate Impacts Programme, http://www.ukcip.org.uk. Accessed September 3, 2010.

ERES Consultants, Inc. (1987) *Pavement Design Principles and Practices*. Champaign, Illinois, National Highway Institute, Washington D.C.

Federal Highway Administration (FHWA). (2001). Traffic Monitoring Guide. FHWA, McLean, VA.

Federal Highway Administration (FHWA). (2010). Long-Term Pavement Performance (LTPP) Database, http://www.fhwa.dot.gov/pavement/ltpp, Accessed October 26, 2010.

Foley A.M. (2010) Uncertainty in regional climate modeling: A review. *Progress in Physical Geography,* vol. 34 no. 5, p: 647-670.

Forest, C.E., et al., (2002). Quantifying uncertainties in climate system properties with the use of recent climate observations. *Science*,295, 113–117.

Forest, C.E., P.H. Stone, and A.P. Sokolov, (2006). Estimated PDFs of climate system properties including natural and anthropogenic forcings. *Geophys. Res. Lett.*, **33**, L01705, doi:10.1029/2005GL023977.

Forster, P.M.D., and K.E. Taylor, 2006: Climate forcings and climate sensitivities diagnosed from coupled climate model integrations. *J. Clim.*, 19, 6181–6194.

Frame, D.J., et al., (2005). Constraining climate forecasts: The role of prior assumptions. *Geophys. Res. Lett.*, 32, L09702, doi:10.1029/2004GL022241.

Gregory, J.M., et al., (2002). An observationally based estimate of the climate sensitivity. *J. Clim.*, 15, 3117–3121.

Haas, R., L.C. Falls, D. MacLeod and S. Tighe. (2004) *Climate Impacts and Adaptations on Roads in Northern Canada*. Cold Climates Conference, Regina, AB. 2004.

Hegerl, G.C., T.J. Crowley, W.T. Hyde, and D.J. Frame, (2006). Climate sensitivity constrained by temperature reconstructions over the past seven centuries. *Nature*, 440, 1029–1032.

Huang, Y.H. (2004). *Pavement Analysis and Design (2nd Edition)*. Prentice Hall Publishing Press, Upper Saddle River, New Jersey.

Intergovernmental Panel on Climate Change (IPCC). (1990) *Climate Change, the IPCC Scientific Assessment*. Edited by J.T. Houghton, G.J. Jenkins and J.J. Ephraums. Cambridge University Press, Cambridge.

Intergovernmental Panel on Climate Change (IPCC). (1995) *The Science of Climate Change*, *Contribution of Working Group I to the Second Assessment Report of the Intergovernmental Panel on Climate Change*. Edited by J.T. Houghton, L.G. Meira Filho, B.A. Callander, N. Harris, A. Kattenberg and K. Maskell.

Intergovernmental Panel on Climate Change (IPCC). (2001) *Climate Change 2001: The Scientific Basis. Contribution of Working Group I to the Third Assessment Report of the Intergovernmental*

Panel on Climate Change. Edited by Houghton, J.T.,Y. Ding, D.J. Griggs, M. Noguer, P.J. van der Linden, X. Dai, K. Maskell, and C.A. Johnson. Cambridge University Press, Cambridge, United Kingdom and New York, NY, USA,

Intergovernmental Panel on Climate Change (IPCC). (2007a) *Summary for Policymakers*. In: Climate Change 2007: The Physical Science Basis. Contribution of Working Group I to the Fourth Assessment Report of the Intergovernmental Panel on Climate Change. Edited by Solomon, S., D. Qin, M. Manning, Z. Chen, M. Marquis, K.B. Averyt, M.Tignor and H.L. Miller. Cambridge University Press, Cambridge, United Kingdom and New York, NY, USA.

Intergovernmental Panel on Climate Change (IPCC). (2007b). *IPCC Fourth Assessment Report: Climate Change 2007 (AR4)*, Cambridge University Press, New York, NY, USA.

Intergovernmental Panel on Climate Change (IPCC). (2011). IPCC Special Report Emissions Scenarios. http://www.ipcc.ch/pdf/special-reports/spm/sres-en.pdf, Accessed on March 15, 2011.

Kheshgi, Haroon S., Roger C. Prince, and Gregg Marland. (2000). The Potential of Biomass Fuels in the Context of Global Climate Change: Focus on Transportation Fuels. *Annual Review of Energy Environments* Vol. 25, 2000, pp:199–244.

Knutti, R., T.F. Stocker, F. Joos, and G.-K. Plattner. (2002). Constraints on radiative forcing and future climate change from observations and climate model ensembles. *Nature*, 416, 719–723.

LaCourseiere, S.A., M.I. Darter, and S.A. Smiley. (1978). Structural Distress Mechanisms in Continuously Reinforced Concrete Pavement. Transportation Engineering Series No. 20, University of Illinois at Urbana-Champaign.

Li J.H., Muench S. T., Mahoney J. P., Sivaneswaran N., Pierce L. M. (2006). Calibration of NCHRP 1-37A Software for the Washington State Department of Transportation: Rigid Pavement Portion. Transportation Research Record: Journal of the Transportation Research Board No. 1949, Transportation Research Board Business Office, Washington, DC, pp 43-53

Li, J.H., Pierce L. M, Uhlmeyer J. S. (2009). Calibration of Flexible Pavement in Mechanistic–Empirical Pavement Design Guide for Washington State. Transportation Research Record: Journal of the Transportation Research Board No. 2095, Transportation Research Board Business Office, Washington, DC, pp 73-83

Meyer M., A. Amekudzi and J.P. O'Har. (2010) *Transportation Asset Management Systems and Climate Change*. In Transportation Research Record: Journal of the Transportation Research Board, No 2160, Transportation Research Board of the National Academies, Washington, D.C., pp.12-20.

Meyer M., and B. Wiegel. (2011). Climate Change and Transportation Engineering. Preparing for a Sustainable Future. *Journal of Transportation Engineering*, Vol. 137, pp. 393-403

Mills, B.N., S.L. Tighe, J. Andrey, J. Smith, S. Parm. and K. Huen. (2007). *The Road Well-Traveled: Implications of Climate Change for Pavement Infrastructure in Southern Canada*. Final Technical Report. University of Waterloo, Canada.

Moulton, U.K. *Highway Subdrainage Design*. (1980) Report No. FHWA-TS-80-224. FHWA.

National Oceanographic and Atmospheric Administration (NOAA). (2010). National Climatic Data Center, http://www.ncdc.noaa.gov. Accessed September 10, 2010.

Papagiannakis, A.T. and E.A. Masad. (2008). *Pavement Design and Materials.* John Wiley and Sons.

Saleh M., M. Mamlouk and E. Owusu-Antwi. Mechanistic roughness model based on vehicle-pavement interaction" In *Transportation Research Record: Journal of the Transportation Research Board*, No. 1699, Transportation Reseaarch Board of the National Academies, Washington D.C., 2000, pp 114-120.

Santer, B.D., Wigley, T.M.L., Schlesinger, M.E. and Mitchell, J.F.B. (1990). *Developing Climate Scenarios from Equilibrium GCM Results*. Max-Planck-Institut für Meteorologie Report No. 47, Hamburg, Germany.

Schneider von Deimling, T., H. Held, A. Ganopolski, and S. Rahmstorf, (2006). Climate sensitivity estimated from ensemble simulations of glacial climate. *Clim. Dyn.*, 27, 149–163.

Selezneva O.I., D. Zollinger, M. Darter. (2001). Mechanistic Analysis of Factors Leading to Punchout Development for Improved CRCP Design Procedures. Proceedings of the 7th International conference on Concrete Pavements, pp. 731-745, September.

Selezneva, O.I. (2002). Development of Mechanistic-Empirical Damage Assessment Procedures for CRC Pavements with Emphasis on Traffic Loading Characteristics. Ph.D. Dissertation, West Virginia University.

Tran Nam H. and Hall Kevin D. (2007). Development and Influence of Statewide Axle Load Spectra on Flexible Pavement Performance, *Transportation Research Record: Journal of the Transportation Research Board*, No. 2037, Transportation Research Board of the National Academies, Washington, D.C., pp. 106–114.

Transportation Research Board (TRB). (2009) *A Transportation Research Program for Mitigating and Adapting to Climate Change and Conserving Energy*. Transportation Research Board Special Report 299, Washington D.C.

Transportation Research Board (TRB) (2010). Mechanistic-Empirical Pavement Design Guide (MEPDG). http://onlinepubs.trb.org/onlinepubs/archive/mepdg/home.htm. Accesses on September 2010.

Transportation Research Board (TRB). (2011). Mechanistic-Empirical Pavement Design Guide: Climate Data, http://onlinepubs.trb.org/onlinepubs/archive/mepdg/climatic_state.htm, accessed on March 10, 2011.

Transportation Research Board. (2008) *Potential Impacts of Climate Change on US Transportation*. Transportation Research Board Special Report 290, Washington D.C., 2008.

U.S. Climate Change Science Program (CCSP). (2008) *Impacts of Climate Change and Variability on Transportation Systems and Infrastructure: Gulf Coast Study, Phase I*. Department of Transportation, Washington, DC, USA, 2008

U.S. Global Change Research Program (USGCRP) (2009). Global Climate Change Impacts in the United States. Thomas R. Karl, Jerry M. Melillo, and Thomas C. Peterson, (eds.). Cambridge University Press, New York, NY, USA. http://downloads.globalchange.gov/usimpacts/pdfs/climate-impacts-report.pdf

Walther, Gian-Reto, Eric Post, Peter Convey, Annette Menzel, Camille Parmesank, Trevor J. C. Beebee, Jean-Marc Fromentin, Ove Hoegh-Guldberg and Franz Bairlein. (2002). Ecological responses to recent climate change. *Nature*, Vol. 416 No. 28.

Wang Kelvin C. P., Li Qiang (2008), Database Support for the New Mechanistic-Empirical Pavement Design Guide (MEPDG). *Transportation Research Record: Journal of the Transportation Research Board*, No: 2087, pp: 109-119.

Washington Department of Transportation (WSDOT). (2011). WSDOT Pavement Guide, http://training.ce.washington.edu/wsdot/. Accessed on July 10, 2011.

Wigley, Tom M.L. (2008). *MAGICC/SCENGEN 5.3: USER MANUAL* (version 2). The National Center for Atmospheric Research (NCAR), Boulder, CO.

Yoder, E.J., and M.W. Witzcak. (1979) *Principles of Pavement Design*. New York: John Wiley & Sons.

Zollinger, D.G., and E.J. Barenberg. (1990). Continuously Reinforced Pavements: Punchouts and Other Distresses and Implications for Design. Project IHR - 518, Illinois Cooperative Highway Research Program, University of Illinois at Urbana-Champaign, March.

Zollinger, D.G., N. Buch, D. Xin, and J. Soares. (1998). Performance of CRCP Volume 6 – CRCP Design, Construction, and Performance. FHWA-RD-97-151, Report, U.S. Department of Transportation, Washington, DC, February.

APPENDIX A Formats of the Integrated Climatic Model Files

The Integrated Climatic Model uses several file formats for modeling pavement temperature and moisture profiles. The format of these files is outlined below.

ICM Files (*.icm)

ICM files are generated by the hourly climatic database and contain all of the information needed to run the Integrated Climatic Model numerical engine.

StartDate(YYYYMMDD) – EndDate(YYYYMMDD): The period for which this file contains data for.

19960701-20011231

Longitude, Latitude, Annual Water Table Depth(-1 if using seasonal), spring water table depth , summer water table, fall water table, winter water table, monthly average humidity (12 total-start January)

-86.23,32.18,227,-
1,10,20,19,10,64.8035,12.8717,44.1237,72.3013,69.6847,65.7183,70.4444,70.5253,75.7314,75.2074,74.7334,74.5993,72.8259,74.0491,75.2558

Month, Day, Year, Sunrise time (decimal-24 hour), sunset, daily solar radiation maximum. Sunrise/Sunset calculated from Lat/Long. Solar radiation data from rad.dat file, correct for Lat/Long.

7 1 1996 4.95899 19.041 3730.48

Hour, temperature, precipitation, wind speed, percent sunshine, hourly ground water depth.

0 72 0 0 100 20
1 71.1 0 0 100 20
2 70 0 3 100 20
3 70 0 0 100 20
4 70 0 3 75 20
5 72 0 0 100 20
6 77 0 6 100 20
7 82 0 6 100 20
8 87.1 0 7 100 20
9 90 0 7 100 20
10 91 0 7 100 20
11 93 0 5 75 20
12 91.9 0 5 25 20
13 93.9 0 6 100 20
14 95 0 5 75 20
15 93 0 5 100 20
16 91 0 6 100 20
17 89.1 0 5 100 20

18 86 0 3 100 20
19 84 0 4 100 20
20 81 0 4 100 20
21 80.1 0 4 100 20
22 79 0 5 100 20
23 77 0 3 100 20

Hourly Climatic Database Files (*.hcd)

Hourly climatic database files contain information for a specific weather station. To add a weather station to those that are available within the ME-PDG, create a new *.hcd file. Assign a number unused in the station.dat file (described below). Add that number to the station.dat file list.

YYYYMMDDHH,Temperature (F),Wind speed (mph),% Sun shine, Precipitation, Relative humidity.

1997060100,57.9,9,0,0.2,97
1997060101,57.9,9,0,0.35,97
1997060102,57.9,5,0,0.18,100
1997060103,59,9,0,0.06,93
1997060104,59,10,0,0.05,93
1997060105,59,12,0,0.07,96
1997060106,59,12,0,0.07,96
1997060107,60.1,9,0,0.03,96
1997060108,61,9,0,0.03,97
1997060109,62.1,9,0,0.06,96
1997060110,63,5,0,0,97
1997060111,64,4,0,0.01,96
1997060112,64.9,3,0,0.04,97
1997060113,68,0,0,0,90
1997060114,69.1,0,0,0,87
1997060115,69.1,0,0,0,84
1997060116,69.1,0,0,0,84
1997060117,69.1,0,0,0,78
1997060118,66.9,0,25,0,87
1997060119,64.9,4,100,0,97
1997060120,64,0,100,0,100
1997060121,62.1,0,50,0,100
1997060122,60.1,3,0,0,100
1997060123,62.1,0,0,0,100
1997060200,62.1,0,0,0,100

Station File (station.dat)

The station.dat file contains all of the hourly climatic database weather stations. Each weather station included has the following information.

Weather station number, weather station abbreviation, location (city|state), latitude, longitude, elevation, first date in file (YYYMMDD)

25704,ADK,ADAK|AK,ADAK NAS,51.53,-176.39,17,19960701

APPENDIX B Weigh-In-Motion (WIM) Traffic Results

This appendix documents the monthly adjustment factors, and vehicle class distribution factors used for each of the case study sections. The figures are organized as follows:

- JPCP pavement section
    - Load specta
        - Class 5 single axles – Figure B-1
        - Class 9 single axles – Figure B-2
        - Class 9 tandem axles – Figure B-3
        - Class 7 tridem axles – Figure B-4
        - Class 10 tridem axles – Figure B-5
    - Monthly adjustment factors – Figure B-6
    - Vehicle class distribution – Figure B-7
- CRCP pavement section
    - Load specta
        - Class 5 single axles – Figure B-8
        - Class 9 single axles – Figure B-9
        - Class 9 tandem axles – Figure B-10
        - Class 7 tridem axles – Figure B-11
        - Class 10 tridem axles – Figure B-12
    - Monthly adjustment factors – Figure B-13
    - Vehicle class distribution – Figure B-14
- AC pavement section
    - Load specta
        - Class 5 single axles – Figure B-15
        - Class 9 single axles – Figure B-16
        - Class 9 tandem axles – Figure B-17
        - Class 7 tridem axles – Figure B-18
        - Class 10 tridem axles – Figure B-19
    - Monthly adjustment factors – Figure B-20
    - Vehicle class distribution – Figure B-21

1. JPCP Pavement Section (09-4008)

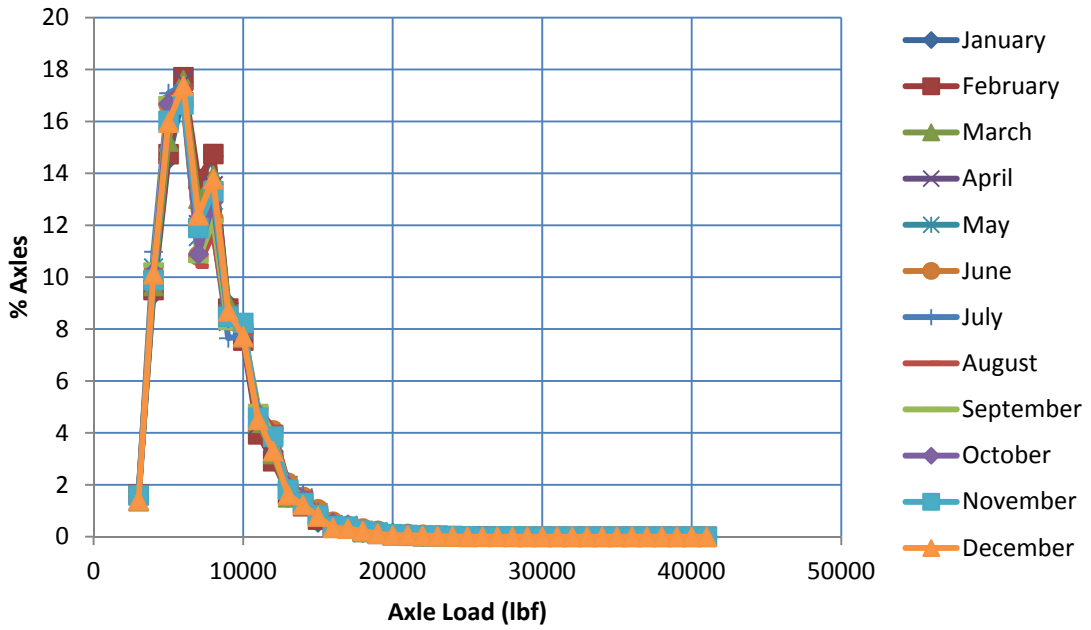

Figure B-1 Load Spectra for Vehicle Class 5 Single Axles

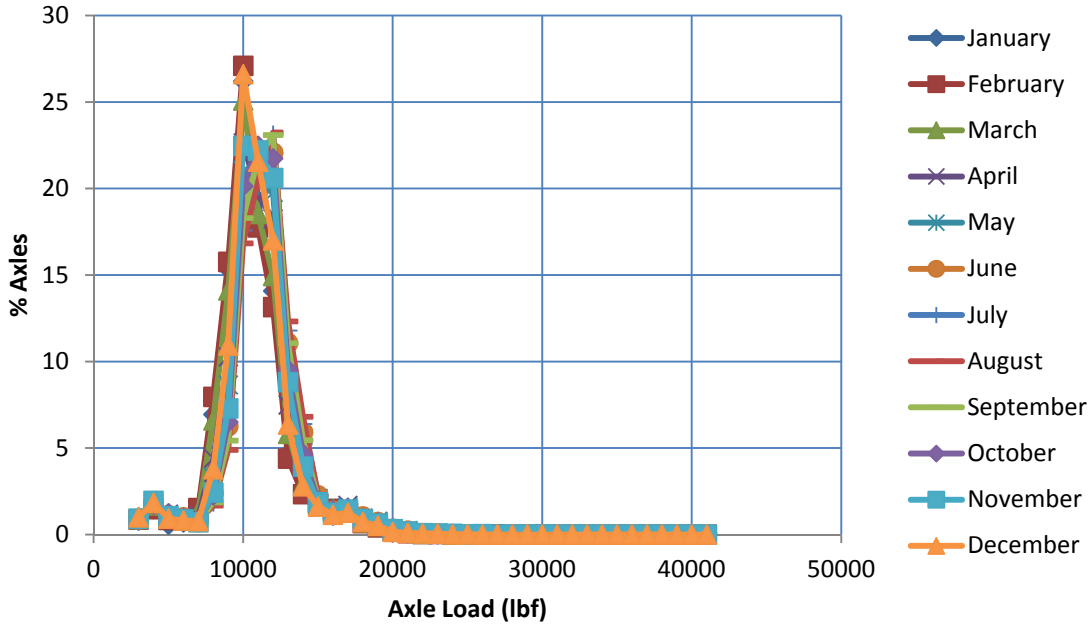

Figure B-2 Load Spectra for Vehicle Class 9 Single Axles

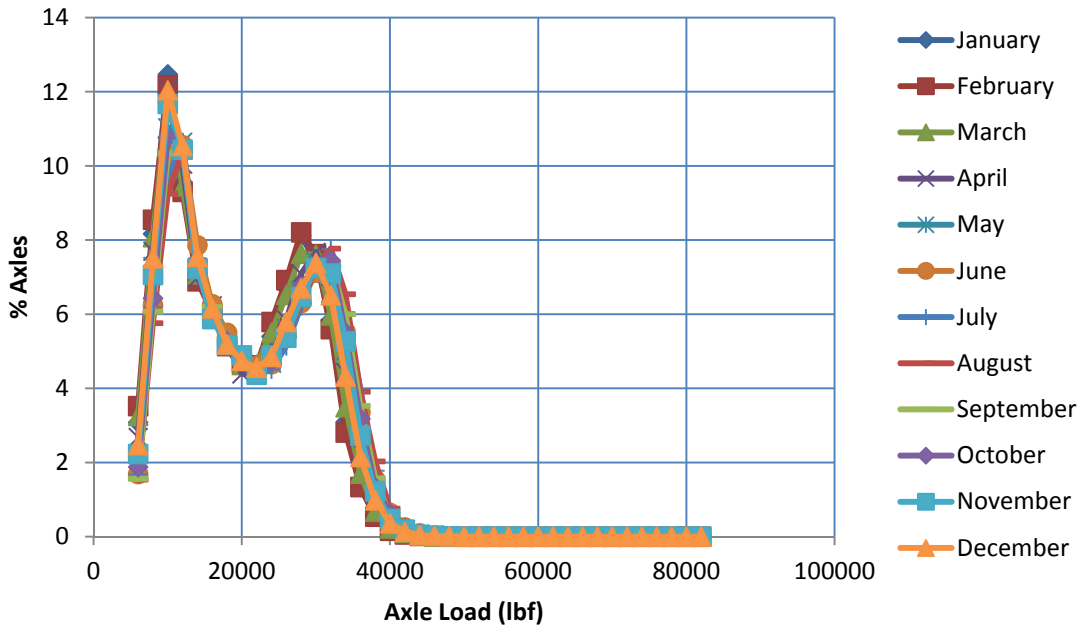

Figure B-3 Load Spectra for Vehicle Class 9 Tandem Axles

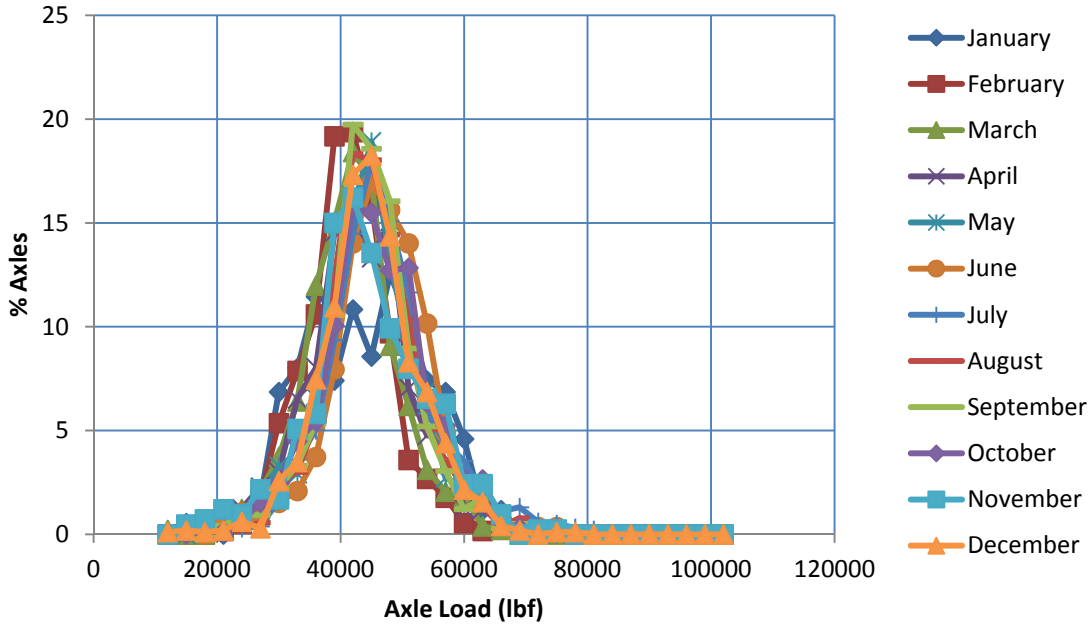

Figure B-4 Load Spectra for Vehicle Class 7 Tridem Axles

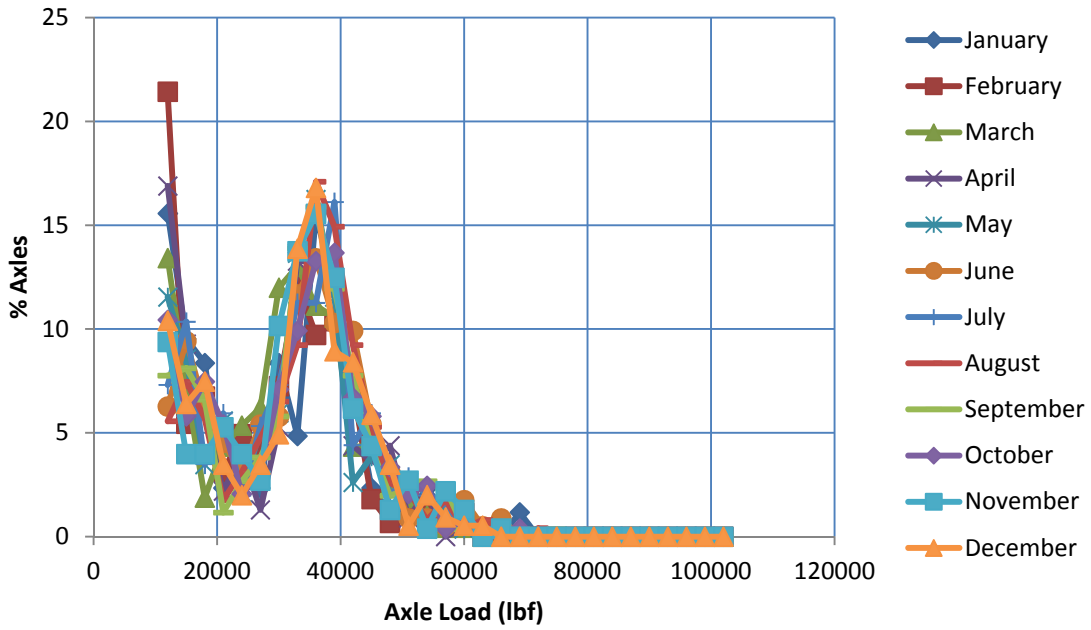

Figure B-5 Load Spectra for Vehicle Class 10 Tridem Axles

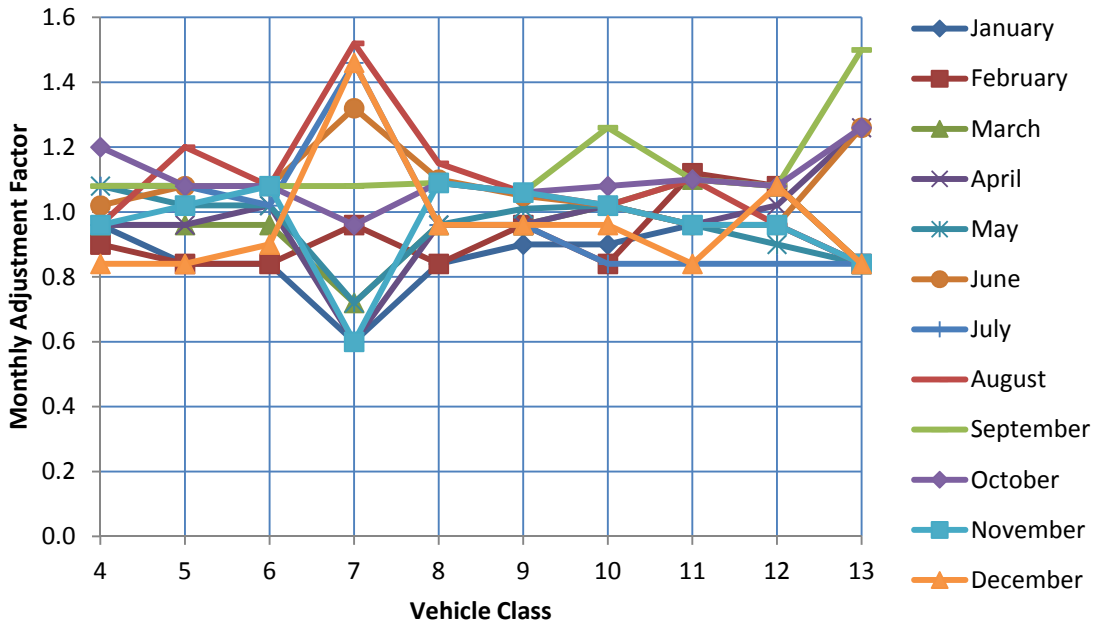

Figure B-6 Monthly Adjustment Factor

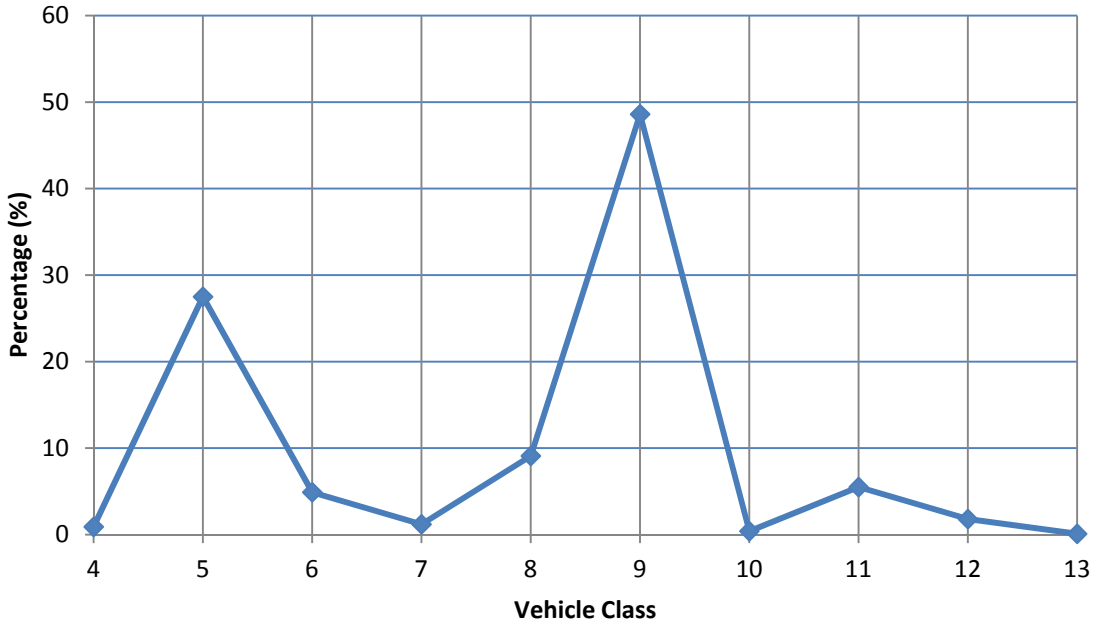

Figure B-7 Vehicle Class Distribution

2. CRCP Pavement Section (10-5004)

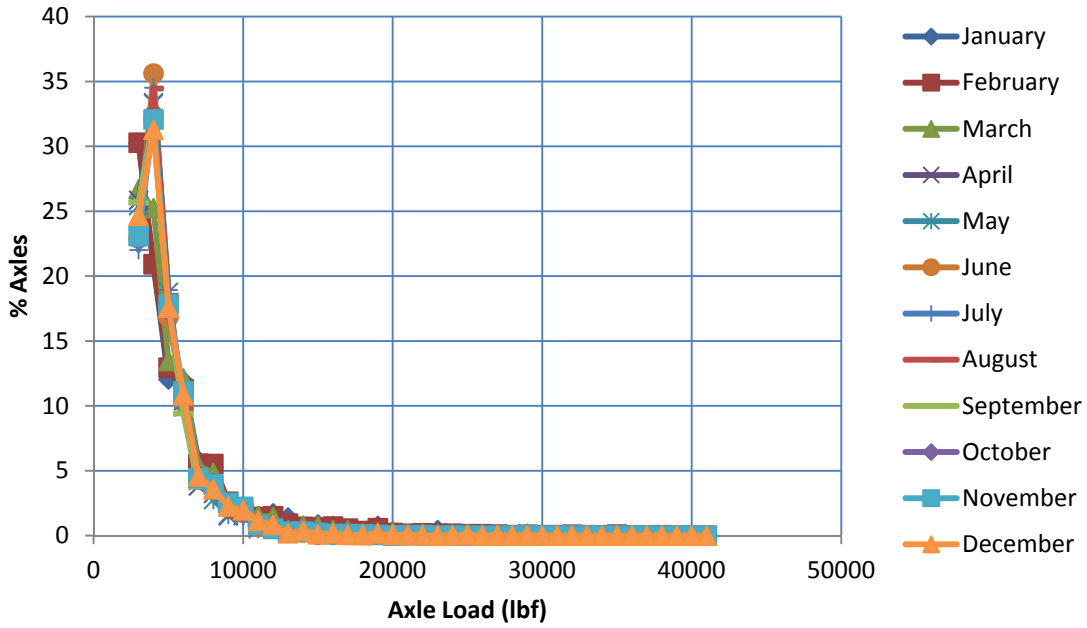

Figure B-8 Load Spectra for Vehicle Class 5 Single Axles

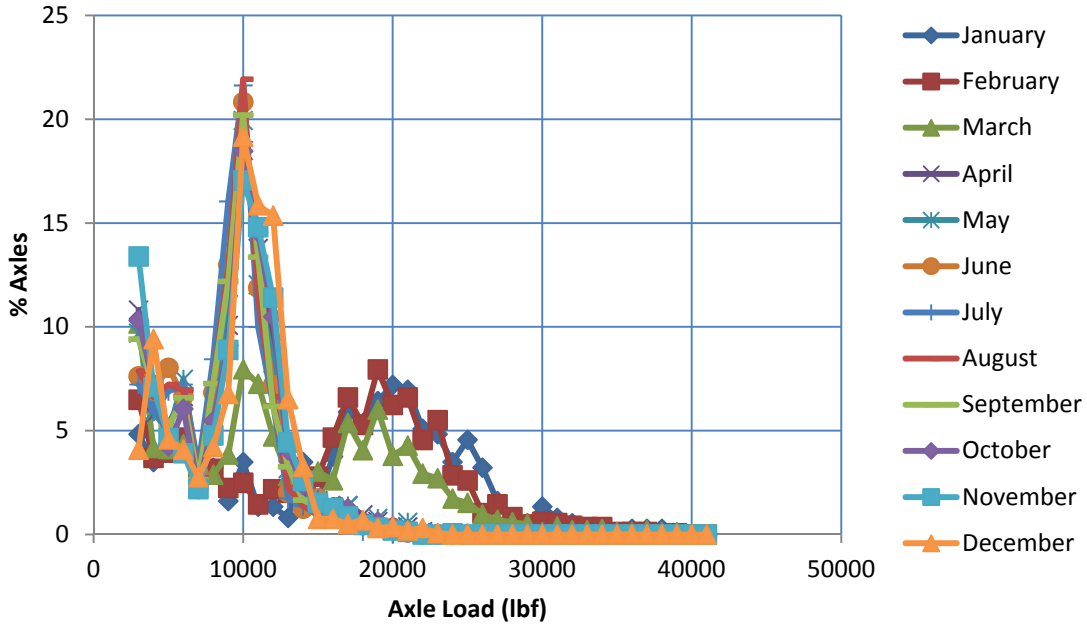

Figure B-9 Load Spectra for Vehicle Class 9 Single Axles

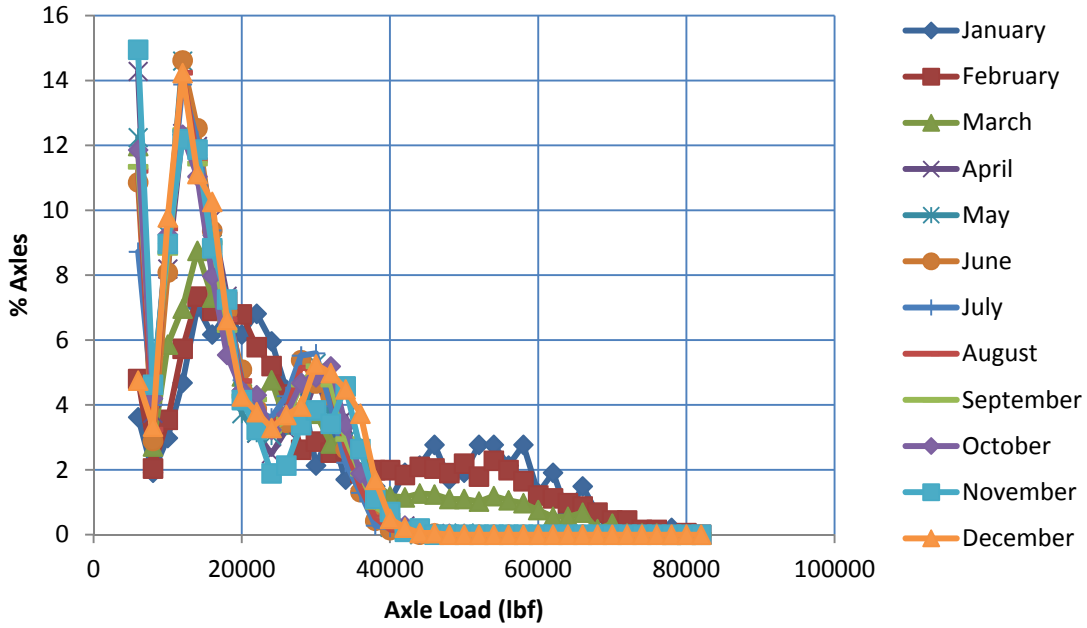

Figure B-10 Load Spectra for Vehicle Class 9 Tandem Axles

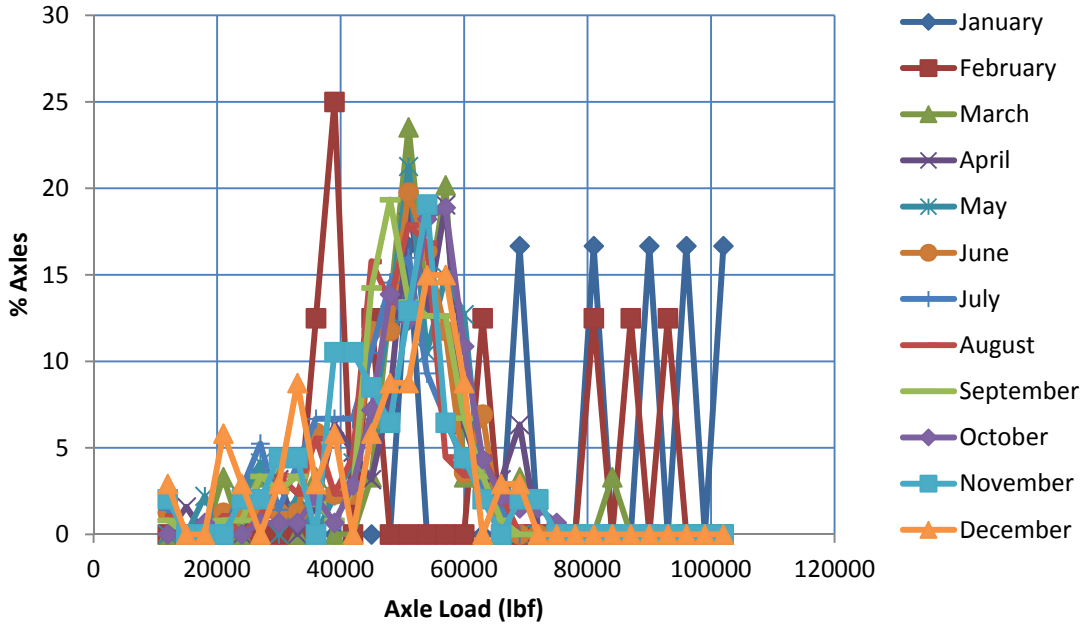

Figure B-11 Load Spectra for Vehicle Class 7 Tridem Axles

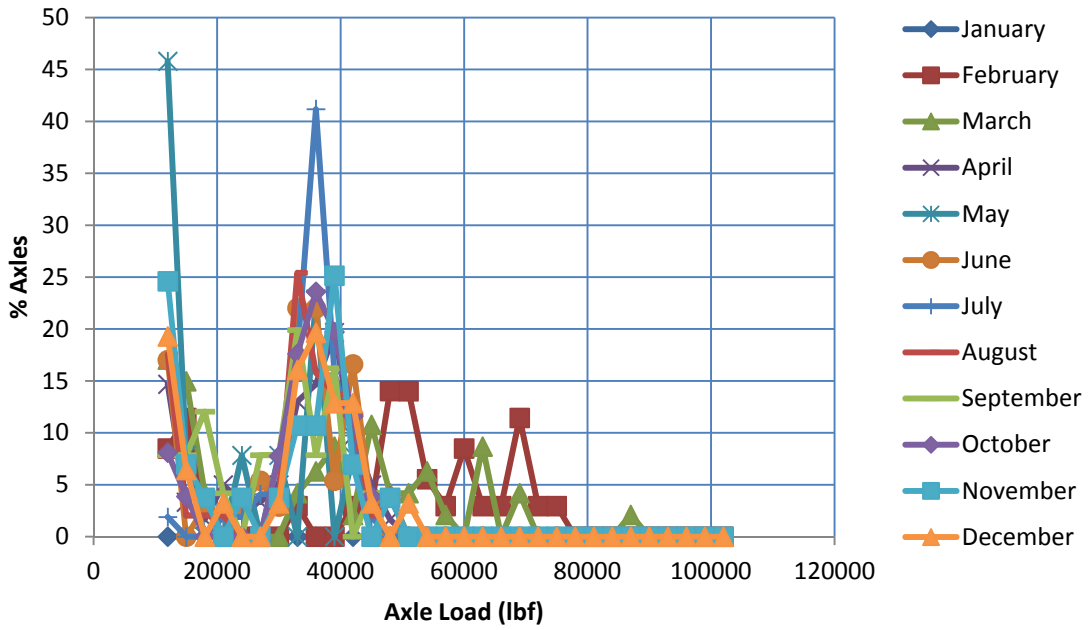

Figure B-12 Load Spectra for Vehicle Class 10 Tridem Axles

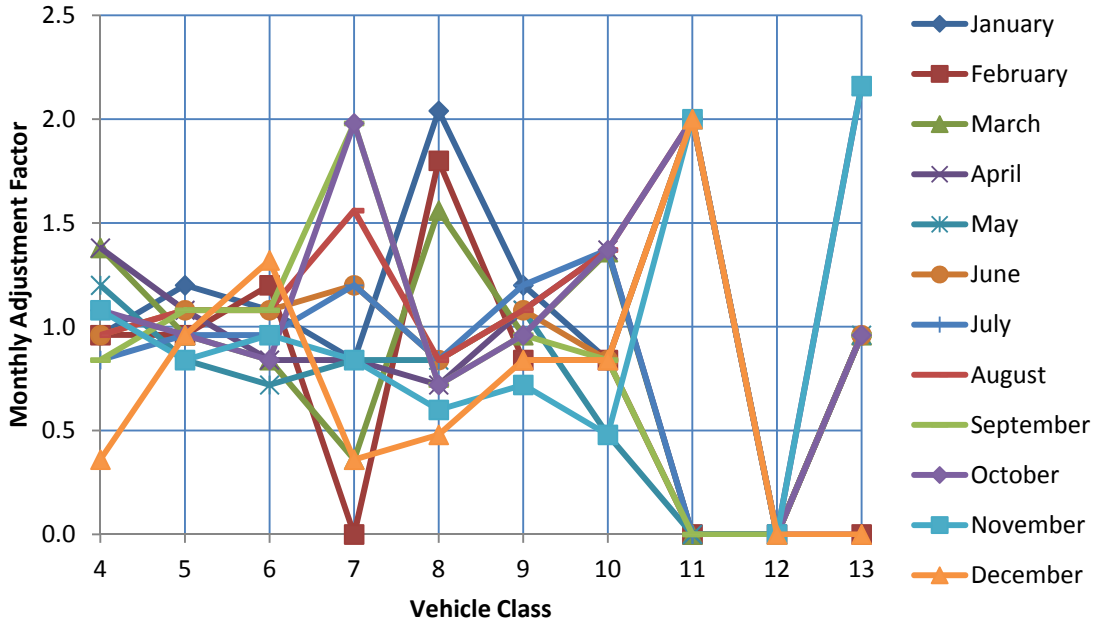

Figure B-13 Monthly Adjustment Factor

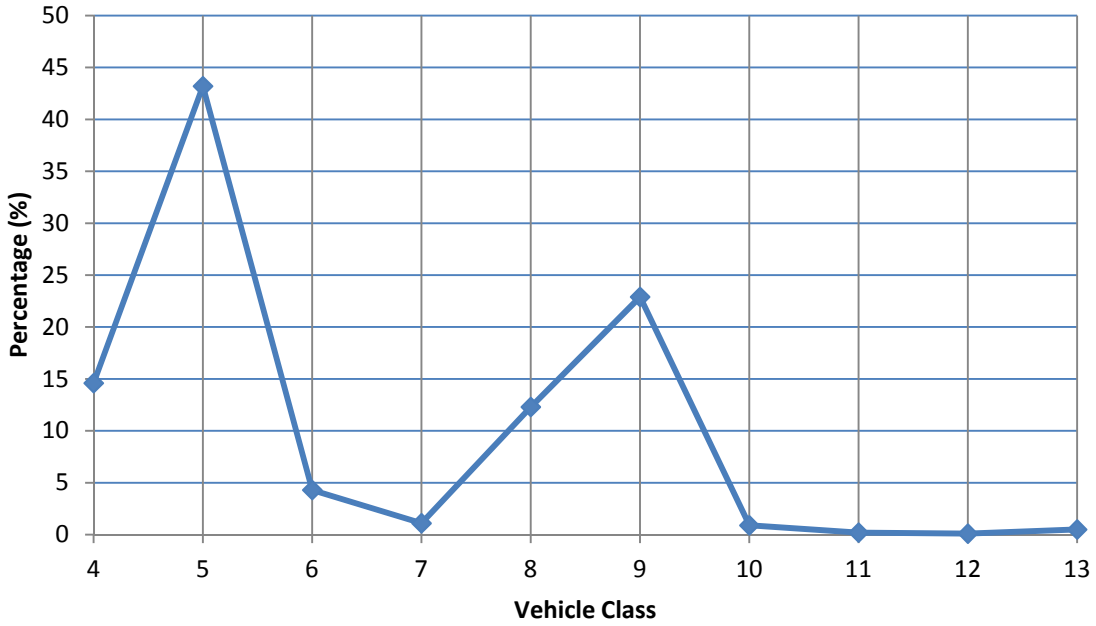

Figure B-14 Vehicle Class Distribution

3. Flexible Pavement Section (34-6507)

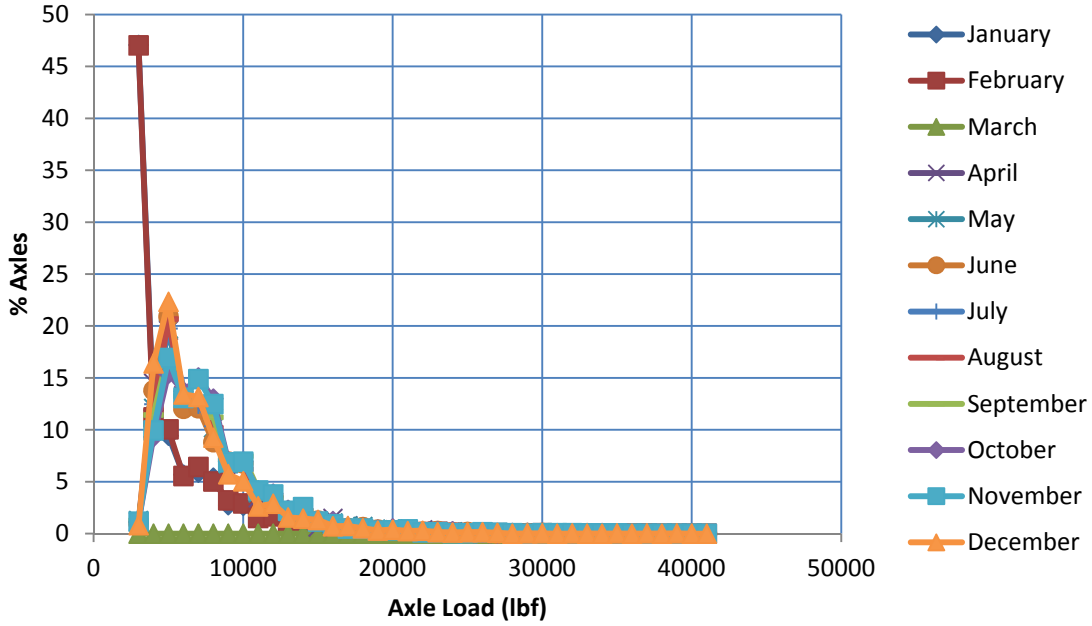

Figure B-15 Load Spectra for Vehicle Class 5 Single Axles

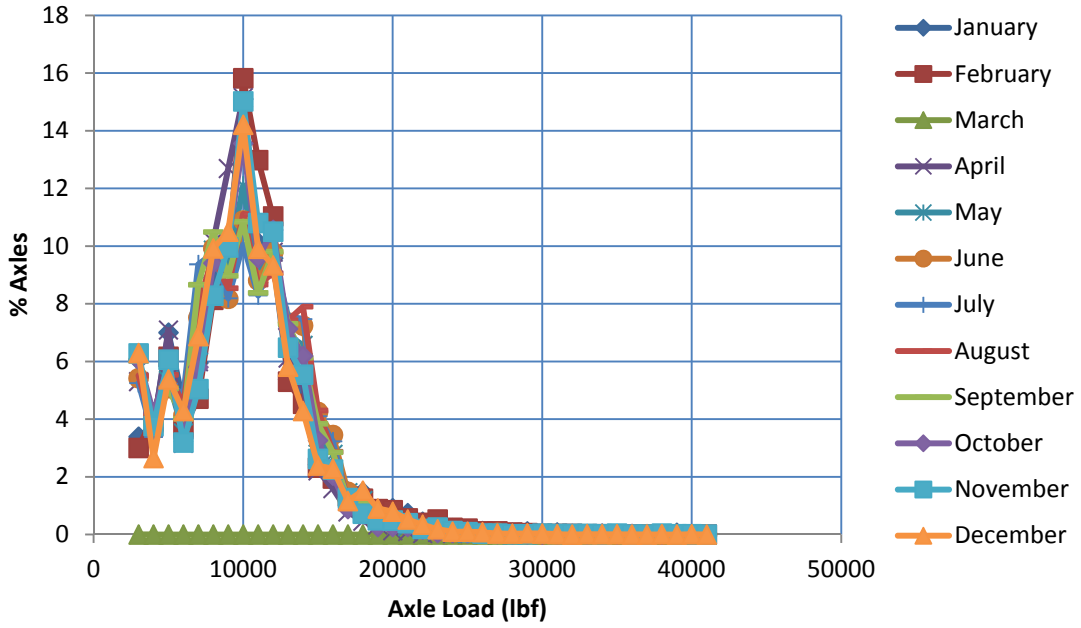

Figure B-16 Load Spectra for Vehicle Class 9 Single Axles

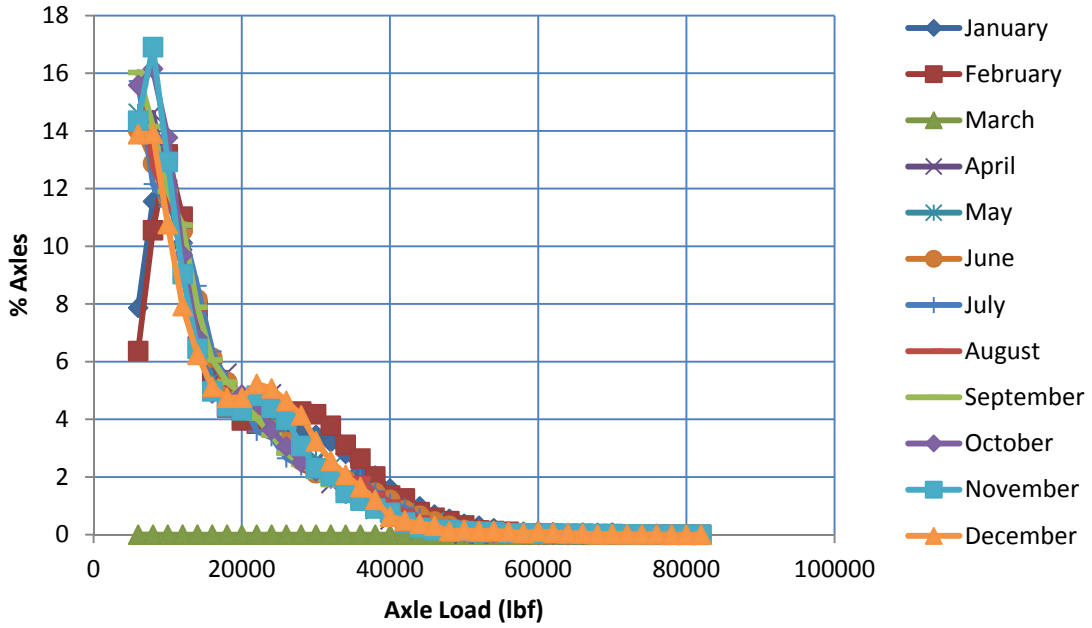

Figure B-17 Load Spectra for Vehicle Class 9 Tandem Axles

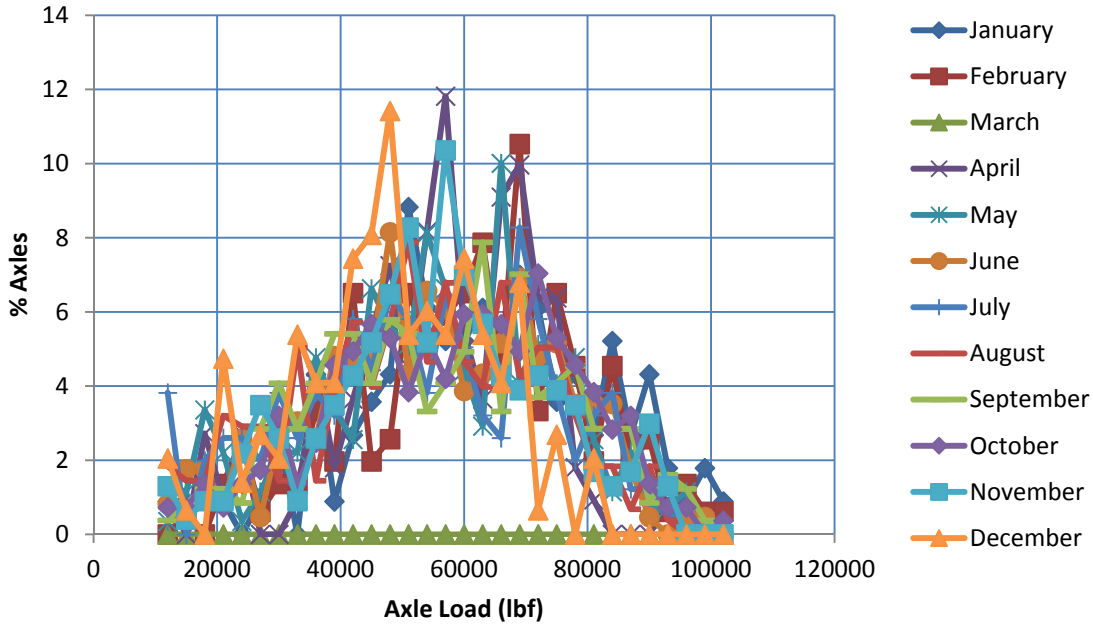

Figure B-18 Load Spectra for Vehicle Class 7 Tridem Axles

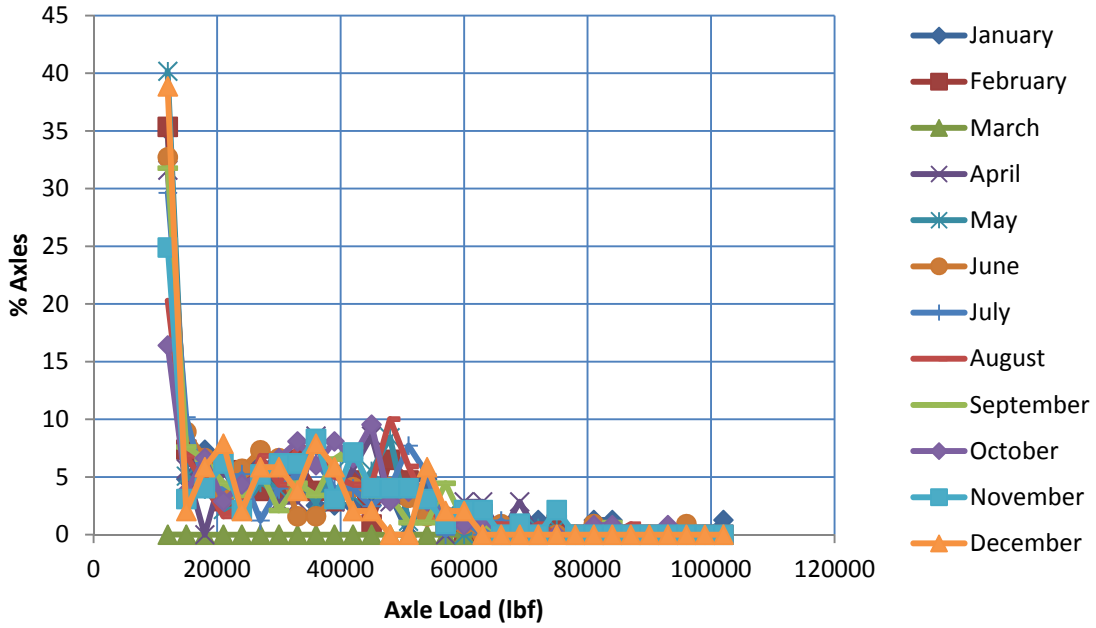

Figure B-19 Load Spectra for Vehicle Class 10 Tridem Axles

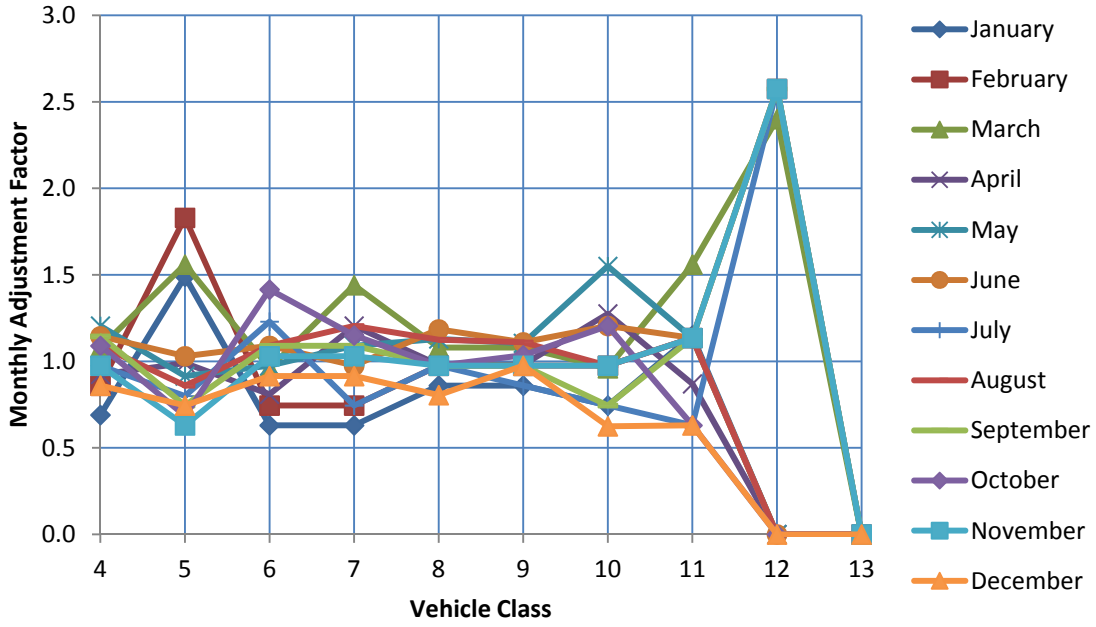

Figure B-20 Monthly Adjustment Factor

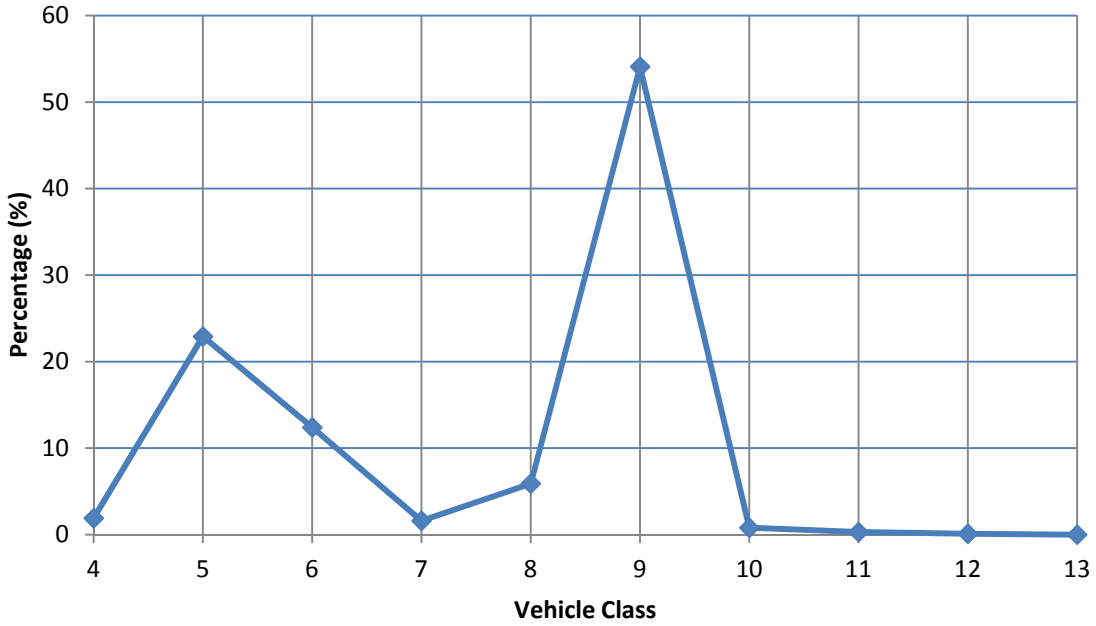

Figure B-21 Vehicle Class Distribution

APPENDIX C Formats of the MEPDG Traffic Import Files

The MEPDG traffic export/import files, 11 in total, come as follows. They contain all the traffic data sets that are required in the MEPDG analysis.

_HourlyTrafficPercentage.txt

MonthlyAdjustmentFactor.txt

VehicleClassDistribution.txt

TrafficGrowth.txt

Traffic.txt

GeneralTraffic.txt

AxlesPerTruck.txt

Single.alf

Tandem.alf

Tridem.alf

Quad.alf

Table C.1 Studies on the 11 Importable Traffic Files for MEPDG

Categories	File Name	Data Included	Notes
Basic Information	Traffic.txt	♦Initial two-way AADTT ♦Number of lanes in the design direction ♦Percent of trucks in the design direction ♦Percent of trucks in the design lane ♦Operational speed	
Traffic Volume Adjustment	MonthlyAdjustmentFactor.txt	Table for Monthly Adjustment Factor	
	VehicleClassDistribution.txt	Percent trucks in Class	10 numbers that sum to 100
	_HourlyTrafficPerc.txt	Hourly truck traffic distribution in 24 hours	
	TrafficGrowth.txt	♦Traffic growth function: 0 or 1 ♦Input growth : No, Linear or Compound ♦Growth Rate – Number (%) growth rate	0 -- Composite vehicle class growth; 1 -- Vehicle-class specific growth;
Axle Load Distribution Factors	single.alf	Axle load distribution factors-single load	1. These files can be opened with WordPad; 2. The formats of these files are same as those in MEPDG
	tandem.alf	Axle load distribution factors- tandem load	
	tridem.alf	Axle load distribution factors- tridem load	
	quad.alf	Axle load distribution factors- quad load	
General Traffic Inputs	GeneralTraffic.txt	MeanWheel Location Traffic Wander Design land width Average Axle Width(edge to edge) Outside dimensions Dual Tire Spacing Tire Pressure Tandem, tridem, and quad axle spacing Short axle spacing Percent trucks with short axle spacing Medium axle spacing Percent of trucks with medium axle spacing Long axle spacing ♦Percent of trucks with long axle spacing	
	AxlesPerTruck.txt	♦Axles per truck at different load categories	

APPENDIX D MAGICC/SCENGEN Climate Change Projection Results

zThis appendix tabulates the MAGICC/SCENGEN climate change projections for the 36 scenarios used in this study. Data for each season (Spring, Summer, Fall and Winter) and for two locations (CT & NJ, and DE) included:

- Change in temperature (Δ(ange)
- Standard deviation of temperature (SDT (%))
- Percentage change in precipitation (Δ(rcen)
- Standard deviation of the percentage change in precipitation (SDP (%))
- Global change in temperature, and
- Global sea level rise (SLR (cm))

The tables are organized as follows:

- A1B-AIM Model
    - 2030
        - Low Variability – Table D1
        - Medium Variability – Table D2
        - High Variability – Table D3
    - 2050
        - Low Variability – Table D4
        - Medium Variability – Table D5
        - High Variability – Table D6
    - 2100
        - Low Variability – Table D7
        - Medium Variability – Table D8
        - High Variability – Table D9
- A2-ASF Model
    - 2030

        - Low Variability – Table D10
        - Medium Variability – Table D11
        - High Variability – Table D12
    - 2050
        - Low Variability – Table D13
        - Medium Variability – Table D14
        - High Variability – Table D15
    - 2100
        - Low Variability – Table D16
        - Medium Variability – Table D17
        - High Variability – Table D18
- B1-IMA Model
    - 2030
        - Low Variability – Table D19
        - Medium Variability – Table D20
        - High Variability – Table D21
    - 2050
        - Low Variability – Table D22
        - Medium Variability – Table D23
        - High Variability – Table D24
    - 2100
        - Low Variability – Table D25
        - Medium Variability – Table D26
        - High Variability – Table D27

- B2-MES Model
    - 2030
        - Low Variability – Table D28
        - Medium Variability – Table D29
        - High Variability – Table D30
    - 2050
        - Low Variability – Table D31
        - Medium Variability – Table D32
        - High Variability – Table D33
    - 2100
        - Low Variability – Table D34
        - Medium Variability – Table D35
        - High Variability – Table D36

Table D-1 A1B-AIM Model, Low Variability, 2030

Grid	Season	ΔT (C)	SDT (%)	ΔP (%)	SDP (%)	Global ΔT (C)	Global SLR (cm)
CT & NJ	Spring	0.72	2.1	3.54	4.11	0.54	3.88
	Summer	0.74	14.21	-0.19	-0.36		
	Fall	0.75	2.31	-0.09	2.58		
	Winter	0.66	-7.94	2.05	-0.76		
DE	Spring	0.73	0.55	4.99	2.68		
	Summer	0.7	7.17	1.58	-2.72		
	Fall	0.74	5.07	-1.09	3.85		
	Winter	0.58	-6.56	2.72	9.39		

Table D-2 A1B-AIM Model, Medium Variability, 2030

Grid	Season	ΔT (C)	SDT (%)	ΔP (%)	SDP (%)	Global ΔT (C)	Global SLR (cm)
CT & NJ	Spring	1.17	3.41	5.76	6.68	0.87	7.99
	Summer	1.2	23.1	-0.31	-0.59		
	Fall	1.22	3.76	-0.15	4.2		
	Winter	1.08	-12.9	3.34	-1.24		
DE	Spring	1.18	0.89	8.11	4.36		
	Summer	1.13	11.16	2.57	-4.43		
	Fall	1.2	8.24	-1.77	6.25		
	Winter	0.95	-10.66	4.2	15.25		

Table D-3 A1B-AIM Model, High Variability, 2030

Grid	Season	ΔT (C)	SDT (%)	ΔP (%)	SDP (%)	Global ΔT (C)	Global SLR (cm)
CT & NJ	Spring	1.69	18.6	8.3	9.63	1.26	13.88
	Summer	1.73	33.31	-0.45	-0.85		
	Fall	1.76	5.42	-0.21	6.05		
	Winter	1.56	-18.61	4.81	-1.79		
DE	Spring	1.7	1.28	11.69	6.28		
	Summer	1.63	16.81	3.71	-6.38		
	Fall	1.72	11.89	-2.55	9.01		
	Winter	1.37	-15.38	6.37	22		

Table D-4 A1B-AIM Model, Low Variability, 2050

Grid	Season	ΔT (C)	SDT (%)	ΔP (%)	SDP (%)	Global ΔT (C)	Global SLR (cm)
CT & NJ	Spring	0.3	3.73	6.3	4.1	0.95	7.01
	Summer	1.31	25.26	-0.34	-0.7		
	Fall	1.34	4.11	-0.16	4.6		
	Winter	1.18	-14.11	3.65	-1.4		
DE	Spring	1.29	0.97	8.87	4.8		
	Summer	1.24	12.75	2.81	-4.8		
	Fall	1.31	9.02	-1.93	6.8		
	Winter	1.04	-11.66	4.83	17		

Table D-5 A1B-AIM Model, Medium Variability, 2050

Grid	Season	ΔT (C)	SDT (%)	ΔP (%)	SDP (%)	Global ΔT (C)	Global SLR (cm)
CT & NJ	Spring	2.13	6.19	10.44	12	1.58	15.13
	Summer	2.17	41.89	-0.56	-1.1		
	Fall	2.22	6.82	-0.27	7.6		
	Winter	1.96	-23.39	6.05	-2.3		
DE	Spring	2.14	1.61	14.71	7.9		
	Summer	2.05	21.14	4.67	-8		
	Fall	2.17	14.95	-3.2	11		
	Winter	1.72	-19.34	8.01	28		

Table D-6 A1B-AIM Model, High Variability, 2050

Grid	Season	ΔT (C)	SDT (%)	ΔP (%)	SDP (%)	Global ΔT (C)	Global SLR (cm)
CT & NJ	Spring	3.13	9.11	15.36	18	2.33	27.09
	Summer	3.2	61.64	-0.83	-1.6		
	Fall	3.26	10.03	-0.4	11		
	Winter	2.88	-34.42	8.91	-3.3		
DE	Spring	3.15	2.38	21.64	12		
	Summer	3.02	31.1	6.87	-12		
	Fall	3.19	21.99	-4.71	17		
	Winter	2.53	-28.45	11.78	41		

Table D-7 A1B-AIM Model, Low Variability, 2100

Grid	Season	ΔT (C)	SDT (%)	ΔP (%)	SDP (%)	Global ΔT (C)	Global SLR (cm)
CT & NJ	Spring	2.25	6.53	11.01	12.77	1.67	14.8
	Summer	2.29	44.17	-0.59	-1.13		
	Fall	2.34	7.19	-0.28	8.03		
	Winter	2.06	-24.67	6.38	-2.37		
DE	Spring	2.26	1.7	15.51	8.33		
	Summer	2.17	22.29	4.92	-8.47		
	Fall	2.29	15.76	-3.38	11.96		
	Winter	1.82	-20.39	8.44	29.17		

Table D-8 A1B-AIM Model, Medium Variability, 2100

Grid	Season	ΔT (C)	SDT (%)	ΔP (%)	SDP (%)	Global ΔT (C)	Global SLR (cm)
CT & NJ	Spring	3.98	11.58	19.52	22.63	2.96	37.1
	Summer	4.06	78.3	-1.05	-2.01		
	Fall	4.15	12.74	-0.5	14.23		
	Winter	3.66	-43.72	11.31	-4.2		
DE	Spring	4	3.02	27.49	14.77		
	Summer	3.84	39.51	8.72	-15.01		
	Fall	4.05	27.94	-5.99	21.19		
	Winter	3.22	-36.15	14.97	51.71		

Table D-9 A1B-AIM Model, High Variability, 2100

Grid	Season	ΔT (C)	SDT (%)	ΔP (%)	SDP (%)	Global ΔT (C)	Global SLR (cm)
CT & NJ	Spring	6.31	18.34	30.93	35.86	4.69	73.2
	Summer	6.43	124.04	-1.66	-3.18		
	Fall	6.57	20.19	-0.8	22.55		
	Winter	5.8	-69.29	17.93	-6.66		
DE	Spring	6.34	4.78	43.56	23.41		
	Summer	6.08	62.61	13.82	-23.78		
	Fall	6.42	44.28	-9.49	33.58		
	Winter	5.1	-57.28	23.72	81.95		

Table D-10 A2-ASF Model, Low Variability, 2030

Grid	Season	ΔT (C)	SDT (%)	ΔP (%)	SDP (%)	Global ΔT (C)	Global SLR (cm)
CT & NJ	Spring	0.66	1.93	3.25	3.77	0.49	3.77
	Summer	0.68	13.04	-0.17	-0.33		
	Fall	0.69	2.12	-0.08	2.37		
	Winter	0.61	-7.28	1.88	-0.7		
DE	Spring	0.67	0.5	4.58	2.46		
	Summer	0.64	6.58	1.45	-2.5		
	Fall	0.67	4.65	-1	3.53		
	Winter	0.54	-6.02	2.49	8.61		

Table D-11 A2-ASF Model, Medium Variability, 2030

Grid	Season	ΔT (C)	SDT (%)	ΔP (%)	SDP (%)	Global ΔT (C)	Global SLR (cm)
CT & NJ	Spring	1.09	3.17	5.34	6.2	0.81	7.85
	Summer	1.11	21.44	-0.29	-0.55		
	Fall	1.14	3.49	-0.14	3.9		
	Winter	1	-11.97	3.1	-1.15		
DE	Spring	1.1	0.83	7.53	4.05		
	Summer	1.05	10.82	2.39	-4.11		
	Fall	1.11	7.65	-1.64	5.8		
	Winter	0.88	-9.9	4.1	14.16		

Table D-12 A2-ASF Model, High Variability, 2030

Grid	Season	ΔT (C)	SDT (%)	ΔP (%)	SDP (%)	Global ΔT (C)	Global SLR (cm)
CT & NJ	Spring	1.59	4.62	7.79	9.03	1.18	13.72
	Summer	1.62	31.26	-0.42	-0.8		
	Fall	1.66	5.09	-0.2	5.68		
	Winter	1.46	-17.46	4.52	-1.68		
DE	Spring	1.6	1.2	10.97	5.9		
	Summer	1.53	15.77	3.48	-5.99		
	Fall	1.62	11.16	-2.39	8.46		
	Winter	1.29	-14.43	5.98	20.64		

Table D-13 A2-ASF Model, Low Variability, 2050

Grid	Season	ΔT (C)	SDT (%)	ΔP (%)	SDP (%)	Global ΔT (C)	Global SLR (cm)
CT & NJ	Spring	1.21	3.52	5.94	6.9	0.9	6.77
	Summer	1.24	23.84	-0.32	-0.6		
	Fall	1.26	3.88	-0.15	4.3		
	Winter	1.11	-13.31	3.45	-1.3		
DE	Spring	1.22	0.92	8.37	4.5		
	Summer	1.17	12.03	2.66	-4.6		
	Fall	1.23	8.51	-1.82	6.5		
	Winter	0.98	-11.01	4.56	16		

Table D-14 A2-ASF Model, Medium Variability, 2050

Grid	Season	ΔT (C)	SDT (%)	ΔP (%)	SDP (%)	Global ΔT (C)	Global SLR (cm)
CT & NJ	Spring	2.01	5.84	9.84	11	1.49	14.59
	Summer	2.05	39.48	-0.53	-1		
	Fall	2.23	6.42	-0.25	7.2		
	Winter	1.85	-22.05	5.71	-2.1		
DE	Spring	2.02	1.52	13.86	7.5		
	Summer	1.94	19.92	4.4	-7.6		
	Fall	2.19	14.09	-3.02	11		
	Winter	1.62	-18.23	7.55	26		

Table D-15 A2-ASF Model, High Variability, 2050

Grid	Season	ΔT (C)	SDT (%)	ΔP (%)	SDP (%)	Global ΔT (C)	Global SLR (cm)
CT & NJ	Spring	2.95	8.59	14.49	17	2.2	26.18
	Summer	3.01	58.12	-0.78	-1.5		
	Fall	3.08	9.46	-0.37	11		
	Winter	2.72	-32.45	8.4	-3.1		
DE	Spring	2.97	2.24	20.4	11		
	Summer	2.85	29.34	6.47	-11		
	Fall	3.01	20.74	-4.45	16		
	Winter	2.39	-26.83	11.11	38		

Table D-16 A2-ASF Model, Low Variability, 2100

Grid	Season	ΔT (C)	SDT (%)	ΔP (%)	SDP (%)	Global ΔT (C)	Global SLR (cm)
CT & NJ	Spring	3	8.74	14.73	17.08	2.23	17.53
	Summer	3.06	59.1	-0.79	-1.51		
	Fall	3.13	9.62	-0.38	10.74		
	Winter	2.76	-33	8.54	-3.17		
DE	Spring	3.02	2.28	20.75	11.15		
	Summer	2.9	29.82	6.58	-11.3		
	Fall	3.06	21.09	-4.52	16		
	Winter	2.43	-27.28	11.3	39.03		

Table D-17 A2-ASF Model, Medium Variability, 2100

Grid	Season	ΔT (C)	SDT (%)	ΔP (%)	SDP (%)	Global ΔT (C)	Global SLR (cm)
CT & NJ	Spring	5.13	14.91	25.14	29.15	3.81	41.71
	Summer	5.23	100.86	-1.35	-2.58		
	Fall	5.34	16.41	-0.65	18.33		
	Winter	4.71	-56.32	14.58	-5.42		
DE	Spring	5.15	3.89	35.41	19.03		
	Summer	4.94	50.9	11.24	-19.3		
	Fall	5.22	35.99	-7.71	27.3		
	Winter	4.15	-46.56	19.28	66.61		

Table D-18 A2-ASF Model, High Variability, 2100

Grid	Season	ΔT (C)	SDT (%)	ΔP (%)	SDP (%)	Global ΔT (C)	Global SLR (cm)
CT & NJ	Spring	7.83	22.77	38.39	44.51	5.82	79.87
	Summer	7.99	154.02	-2.07	-3.95		
	Fall	8.15	25.06	-0.99	28		
	Winter	7.2	-86.01	22.26	-8.27		
DE	Spring	7.87	5.94	54.07	29.06		
	Summer	7.55	77.72	17.16	-29.5		
	Fall	7.97	54.96	-11.78	41.69		
	Winter	6.33	-71.1	29.44	101.7		

Table D-19 B1-IMA Model, Low Variability, 2030

Grid	Season	ΔT (C)	SDT (%)	ΔP (%)	SDP (%)	Global ΔT (C)	Global SLR (cm)
CT & NJ	Spring	0.61	1.78	3	3.48	0.45	3.61
	Summer	0.62	12.04	-0.16	-0.31		
	Fall	0.64	1.96	-0.08	2.19		
	Winter	0.56	-6.72	1.74	-0.65		
DE	Spring	0.62	0.46	4.23	2.27		
	Summer	0.59	6.07	1.34	-2.31		
	Fall	0.62	4.3	-0.92	3.26		
	Winter	0.49	-5.56	2.3	7.95		

Table D-20 B1-IMA Model, Medium Variability, 2030

Grid	Season	ΔT (C)	SDT (%)	ΔP (%)	SDP (%)	Global ΔT (C)	Global SLR (cm)
CT & NJ	Spring	1.02	2.97	5	5.8	0.76	7.63
	Summer	1.04	20.08	-0.27	-0.51		
	Fall	1.06	3.27	-0.13	3.65		
	Winter	0.94	-11.21	2.9	-1.08		
DE	Spring	1.03	0.77	7.05	3.79		
	Summer	0.98	10.13	2.24	-3.85		
	Fall	1.04	7.16	-1.54	5.43		
	Winter	0.83	-9.27	3.84	13.26		

Table D-21 B1-IMA Model, High Variability, 2030

Grid	Season	ΔT (C)	SDT (%)	ΔP (%)	SDP (%)	Global ΔT (C)	Global SLR (cm)
CT & NJ	Spring	1.5	4.37	7.37	8.55	1.12	13.44
	Summer	1.53	29.58	-0.4	-0.76		
	Fall	1.57	4.81	-0.19	5.38		
	Winter	1.38	-16.52	4.27	-1.59		
DE	Spring	1.51	1.14	10.38	5.58		
	Summer	1.45	14.93	3.3	-5.67		
	Fall	1.53	10.56	-2.26	8.01		
	Winter	1.22	-13.66	5.65	19.54		

Table D-22 B1-IMA Model, Low Variability, 2050

Grid	Season	ΔT (C)	SDT (%)	ΔP (%)	SDP (%)	Global ΔT (C)	Global SLR (cm)
CT & NJ	Spring	0.92	2.7	4.51	5.2	0.68	5.77
	Summer	0.94	18	-0.24	-0.5		
	Fall	0.96	2.9	-0.12	3.3		
	Winter	0.85	-10	2.61	-1		
DE	Spring	0.92	0.7	6.35	3.4		
	Summer	0.89	9.1	2.02	-3.5		
	Fall	0.94	6.5	-1.38	4.9		
	Winter	0.74	-8	3.46	12		

Table D-23 B1-IMA Model, Medium Variability, 2050

Grid	Season	ΔT (C)	SDT (%)	ΔP (%)	SDP (%)	Global ΔT (C)	Global SLR (cm)
CT & NJ	Spring	1.57	4.6	7.69	8.9	1.17	12.92
	Summer	1.6	31	-0.41	-0.8		
	Fall	1.63	5	-0.2	5.6		
	Winter	1.44	-17	4.46	-1.7		
DE	Spring	1.58	1.2	10.83	5.8		
	Summer	1.51	16	3.44	-5.9		
	Fall	1.6	11	-2.36	8.4		
	Winter	1.27	-14	5.9	20		

Table D-24 B1-IMA Model, High Variability, 2050

Grid	Season	ΔT (C)	SDT (%)	ΔP (%)	SDP (%)	Global ΔT (C)	Global SLR (cm)
CT & NJ	Spring	2.37	6.9	11.63	13	1.76	23.71
	Summer	2.42	47	-0.63	-1.2		
	Fall	2.47	7.6	-0.3	8.5		
	Winter	2.18	-26	6.74	-2.5		
DE	Spring	2.38	1.8	16.37	8.8		
	Summer	2.29	24	5.2	-8.9		
	Fall	2.41	17	-3.57	13		
	Winter	1.92	-22	8.91	31		

Table D-25 B1-IMA Model, Low Variability, 2100

Grid	Season	ΔT (C)	SDT (%)	ΔP (%)	SDP (%)	Global ΔT (C)	Global SLR (cm)
CT & NJ	Spring	1.37	3.99	6.73	7.81	1.02	10.41
	Summer	1.4	27.01	-0.36	-0.69		
	Fall	1.43	4.4	-0.17	4.91		
	Winter	1.26	-15.08	3.9	-1.45		
DE	Spring	1.38	1.04	9.48	5.1		
	Summer	1.32	13.63	3.01	-5.8		
	Fall	1.4	9.64	-2.07	7.31		
	Winter	1.11	-12.47	5.16	17.8		

Table D-26 B1-IMA Model, Medium Variability, 2100

Grid	Season	ΔT (C)	SDT (%)	ΔP (%)	SDP (%)	Global ΔT (C)	Global SLR (cm)
CT & NJ	Spring	2.53	7.35	12.4	14.4	1.88	27.4
	Summer	2.58	49.74	-0.67	-1.27		
	Fall	2.63	8.09	-0.32	9.04		
	Winter	2.32	-27.77	7.19	-2.67		
DE	Spring	2.54	1.92	17.46	9.38		
	Summer	2.44	25.1	5.54	-9.53		
	Fall	2.57	17.75	-3.8	13.5		
	Winter	2.04	-22.96	9.51	32.9		

Table D-27 B1-IMA Model, High Variability, 2100

Grid	Season	ΔT (C)	SDT (%)	ΔP (%)	SDP (%)	Global ΔT (C)	Global SLR (cm)
CT & NJ	Spring	4.16	12.1	20.39	23.6	3.09	55.71
	Summer	4.24	81.82	-1.1	-2.1		
	Fall	4.33	13.31	-0.53	14.9		
	Winter	3.82	-45.69	11.82	-4.39		
DE	Spring	4.18	3.15	28.72	15.4		
	Summer	4.01	41.29	9.12	-15.7		
	Fall	4.24	29.2	-6.26	22.1		
	Winter	3.36	-37.77	15.64	54		

Table D-28 B2-MES Model, Low Variability, 2030

Grid	Season	ΔT (C)	SDT (%)	ΔP (%)	SDP (%)	Global ΔT (C)	Global SLR (cm)
CT & NJ	Spring	0.69	2.01	3.39	3.93	0.51	3.73
	Summer	0.71	13.61	-0.18	-0.35		
	Fall	0.72	2.21	-0.09	2.47		
	Winter	0.64	-7.6	1.97	-0.73		
DE	Spring	0.7	0.52	4.78	2.57		
	Summer	0.67	6.87	1.52	-2.61		
	Fall	0.7	4.86	-1.04	3.68		
	Winter	0.56	-6.28	2.6	8.99		

Table D-29 B2-MES Model, Medium Variability, 2030

Grid	Season	ΔT (C)	SDT (%)	ΔP (%)	SDP (%)	Global ΔT (C)	Global SLR (cm)
CT & NJ	Spring	1.15	3.34	5.63	6.53	0.85	7.94
	Summer	1.17	22.6	-0.3	-0.58		
	Fall	1.2	3.68	-0.15	4.11		
	Winter	1.06	-12.62	3.27	-1.21		
DE	Spring	1.15	0.87	7.93	4.26		
	Summer	1.11	11.4	2.52	-4.33		
	Fall	1.17	8.07	-1.73	6.12		
	Winter	0.93	-10.43	4.32	14.93		

Table D-30 B2-MES Model, High Variability, 2030

Grid	Season	ΔT (C)	SDT (%)	ΔP (%)	SDP (%)	Global ΔT (C)	Global SLR (cm)
CT & NJ	Spring	1.68	4.9	8.26	9.57	1.25	14.03
	Summer	1.72	33.12	-0.44	-0.85		
	Fall	1.75	5.39	-0.21	6.02		
	Winter	1.55	-18.5	4.79	-1.78		
DE	Spring	1.69	1.28	11.63	6.25		
	Summer	1.62	16.71	3.69	-6.35		
	Fall	1.71	11.82	-2.53	8.96		
	Winter	1.36	-15.29	6.33	21.87		

Table D-31 B2-MES Model, Low Variability, 2050

Grid	Season	ΔT (C)	SDT (%)	ΔP (%)	SDP (%)	Global ΔT (C)	Global SLR (cm)
CT & NJ	Spring	1.07	3.11	5.25	6.08	0.8	6.12
	Summer	1.09	21.04	-0.28	-0.54		
	Fall	1.11	3.42	-0.14	3.82		
	Winter	0.98	-11.75	3.04	-1.13		
DE	Spring	1.08	0.81	7.39	3.97		
	Summer	1.03	10.62	2.34	-4.03		
	Fall	1.09	7.51	-1.61	5.7		
	Winter	0.87	-9.71	4.02	13.9		

Table D-32 B2-MES Model, Medium Variability, 2050

Grid	Season	ΔT (C)	SDT (%)	ΔP (%)	SDP (%)	Global ΔT (C)	Global SLR (cm)
CT & NJ	Spring	1.81	5.27	8.89	10.31	1.35	13.82
	Summer	1.85	35.68	-0.48	-0.91		
	Fall	1.89	5.81	-0.23	6.48		
	Winter	1.67	-19.92	5.16	-1.92		
DE	Spring	1.82	1.38	12.52	6.73		
	Summer	1.75	18	3.97	-6.84		
	Fall	1.85	12.73	-2.73	9.66		
	Winter	1.47	-16.47	6.82	23.56		

Table D-33 B2-MES Model, High Variability, 2050

Grid	Season	ΔT (C)	SDT (%)	ΔP (%)	SDP (%)	Global ΔT (C)	Global SLR (cm)
CT & NJ	Spring	2.73	7.93	13.37	15.5	2.03	25.41
	Summer	2.78	53.63	-0.72	-1.37		
	Fall	2.84	8.73	-0.34	9.75		
	Winter	2.51	-29.95	7.75	-2.88		
DE	Spring	2.74	2.07	18.83	10.12		
	Summer	2.63	27.06	5.97	-10.28		
	Fall	2.78	19.14	-4.1	14.52		
	Winter	2.21	-24.76	10.25	35.42		

Table D-34 B2-MES Model, Low Variability, 2100

Grid	Season	ΔT (C)	SDT (%)	ΔP (%)	SDP (%)	Global ΔT (C)	Global SLR (cm)
CT & NJ	Spring	1.98	5.75	9.69	11.23	1.47	12.88
	Summer	2.02	38.88	-0.52	-1		
	Fall	2.06	6.33	-0.25	7.07		
	Winter	1.82	-21.71	5.62	-2.09		
DE	Spring	1.99	1.5	13.65	7.33		
	Summer	1.91	19.62	4.33	-7.45		
	Fall	2.01	13.87	-2.97	10.52		
	Winter	1.6	-17.95	7.43	25.67		

Table D-35 B2-MES Model, Medium Variability, 2100

Grid	Season	ΔT (C)	SDT (%)	ΔP (%)	SDP (%)	Global ΔT (C)	Global SLR (cm)
CT & NJ	Spring	3.49	10.16	17.13	19.86	2.6	32.68
	Summer	3.56	68.73	-0.92	-1.76		
	Fall	3.64	11.18	-0.44	12.49		
	Winter	3.21	-38.38	9.93	-3.69		
DE	Spring	3.51	2.65	24.13	12.97		
	Summer	3.37	34.68	7.66	-13.17		
	Fall	3.56	24.53	-5.26	18.6		
	Winter	2.83	-31.73	13.14	45.39		

Table D-36 B2-MES Model, High Variability, 2100

Grid	Season	ΔT (C)	SDT (%)	ΔP (%)	SDP (%)	Global ΔT (C)	Global SLR (cm)
CT & NJ	Spring	5.54	16.12	27.18	31.51	4.12	65.15
	Summer	5.65	109.02	-1.46	-2.79		
	Fall	5.77	17.74	-0.7	19.82		
	Winter	5.1	-60.88	15.75	-5.85		
DE	Spring	5.57	4.2	38.27	20.57		
	Summer	5.34	55.01	12.15	-20.9		
	Fall	5.64	38.91	-8.34	29.51		
	Winter	4.48	-50.33	20.84	72		

APPENDIX E Pavement Performance Comparison Results: Before and After Climate Change

This Appendix includes figures representing for the different scenarios for:

- JPCP
  - Change in IRI, fatigue and transverse cracking for different
    - Analysis years (2030, 2050, 2100) – Figure E.1
    - Emission models (A1B-AIM, A2-ASF, B1-IMA, B2-MES – Figure E2,
    - Climate change variability (low, medium, high) – Figure E3
  - Validation of calibration coefficients – Figure E4
- CRCP
  - Change in IRI and punchouts,
    - Analysis years (2030, 2050, 2100) – Figure E.5
    - Emission models (A1B-AIM, A2-ASF, B1-IMA, B2-MES – Figure E6,
    - Climate change variability (low, medium, high) – Figure E7
  - Validation of calibration coefficients – Figure E8
- AC
  - Change in IRI, total rutting, top down cracking and bottom up cracking,
    - Analysis years (2030, 2050, 2100) – Figure E.9
    - Emission models (A1B-AIM, A2-ASF, B1-IMA, B2-MES – Figure E10,
    - Climate change variability (low, medium, high) – Figure E11
  - Validation of calibration coefficients – Figue E12

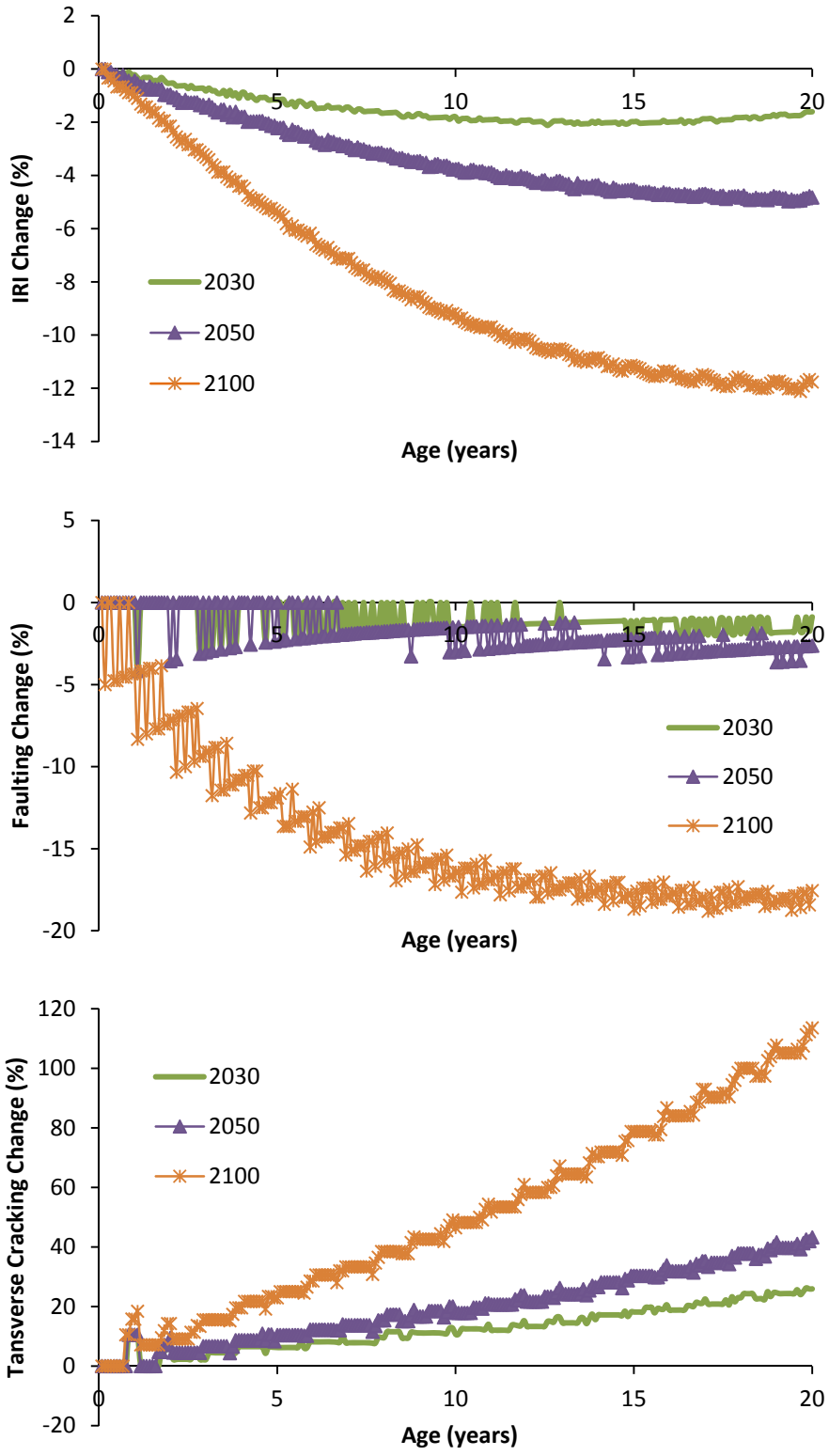

Figure E.1 JPCP: Analysis year comparisons (to the 2010 baseline design)

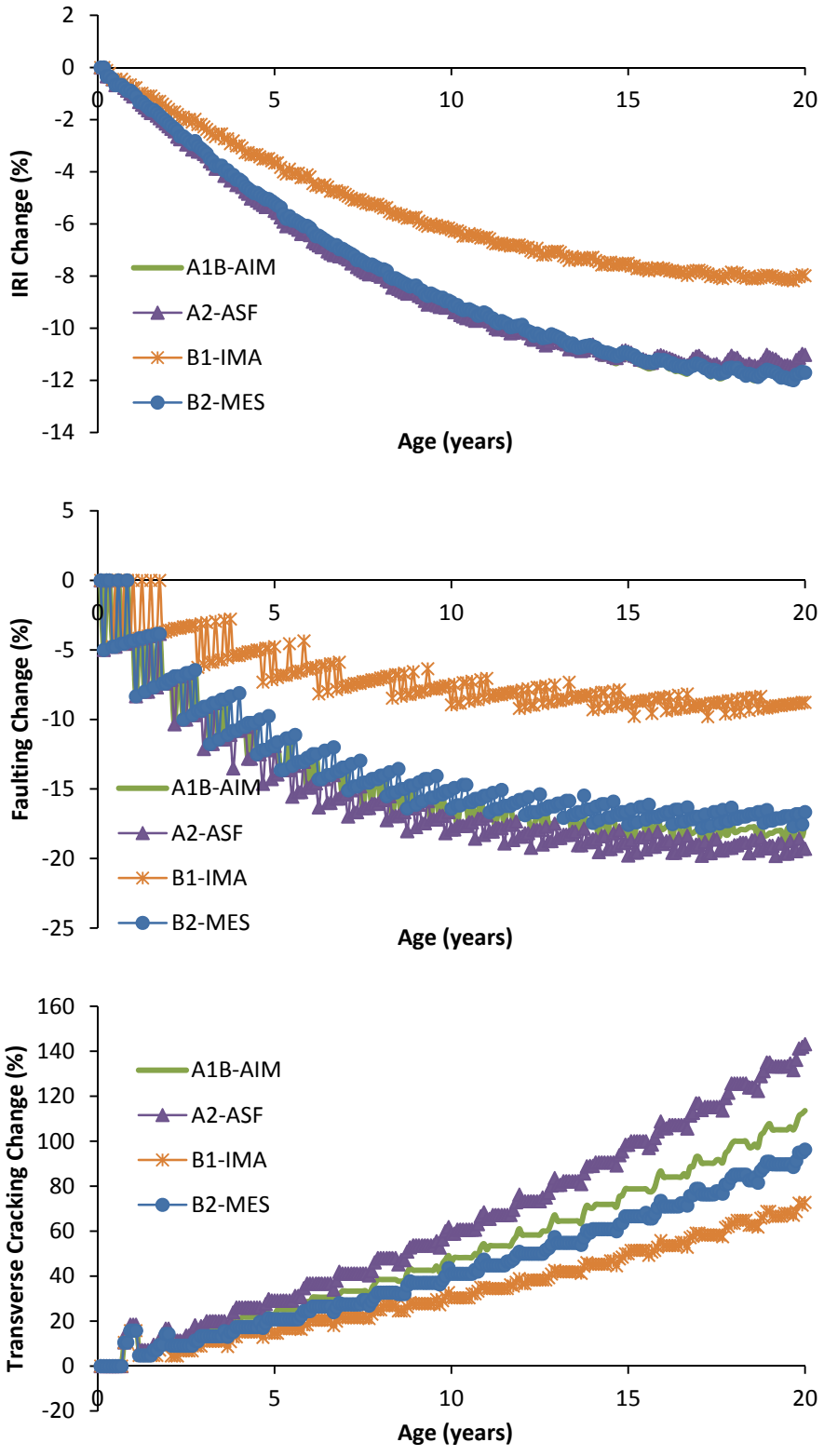

Figure E.2 JPCP: Emission model comparisons (to the 2010 baseline design)

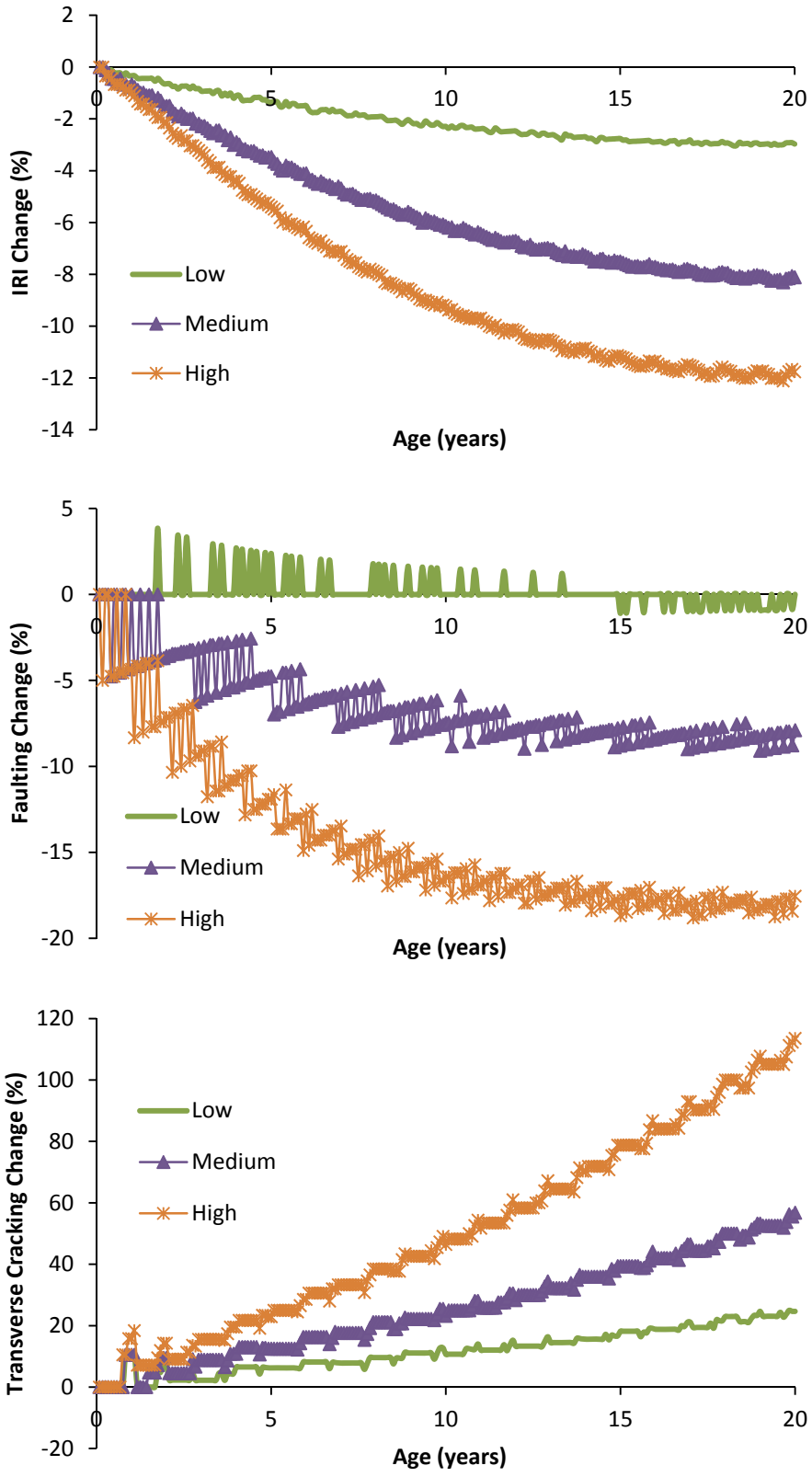

Figure E.3 JPCP: Climate change variability level comparisons (to the 2010 baseline design)

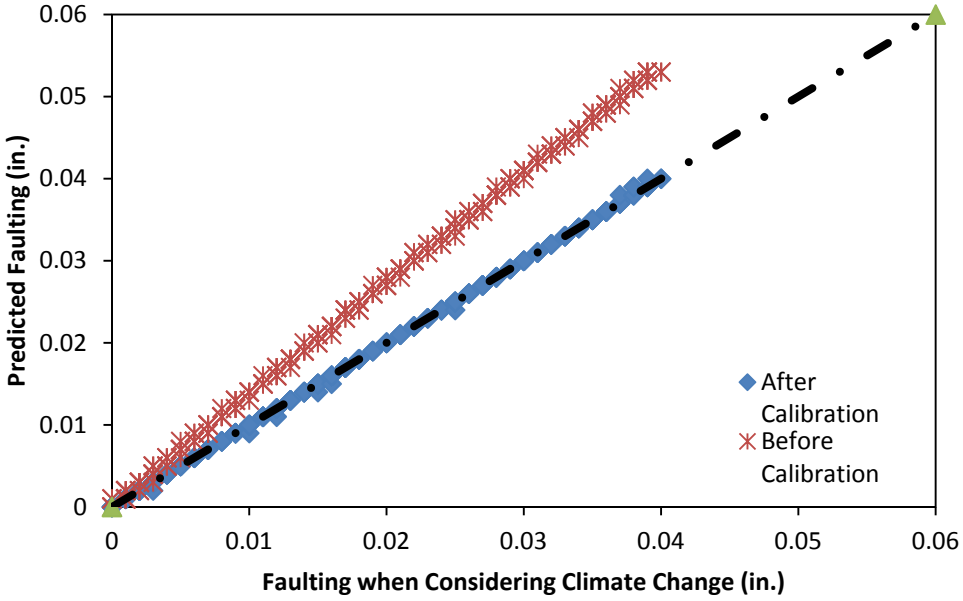

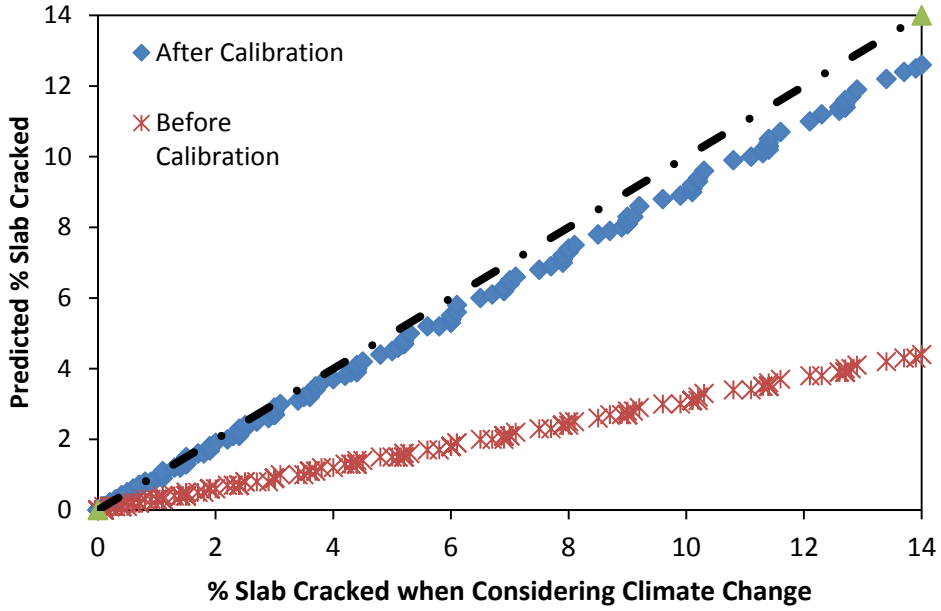

Figure E.4 JPCP: Validation of the calibration coefficients

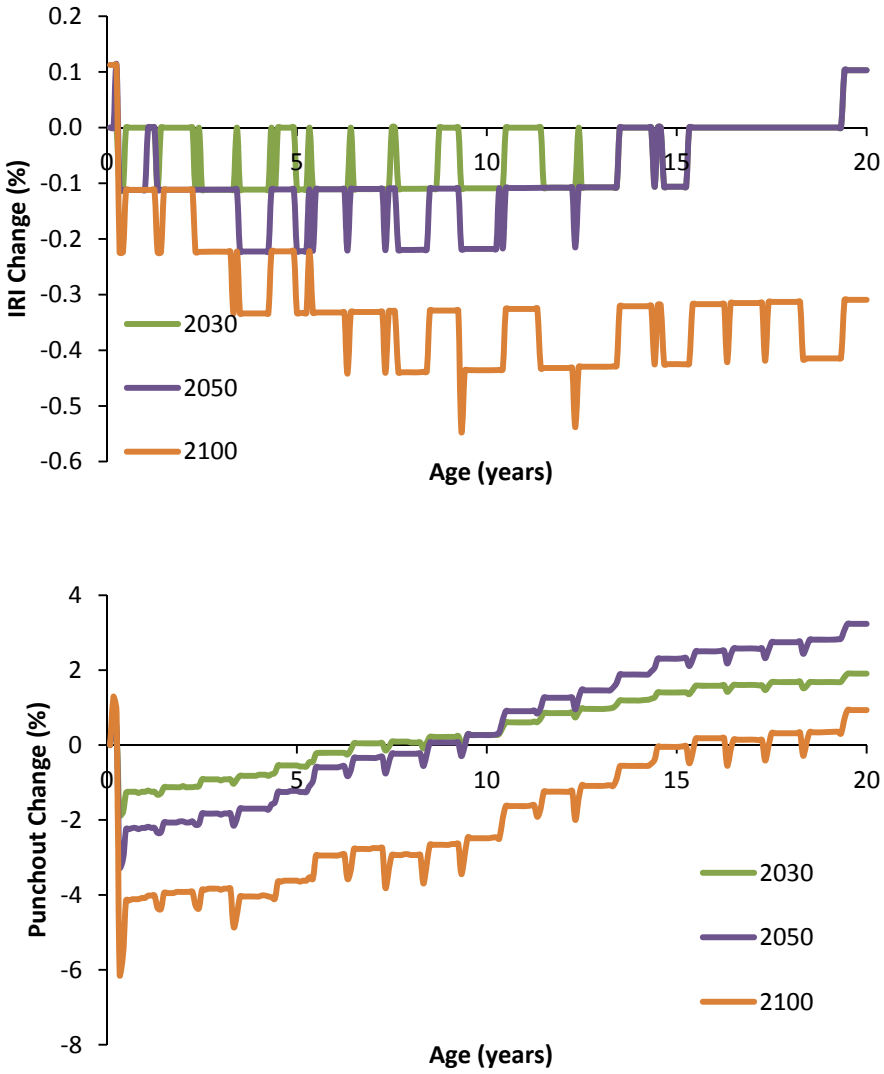

Figure E.5 CRCP: Analysis year comparisons (to the 2010 baseline design)

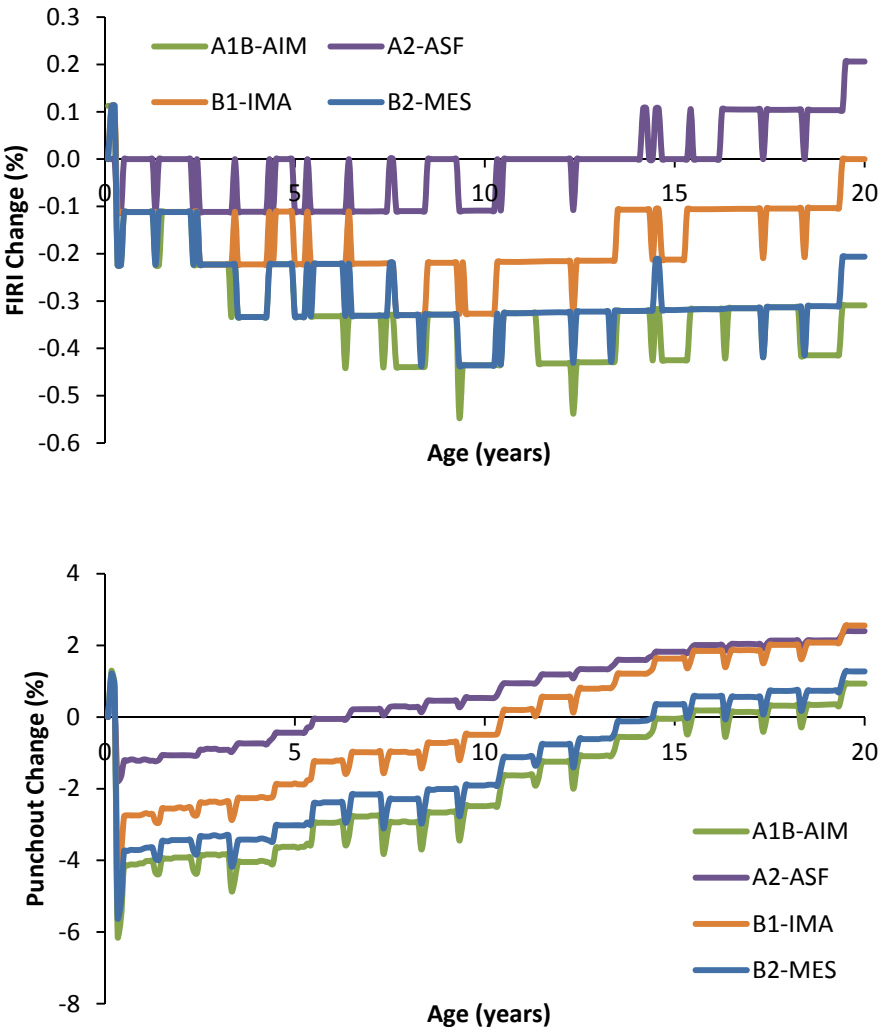

Figure E.6 CRCP: Emission model comparisons (to the 2010 baseline design)

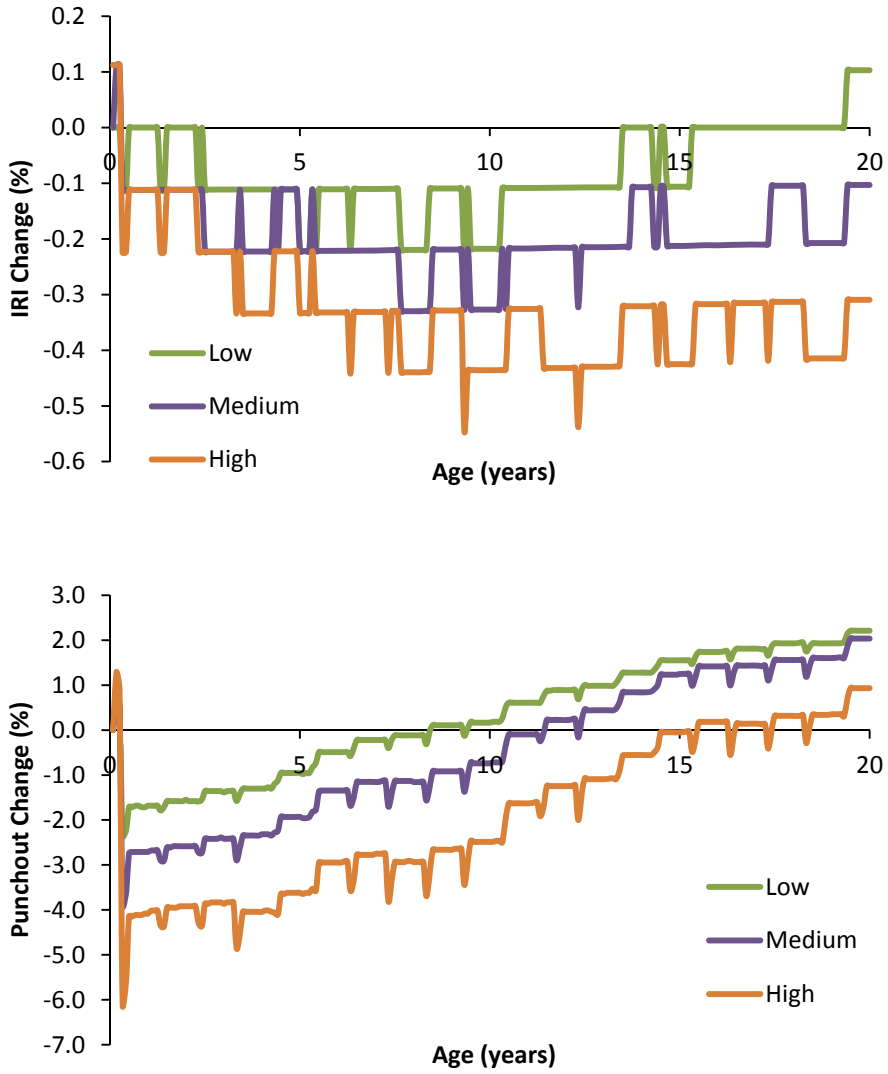

Figure E.7 CRCP: Climate change variability level comparisons (to the 2010 baseline design)

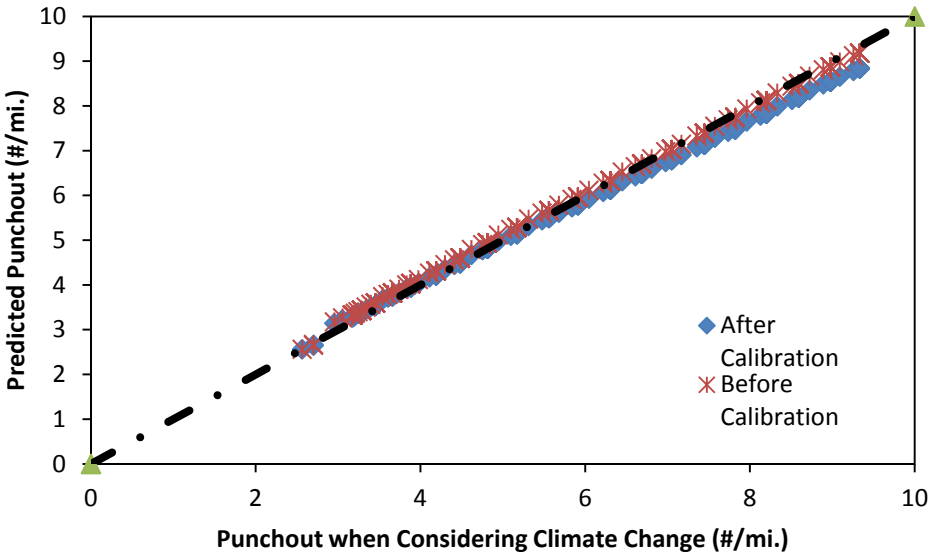

Figure E.8 CRCP: Validation of the calibration coefficients

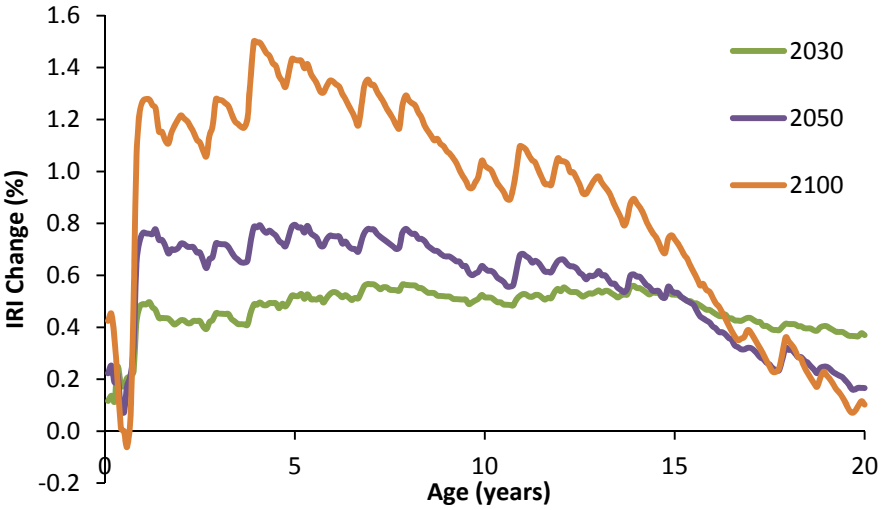
IRI Change (%)
1.6
1.4
1.2
1.0
0.8
0.6
0.4
0.2
0.0
-0.2
0
5
10
15
20
Age (years)
2030
2050
2100

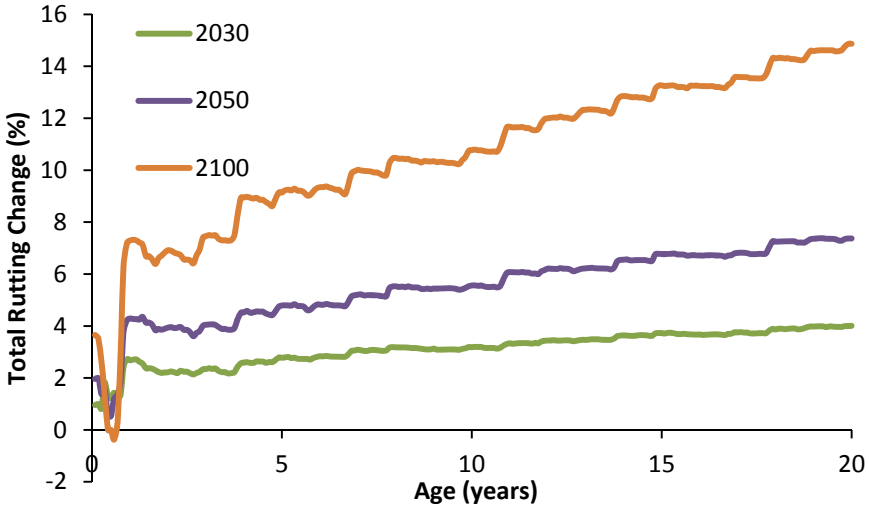
Total Rutting Change (%)
16
14
12
10
8
6
4
2
0
-2
0
5
10
15
20
Age (years)
2030
2050
2100

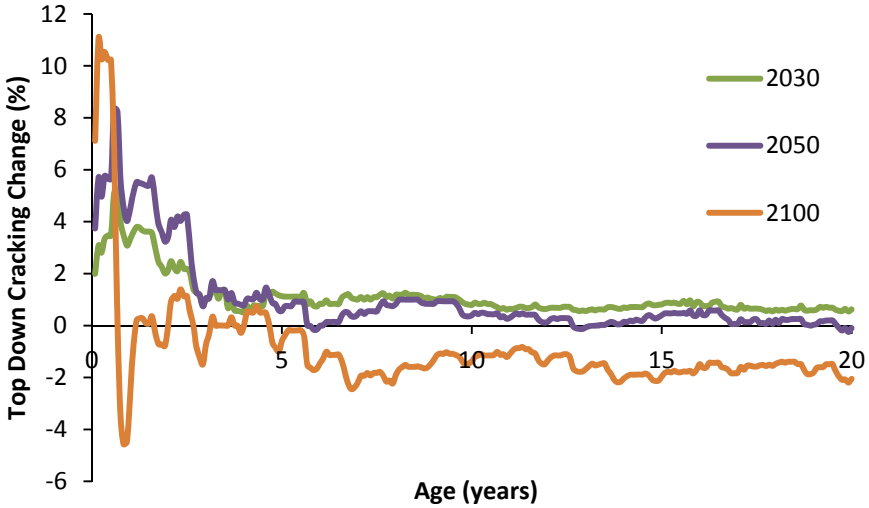
Top Down Cracking Change (%)
12
10
8
6
4
2
0
-2
-4
-6
0
5
10
15
20
Age (years)
2030
2050
2100

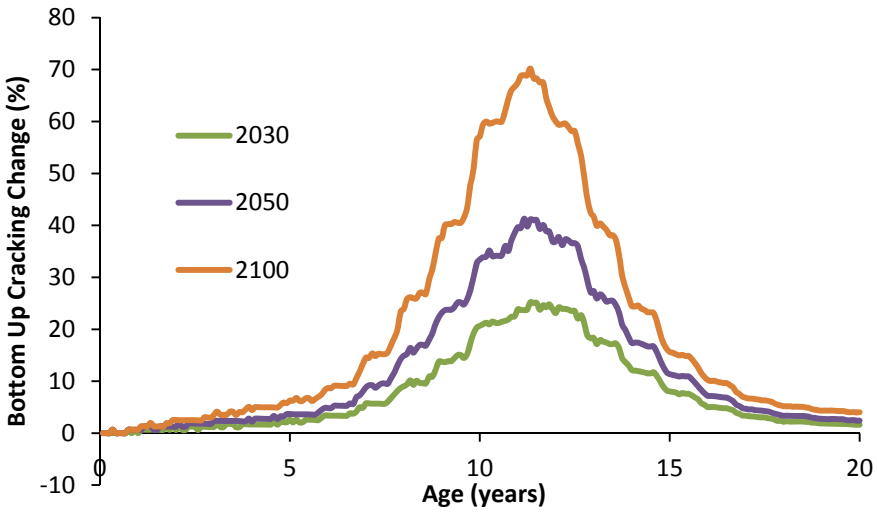

Figure E.9 AC: Analysis year comparisons (to the 2010 baseline design)

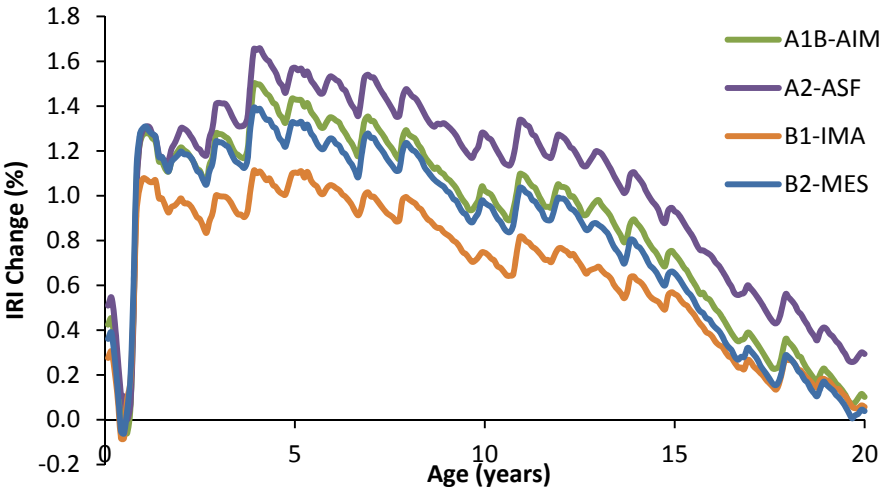
IRI Change (%)
1.8
1.6
1.4
1.2
1.0
0.8
0.6
0.4
0.2
0.0
-0.2
0
5
10
15
20
Age (years)
A1B-AIM
A2-ASF
B1-IMA
B2-MES

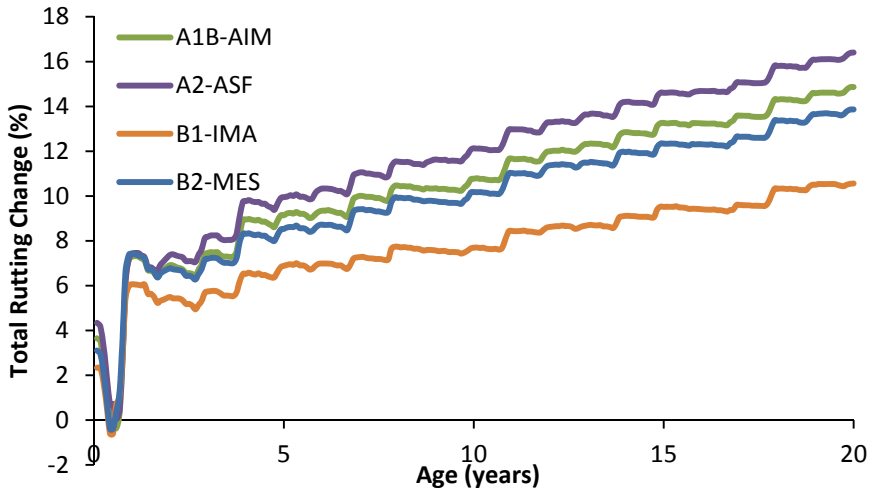
Total Rutting Change (%)
18
16
14
12
10
8
6
4
2
0
-2
0
5
10
15
20
Age (years)
A1B-AIM
A2-ASF
B1-IMA
B2-MES

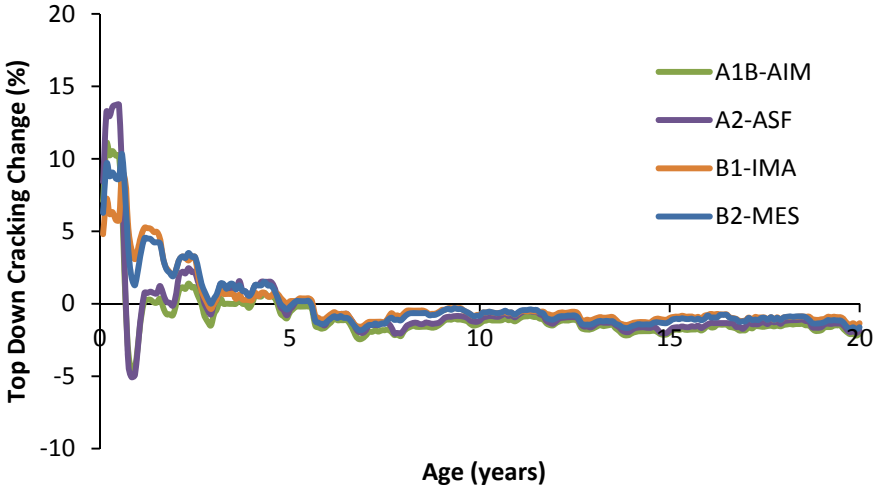
Top Down Cracking Change (%)
20
15
10
5
0
-5
-10
0
5
10
15
20
Age (years)
A1B-AIM
A2-ASF
B1-IMA
B2-MES

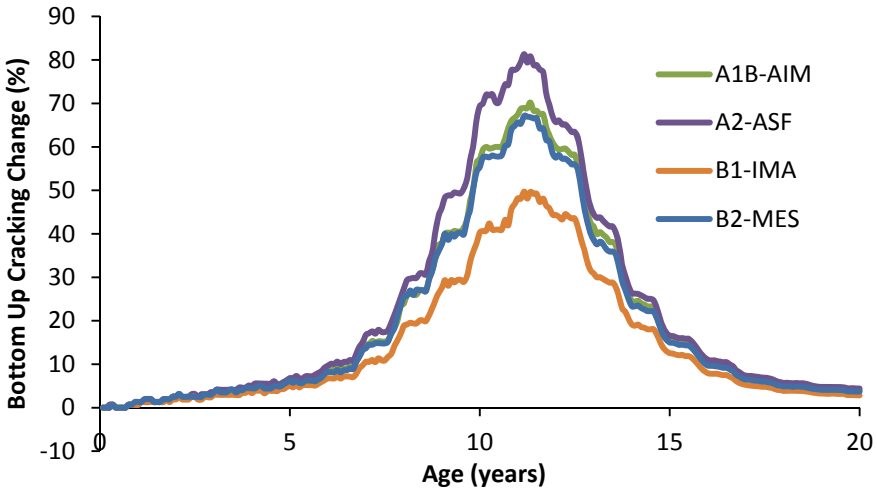

Figure E.10 AC: Emission model comparisons (to the 2010 baseline design)

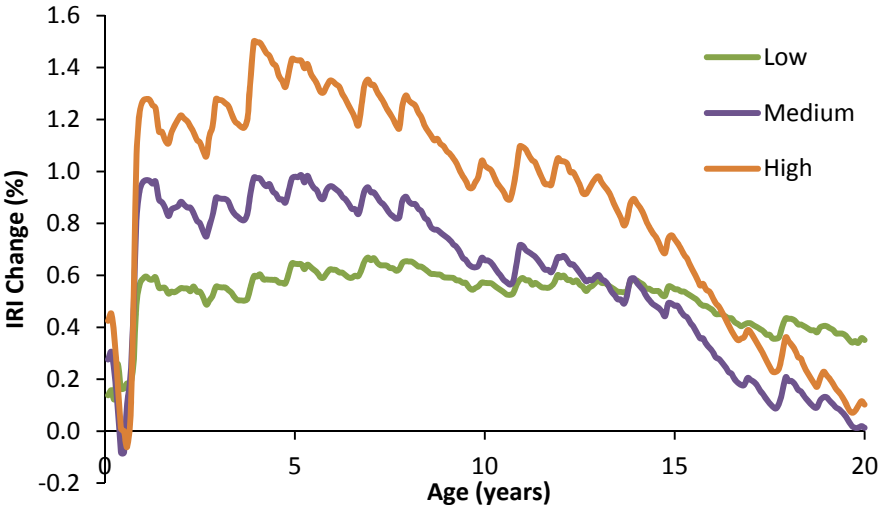
IRI Change (%)
1.6
1.4
1.2
1.0
0.8
0.6
0.4
0.2
0.0
-0.2
0
5
10
15
20
Age (years)
Low
Medium
High

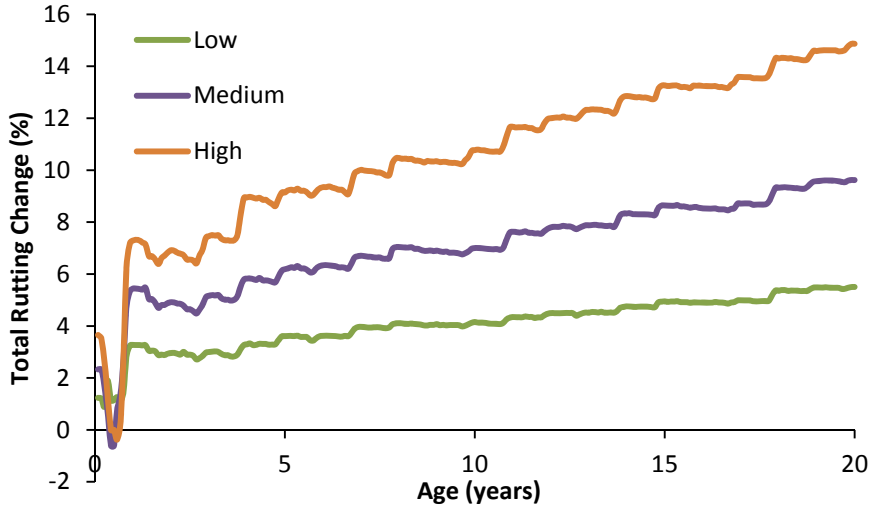
Total Rutting Change (%)
16
14
12
10
8
6
4
2
0
-2
0
5
10
15
20
Age (years)
Low
Medium
High

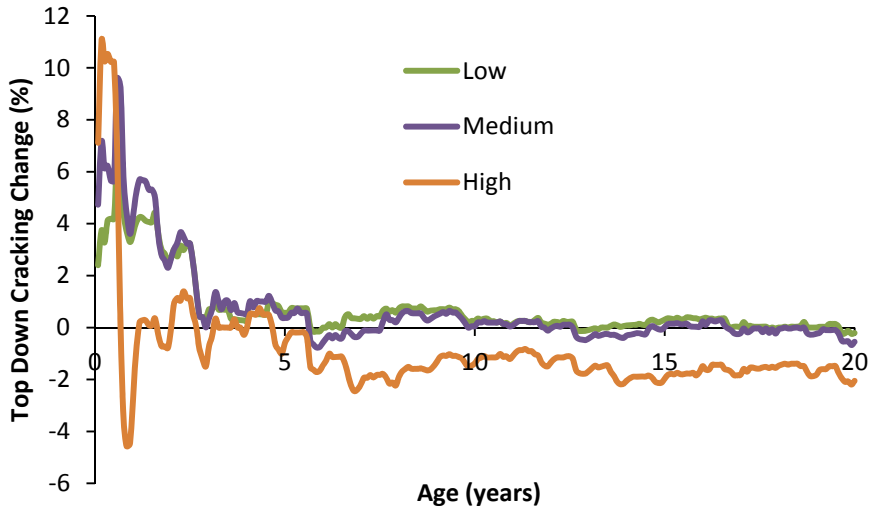
Top Down Cracking Change (%)
12
10
8
6
4
2
0
-2
-4
-6
0
5
10
15
20
Age (years)
Low
Medium
High

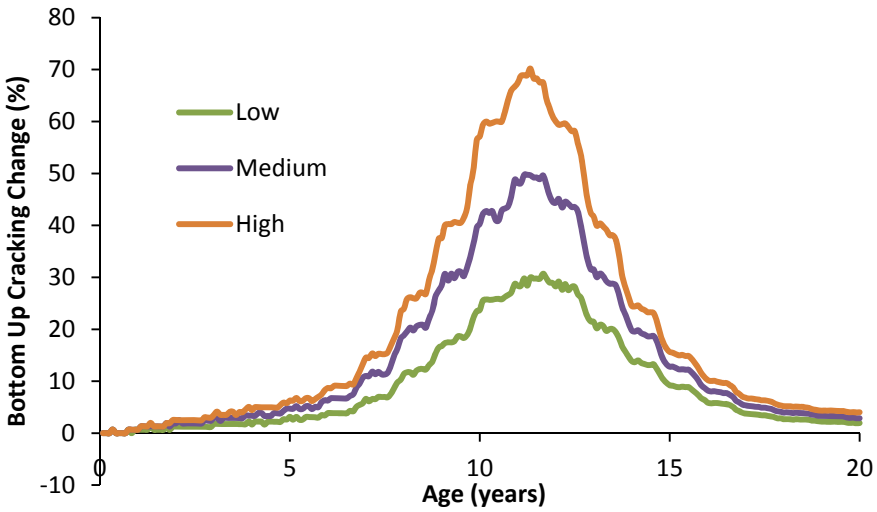

Figure E.11 AC: Climate change variability level comparisons (to the 2010 baseline design)

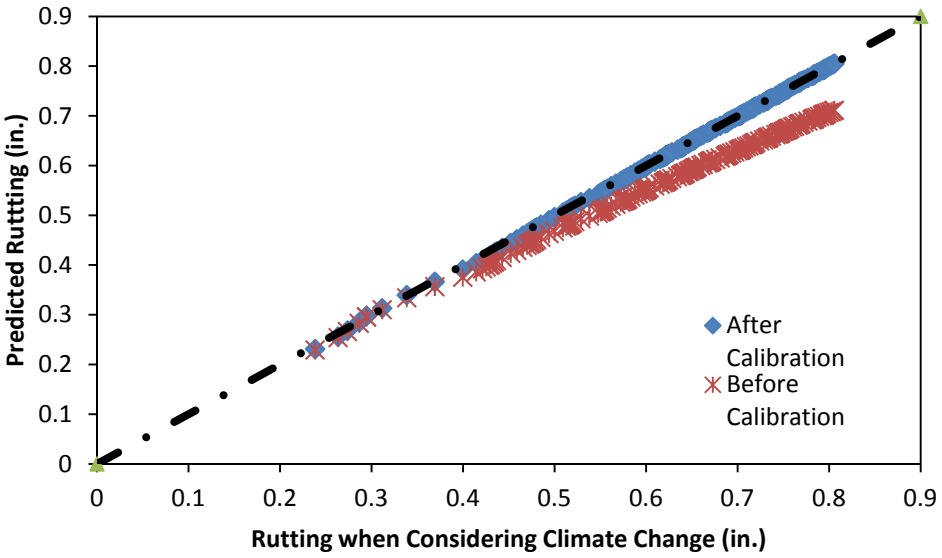
Predicted Ruttting (in.)
0.9
0.8
0.7
0.6
0.5
0.4
0.3
0.2
0.1
0
0
0.1
0.2
0.3
0.4
0.5
0.6
0.7
0.8
0.9
Rutting when Considering Climate Change (in.)
After Calibration
Before Calibration

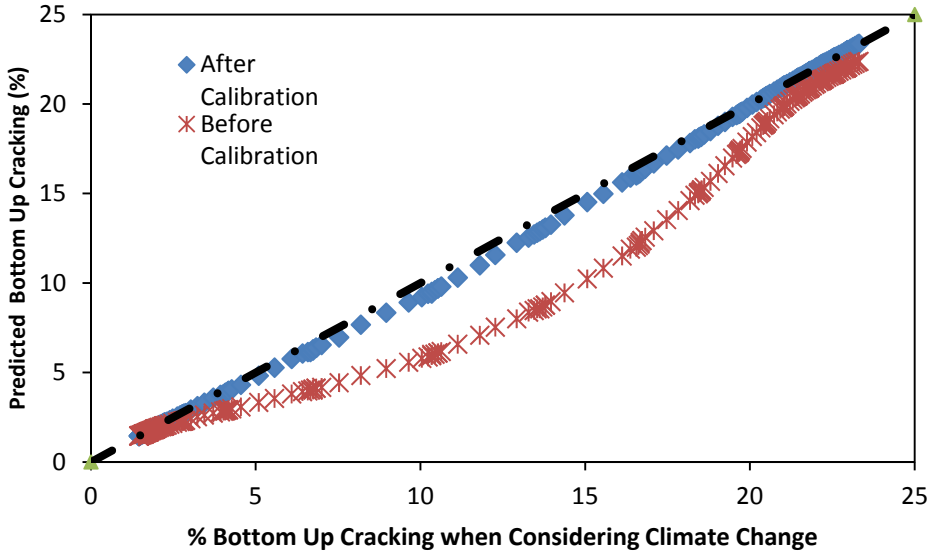
Predicted Bottom Up Cracking (%)
25
20
15
10
5
0
0
5
10
15
20
25
% Bottom Up Cracking when Considering Climate Change
After Calibration
Before Calibration

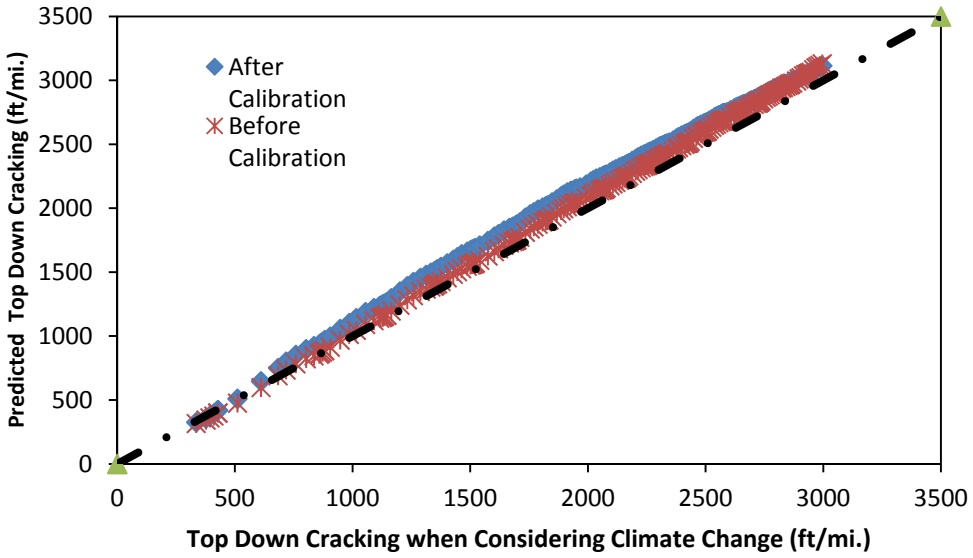

Figure E.12 AC: Validation of the calibration coefficients